# Defects in Amorphous Silicon: Dynamics and Role on Crystallization

Thesis by

Jung H. Shin

In Partial Fulfillment of the Requirements

for the Degree of

Doctor of Philosophy

California Institute of Technology

Pasadena, California

1994

(Submitted November, 1993)

# Acknowledgments

First and foremost, I would like to thank my family for their loving support and encouragement. I am here because of them.

My growth as a scientist here at Caltech would have been impossible without the help and support of Prof. Harry A. Atwater, and I would like to express my deepest gratitude to him. Not only did he provide invaluable guidance, he also showed Zen-like patience and faith during the early part of my research, when nothing seemed to be going right. I am still amazed that I was not thrown out. Thanks.

I also would like to thank Prof. Marc A. Nicolet for allowing me to use his implanter and other equipment in his lab. They have been invaluable in my research. Many thanks also go to Prof. James S. Im, who not only helped me, fresh out of college, get started on research, but also provided me with countless midnight meals. Thanks.

I would like to express special thanks to: Jimmy Yang, who helped me with all matters concerning computers (I still am not sure what CONFIG.SYS does); Peter Stolk, who provided me with his measurements of density of electronic states of amorphous silicon; to Jason Reid, who deposited

diffusion barrier and silver contacts for some of the samples; to Kyong-Hee Kim, for performing X-ray analysis of some of the samples; to Edward Ryan and Loren Funk of High Voltage Electron Microscope/Tandem Accelerator at Argonne National Laboratory for their expert assistance; Imran Hashim and Ramana Murty, for their help with transmission electron microscopy; Maggie Taylor and Ruth Brain, for proofreading this thesis; and to Carol Garland, for her help with transmission electron microscopy, and also for steering me toward the research area of structural relaxation.

I would also like to express my deep thanks to people who have provided me with friendship and good times while here at Caltech: Dr. Shouleh Nikzad, Dr. Byungwoo Park, Dr. Cho Jen Tsai, Dr. Channing Ahn, Selmer Wong, Heather Frase, Gang He, and Kirill Shcheglov. Thanks.

# Abstract

Defects play a crucial role in determining the properties of many materials of scientific and technological interest. With ion irradiation, it is possible to controllably inject defects, and thus carefully study the dynamics of defect creation and annihilation, as well as the effects such defect injection has on materials properties and phase transformations. Amorphous silicon is a model system for the study of amorphous solids characterized as continuous random networks. In hydrogenated form, it is an important material for semiconductor devices such as solar cells and thin film transistors. It is the aim of this thesis to elucidate the dynamics of defects in an amorphous silicon matrix, and the role such defects can play on crystallization of amorphous silicon.

In the first chapter, the concept of a continuous random network that characterizes amorphous silicon is presented as an introduction to amorphous silicon. Structural relaxation, or annihilation of non-equilibrium defects in an amorphous matrix, is introduced. Also developed are the concept of the activation energy spectrum theory for structural relaxation of amorphous solids and the density of relaxation states. In the second chapter, the density of re-

laxation states for the structural relaxation of amorphous silicon is measured by measuring changes in electrical conductivity, using ion irradiation and thermal anneal to create and annihilate defects, respectively. A new quantitative model for defect creation and annihilation, termed the generalized activation energy spectrum theory, is developed in Chapter 3, and is found to be superior to previous models in describing defect dynamics in amorphous silicon. In Chapter 4, the effect of irradiation on the crystallization of amorphous silicon is investigated. It is found that irradiation affects crystallization even when the growth kinetics of crystal grains is unaffected, and that defects injected into amorphous matrix by irradiation probably play a role in affecting the thermodynamic quantities that control nucleation. The role of defect injection in affecting the thermodynamic quantities is investigated in Chapter 5, where we estimate the change in the free energy of amorphous silicon under the irradiation conditions of Chapter 4, using the generalized activation energy theory of Chapter 3. The experimental data and its interpretation are consistent with predictions of generalized activation energy spectrum theory.

# List of Publications

Parts of this thesis have been, or will be published under the following titles.

1) J. H. Shin, J. S. Im, and H. A. Atwater; "Dynamics of Change in Electrical Conductivity of Ion Irradiated Amorphous Silicon."; *Phase Formation and Modification by Beam-Solid Interactions,* edited by G. S. Was, D. M. Follstaedt, and L. E. Rehn, Mat. Res. Soc. Symp. Proc. **235**, p. 21 (1992).

2) J. H. Shin and H. A. Atwater; "*In situ* Analysis of Irradiation-Induced Crystal Nucleation in Amorphous Silicon: A Microscope for Thermodynamic Processes in Nucleation."; Nucl. Inst. Meth. B **80** 973 (1993).

3) J. H. Shin and H. A. Atwater; "Ion Irradiated Amorphous Silicon: A Model Approach to Dynamics of Defect Creation and Annihilation."; *Thermodynamics and Kinetics of Phase Transformation in Thin Films*, edited by M. Atzmon, A. Greer, J. Harper, and M. Libera, Mat. Res. Soc. Symp. Proc. **311**.

4) J. H. Shin and H. A. Atwater; "Activation Energy Spectrum and Structural Relaxation Dynamics of Amorphous Silicon."; Phys. Rev. B **48** 5964 (1993).

5) J. H. Shin and H. A. Atwater; "Generalized Activation Energy Spec-

trum Theory: A New Approach to Modelling Structural Relaxation in Amorphous Solids."; submitted to Phys. Rev. Lett.

In addition, the author also contributed to:

6) J. S. Im, J. H. Shin, and H. A. Atwater, "Suppression of Crystal Nucleation in Amorphous Silicon Thin Films by High Energy Ion Irradiation at Intermediate Temperatures."; edited by H. A. Atwater, F. A. Houle, D. H. Lowndes, Mat. Res. Soc. Symp. Proc. **235**, p. 357 (1991).

7) J. S. Im, J. H. Shin, and H. A. Atwater; "Suppression of Nucleation during Crystallization of Amorphous Thin Si Films."; Appl. Phys. Lett. **59** 2314 (1991).

# Contents

**Acknowledgments** i

**Abstract** iii

**List of Publications** v

**1 Defects in Amorphous Silicon and Activation Energy Spectrum Theory** 1

1.1 Introduction . . . . . 1

1.2 Defects in Amorphous Silicon . . . . . 3

1.3 Activation Energy Spectrum Theory . . . . . 4

**2 The Activation Energy Spectrum of Amorphous Silicon** 18

2.1 Introduction . . . . . 18

2.2 Electron Transport in Amorphous Semiconductors . . . . . 20

2.3 Experimental Procedure . . . . . 28

2.4 Experimental Conductivity Measurements . . . . . 32

2.4.1 Temperature Dependent Conductivity of Relaxed Amorphous Silicon . . . . . 32

2.4.2 Variation of Room Temperature Conductivity with Anneal Temperature . . . . . 33

2.4.3 *In Situ* Measurements of Conductivity . . . . . 35

2.5 Activation Energy Spectrum . . . . . 41

2.6 Discussion . . . . . 52

2.7 Conclusion . . . . . 56

**3 Generalized Activation Energy Spectrum Theory 63**

3.1 Introduction . . . . . 63

3.2 Generalized Activation Energy Spectrum Theory . . . . . 65

3.3 Defect Dynamics of Amorphous Silicon: Modelling and Experiments . . . . . 67

3.3.1 Modelling Defect Dynamics . . . . . 67

3.3.2 Experiments . . . . . 71

3.4 Results and Discussion . . . . . 74

3.4.1 Evolution of Defect Density vs. Irradiation Dose . . . . 74

3.4.2 Evolution of Defect Density During Anneal . . . . . 84

3.4.3 *In Situ* Measurements of Conductivity . . . . . 89

3.5 Conclusion . . . . . 93

**4 Modification of Crystallization Dynamics of Amorphous Silicon by Irradiation** **97**

4.1 Introduction . . . . . 97

4.2 Classical Theory of Nucleation . . . . . 101

4.2.1 Formulation of the Theory . . . . . 101

4.2.2 Solutions to the Problem . . . . . 106

4.3 Experiments . . . . . 114

4.4 Results and Discussion . . . . . 117

4.5 Conclusion . . . . . 134

**5 Estimate of Change in the Free Energy of Crystallization Using Generalized Activation Energy Theory** **139**

5.1 Introduction . . . . . 139

5.2 Estimates of Change in the Free Energy . . . . . 140

5.2.1 Estimating the Defect Population . . . . . 140

5.3 Conclusion . . . . . 146

**Conclusion** **148**

**A Growth Rate and Interface Rearrangement** **150**

**B Code for Simulation of Thermal Anneal** **155**

**C Code for Simulation of Irradiation** **164**

# List of Figures


2.1 Electronic density of states of amorphous silicon . . . . . 23

2.2 Schematic of the experimental setup used for *in situ* conductivity measurements. . . . . 31

2.3 Temperature dependence of the electrical conductivity of relaxed a-Si . . . . . 34

2.4 Room temperature conductivity of a-Si as a function of the anneal temperature . . . . . 36

2.5 *In situ* measurements of the conductivity during and after irradiation . . . . . 38

2.6 *In situ* measurements of the conductivity at 773 K . . . . . 40

2.7 Conductivity transients for *in situ* measurements . . . . . 46

2.8 Density of the defect states of amorphous silicon . . . . . 50

3.1 Schematic of experimental setup for the second sets of *in situ* measurement of conductivity . . . . . 73

3.2 Defect population vs. dose . . . . . 75

3.3 Defect population vs. dpa . . . . . 77

3.4 Cascade generated by a 190 KeV Ne ion. . . . . 79

3.5 Cascade generated by a 600 KeV Xe ion. . . . . 80

3.6 Time evolution of the defect population . . . . . 82

3.7 Time evolution of the low activation energy defect population 83

3.8 $N(Q)$ after isochronal anneals . . . . . 85

3.9 Defect density after isochronal anneals . . . . . 87

3.10 *In situ* measurement of decay transient following irradiations at different ion fluxes . . . . . 91

3.11 The "cross-over" effect, shown in detail . . . . . 92

4.1 Free energy of formation for silicon. . . . . 111

4.2 Experimental setup for nucleation enhancement, performed at Caltech . . . . . 116

4.3 Comparison of grain morphology of grains grown under thermal and irradiation-enhanced growth conditions . . . . . 119

4.4 Grain density vs. time, performed at Caltech . . . . . 120

4.5 Growth rate of nucleated grains . . . . . 121

4.6 *In situ* measurements of the nucleation rate for samples for which steady state nucleation under irradiation is observed. . . 123

4.7 *In situ* measurements of the nucleation rate for samples for which irradiation is terminated before steady state nucleation under irradiation is observed. . . . . 124

4.8 Comparison of the free energies of formation . . . . . 128

4.9 Comparison of the calculated cluster size distribution . . . . . 129

4.10 Comparison of the gradient of calculated cluster size distribution 130

4.11 Schematic description of evolution of the cluster size distribution function and the nucleation rate for samples for which steady state nucleation under irradiation is not observed. . . . 132

4.12 Schematic description of evolution of the cluster size distribution function and the nucleation rate for samples for which steady state nucleation under irradiation is observed. . . . . 133

5.1 Effect of changing $Q_{min}$ on steady state defect concentration under irradiation. . . . . 143

5.2 Effect of changing the time step on steady state defect concentration under irradiation. $Q_{min} = 0.6$ eV. . . . . 144

A.1 Schematic of activation energy for interfacial jump . . . . . 153

# List of Tables

3.1 Theories discussed in this paper, along with significant assumptions associated with them. . . . . 72

4.1 Comparison of the irradiation enhanced and the thermal values of the nucleation rate and the incubation time . . . . . 118

4.2 Calculated changes in thermodynamic parameters controlling nucleation. . . . . 127

5.1 Effect of changing $Q_{min}$ on steady state defect concentration under irradiation. . . . . 142

5.2 Effect of changing timestep on steady state defect concentration under irradiation. $Q_{min} = 0.6$ eV. . . . . 142

# Chapter 1

# Defects in Amorphous Silicon and Activation Energy Spectrum Theory

## 1.1 Introduction

Amorphous silicon (a-Si) is a metastable phase of silicon which undergoes a first-order phase transition to either crystalline or liquid form at elevated temperatures. Therefore, it is distinct from traditional "glasses," which are characterized as configurationally frozen liquids. It is produced most commonly through either low-temperature ion irradiation of crystalline silicon (c-Si), or low temperature vapor deposition of a silicon thin film. It is also possible to produce a thin layer of a-Si by rapid solidification following pulsed laser melting of crystalline silicon, if the quenching rate is fast enough. In its

hydrogenated form, it is used extensively as the material for solar cells and for thin film transistors used to control active matrix displays. However, this thesis will address exclusively the pure, unhydrogenated form of amorphous silicon.

Amorphous silicon is modelled as a continuous random network (CRN) of silicon atoms, in which all silicon atoms have four covalently bonded nearest neighbor atoms in a roughly tetrahedral arrangement. Consequently, the short range order of amorphous silicon is very similar to that of crystalline silicon. However, slight variations in bond angle and, to a much lesser degree, bond length, destroy any long-range order. One result of the lack of long range order is the presence of rings other than six membered rings in the network, which is not allowed in crystalline silicon. The validity of the CRN model for the structure of amorphous silicon, constructed either by ball-and-stick method [1] or by computer simulation [2], is convincingly demonstrated by the close agreement between the predicted and measured radial distribution functions of a-Si. On the other hand, the microcrystalline model of a-Si [3, 4] fails to give satisfactory agreement with experiments, and is no longer considered a viable candidate for modelling a-Si [5, 6].

## 1.2 Defects in Amorphous Silicon

Such continuous random networks, however, represent an "ideal" a-Si, since they do not contain any defects. "Real" amorphous silicon produced experimentally, however, contains a very large number of defects, up to $\approx$ 1 atomic percent [7]. Experimentally produced a-Si is 1.8 $\pm$0.1% less dense than c-Si [8], while "ideal" a-Si (continuous random network of silicon atoms without any defect) is found to be 4% more dense than c-Si [2]. Prolonged anneals at elevated temperatures can be employed to reduce the defect concentration of a-Si, but only up to a factor of about 2-5 [9, 10]. This annihilation of non-equilibrium defects, while still maintaining the amorphous phase, is denoted by the term structural relaxation. With ion irradiation, it is possible to controllably introduce non-equilibrium defects into a-Si. This reverses the effects of a thermal anneal, and is known as structural unrelaxation. The defect concentration does not increase indefinitely, however, and saturates at $\approx$ 1 atomic percent at room temperature. The exact nature of these defects in a-Si is still somewhat unclear. However, the general consensus is that they are point defects. Electron paramagnetic resonance measurements have revealed the presence of dangling bonds in a-Si [11]. Mössbauer spectroscopy

and positron annihilation showed the presence of vacancies in a-Si [12, 13]. Differential scanning calorimetry (DSC) of irradiated a-Si and c-Si provided further proof that structural relaxation in a-Si is associated with annihilation of point defects [7]. The point defects in a-Si are topological defects in CRN, and are analogous to point defects in c-Si. They are distinct from the macroscopic voids that are sometimes present in vapor deposited a-Si.

Given the high concentration of defects in a-Si, it is not surprising that many properties of a-Si (e. g. , refractive index [14], spin density [11], viscosity [15], enthalpy [16, 17], vibrational properties [18, 19], diffusivity [9, 10, 20], shear viscosity [21], and electrical conductivity [22, 23]) are dependent upon the extent of structural relaxation, or the defect concentration. The effects can be quite dramatic. For example, irradiating well-relaxed a-Si to defect saturation at room temperature nearly doubles the free energy difference between a-Si and c-Si, and increases the electrical conductivity of a-Si by nearly 4 orders of magnitude.

## 1.3 Activation Energy Spectrum Theory

As is true with other amorphous solids, the structural relaxation kinetics (defect annihilation kinetics) of a-Si is not characterized by a single activation

energy. In such cases, the activation energy spectrum theory is often invoked. The activation energy spectrum theory was originally developed in the study of structural relaxation in metallic glasses, but is applicable to amorphous solids in general. In studies of metallic glasses, it was shown to be successful in describing reversible and irreversible property changes, and the "ln(t)" behavior that characterizes many relaxation processes under isothermal anneal [24, 25]. It also has been invoked in studies of structural relaxation in a-Si [7, 26, 27].

As treated by Narayanaswami [28] and Primak [29], and further developed by Gibbs *et al.* [30], the main assumption of the activation energy spectrum theory is that the activation energies of processes (i.e., any thermally activated transport or rearrangement of single atoms or groups of atoms) that contribute to structural relaxation are continuously distributed in activation energy. Therefore, the defect population is described by $N(Q)$, such that $N(Q)dQ$ is the density of defects with activation energy between $Q$ and $Q + dQ$.

The density of defects, $N(Q)$, however, can vary from one sample to another, depending on its history. Therefore, it is useful to develop another concept, the density of defect states, $D(Q)$, such that $D(Q)dQ$ is the density

of defect states that have activation energy between $Q$ and $Q + dQ$. Physically, $D(Q)$ is the theoretical upper limit of $N(Q)$ that is intrinsic to a given amorphous solid, such as could be obtained by fully unrelaxinga given sample at 0 K. As defects are being introduced, the actual defect density $N(Q)$ would evolve toward the density of defect states, $D(Q)$.

The density of defect states $D(Q)$ differs from other commonly used density of states functions, such as the electronic density of states in a solid. It is not uniquely determined by a fundamental equation, and thus would be very difficult to derive from an *ab initio* calculation. However, the existence of such an upper limit of defects as a function of activation energy may still be understood as follows. Defects cannot accumulate indefinitely in an amorphous solid while still maintaining the structural integrity of the amorphous solid. For example, a continuous random network cannot contain more defects than the percolation threshold for such a network and still remain continuous. Therefore, there must exist an upper limit to the total defect concentration, most likely much lower than the percolation threshold. Furthermore, in a given amorphous solid, there probably exists a continuum of possible defect configurations, each particular configuration being associated with a particular activation energy. We then may define the density of

defect states, $D(Q)$ by the relationship

$$D(Q) \;=\; p(Q) \times \text{Maximum total defect density}, \tag{1.1}$$

where $p(Q)$ is the probability function, intrinsic to the material under study, that a random defect will have activation energy between $Q$ and $Q + dQ$. In the case of metallic glasses, $p(Q)$ may be the normalized distribution of the free volume around an atom. In the case of amorphous semiconductors, it may be the normalized degree of bond angle distortions around a point defect.

In the case of the amorphous silicon, there are many experimental evidences which support the idea that such a density of defect states exists, and that it is intrinsic to amorphous silicon. For example, the maximum defect density obtainable at room temperature seems to be of the order of 1 atomic percent, even when measured with many different methods [7, 10, 26]. Futhermore, experimental data show that the density of defect states does not vary arbitrarily from sample to sample, but has a consistent form [7, 31].

Finally, we define the characteristic annealing function, $f(Q, T(t), t)$, such that

$$N(Q,t) = f(Q,T(t),t)N(Q,0) \tag{1.2}$$

where $T(t)$ is the thermal history of the sample, and $t$ is the time. It may be possible that rather than annihilating, defects recombine to form other defects, such that $f(Q,T(t),t)$ is a function of initial defect distribution as well. In this thesis, we shall neglect that possibility.

The characteristic annealing function $f(Q,T(t),t)$ is determined by the dynamics of structural relaxation. In order to accurately model the dynamics of structural relaxation, the possibility of interaction between defects with different activation energies must be taken into account. However, in the activation energy spectrum theory that has been used so far, a simplifying assumption is made that the defects with different activation energies are independent of each other. That is, activation of relaxation processes within an energy range between $Q$ and $Q+dQ$ is assumed not to affect the relaxation processes in other activation energy ranges. With this simplification, we can write down the dynamics of structural relaxation as

$$\frac{dN(Q,t)}{dt} = -\nu_o \exp\left(\frac{-Q}{kT(t)}\right) N(Q,t)^n, \tag{1.3}$$

where $\nu_o$ is the reaction constant, and $n$ is the order of the reaction.

In the case of an isothermal anneal, $f(Q,T,t)$ can easily be written down. If structural relaxation occurs through a first-order reaction, then

$$f(Q,T,t) = \exp\left[-\nu t \exp\left[\frac{-Q}{kT}\right]\right]. \tag{1.4}$$

If relaxation occurs through a second-order reaction, then

$$f(Q,T,t) = \frac{1}{1+\nu t \exp\left[-Q/kT\right]}. \tag{1.5}$$

For both Eq. (1.4) and Eq. (1.5), $\nu$ is expected to be of the order of the Debye frequency, or $10^{12}$ - $10^{14}\text{sec}^{-1}$. For a first order reaction, $\nu = \nu_o$, and for second order reaction, $\nu = \nu_o N(Q,0)$.

The density of defects, and thus the dynamics of structural relaxation, usually cannot be measured directly. However, it can be inferred by measuring a change of some property $P$ which changes as the material relaxes. We can write the property change $\Delta P$ as follows:

$$\Delta P = \int dp = \int \frac{dp(Q)}{dQ} dQ = \int C(Q) N_t^{rel}(Q) dQ, \tag{1.6}$$

where $dp(Q)$ is the change in property being measured due to activation of relaxation processes with activation energy between $Q$ and $Q+dQ$. $N_t^{rel}(Q)$ is the density of defects that have contributed to relaxation at time $t$,, which is simply $[(1-f(Q,T,t))N(Q,0)]$. The term $C(Q)$ is the function that relates property change $dp(Q)$ to the defect density $N_t^{rel}(Q)$.

For reasonably high values of $\nu$ ($\nu > 10^{10}$ sec$^{-1}$), $f(Q,T,t)$ changes rapidly from 0.05 to 0.95 within a fairly narrow range of activation energies, of the order of a few $kT$. Thus, it has been customary to approximate $f(Q,T,t)$ during an isothermal anneal by a step function such that

$$\begin{aligned} f(Q,T,t) &= 0, \quad Q < Q_\Theta \\ f(Q,T,t) &= 1, \quad Q > Q_\Theta, \end{aligned} \tag{1.7}$$

where

$$Q_\Theta = kT\ln(\nu t). \tag{1.8}$$

In other words, we make the approximation that all of the defects with activation energy $Q < Q_\Theta$ have been annihilated, while none of the defects

with activation energy $Q > Q_\Theta$ have been annihilated. This approximation is valid for both first and second order reaction kinetics. Indeed, the main conclusions of Gibbs' activation energy spectrum theory do not depend sensitively on the order of the reaction. This also implies, however, that it is not possible to distinguish between different orders of reaction using this method.

Since $Q_\Theta$ depends linearly on the anneal temperature but only logarithmically on the anneal time, during an isothermal anneal of a typical experimental duration, it will sweep only a narrow activation energy range after a brief transient. Therefore, if both $N(Q)$ and $C(Q)$ are broad with no sharp features of the order of the energy range swept by $Q_\Theta$, we can greatly simplify Eq. (1.6) as follows:

$$\Delta P = \int^{Q_\Theta} C(Q) N_t^{rel}(Q) dQ = \overline{C}\,\overline{N} kT \ln(\nu t) \propto \ln(t), \tag{1.9}$$

where $\overline{C}$ and $\overline{N}$ are the average values of $C(Q)$ and $N(Q)$, respectively, within the activation energy range swept by $Q_\Theta$ during an isothermal anneal (after a brief transient). Thus, after a brief transient, a property of an amorphous material will change logarithmically with time during an isothermal anneal if there exists a density of relaxation states, and if the approximations used

in deriving Eq. (1.9) are valid.

# Bibliography


[1] D. E. Polk, J. Non-Crystalline Solids, **5**, 365 (1971).

[2] F. Wooten and D. Weaire, in *Solid State Physics: Advances in Research Applications*, edited by D. Turnbull and H. Ehrenreich (Academic Press, New York 1987) Vol. **40**, pp. 2-42.

[3] A. Howie, O. Krivanek, and M. L. Ruidee, Phil. Mag., **27** (1) 235.

[4] A. Grigorovici, Thin Solid Films, **9** 1 (1971).

[5] J. F. Graczyk, P. Chaudhari, Phys. Stat. Solidi B, **58**, 163 (1973).

[6] Richard Zallen, *The Physics of Amorphous Solids*, (Wiley, New York 1983). p. 81.

[7] S. Roorda, W. C. Sinke, J. M. Poate, D. C. Jacobson, S. Dierker, B. S. Dennis, D. J. Eaglesham, F. Spaepen, and P. Fuoss, Phys. Rev. B **44** 3702 (1991).

[8] J. M. Poate, S. Coffa, D. C. Jacobson, A. Polman, J. A. Roth, G. L. Olson, S. Roorda, W. Sinke, J. S. Custer, M. O. Thompson, F. Spaepen, and E. Donovan:ch1, Nucl. Inst. Methods B **55**, 533 (1991).

[9] S. Coffa, J. M. Poate, D. C. Jacobson, W. Frank, and W. Gustin, Phys. Rev. B **45**, 8355 (1992).

[10] A. Polman, D. C. Jacobson, S. Coffa, J. M. Poate.

[11] P. A. Thomas, M. H. Bordsky, D. Kaplan, and D. Lepine, Phys. Rev. **18**, 3059 (1978).

[12] G. N Vandehoven, A. N. Liang, L. Niesen, and J. S. Custer, Phys. Rev. Lett. **68** 3714 (1992).

[13] S. Roorda, R. A. Hakvoort, A. van Veen, P. A. Stolk, and F. W. Saris, in *Phase Formation and Modification by Beam-Solid Interactions,* edited by G. S. Was, D. M. Follstaedt, and L. E. Rehn, Mat. Res. Soc. Symp. Proc. **235**, 39 (1992).

[14] C. N. Waddell, W. G. Spitzer, J. E. Frederickson, G. K. Hubler, and T. A. Kennedy, J. Appl. Phys. **55**, 4361 (1984).

[15] A. Witvrouw and F. Spaepen, in *Kinetics of Phase Transformations,* edited by M. M. Thompson, M. J. Aziz, and G. B. Stephenson, Mat. Res. Soc. Symp. Proc. **205**, 21 (1991).

[16] S. Roorda, S. Doorn, W. C. Sinke, P. M. L. O. Scholte, and E. van Loenen, Phys. Rev. Lett. **62**, 1880 (1989).

[17] E. P. Donovan, F. Spaepen, J. M. Poate, and D. C. Jacobson, Appl. Phys. Lett. **55**, 1516 (1989).

[18] J. S. Lannin, L. J. Pilione, S. T. Kshirsagar, R. Messier, and R. C. Ross, Phys. Rev. B **26**, 3506 (1982).

[19] W. C. Sinke, T. Wabarisako, M. Miyao, T. Tokuyama, S. Roorda, and F. W. Saris, J. Non-Cryst. Solids, **99**, 308 (1988).

[20] B. Park, F. Spaepen, J. M. Poate, and D. C. Jacobson, J. Appl. Phys. **69**, 6430 (1991).

[21] C. A. Volkert, J. Appl. Phys. **70**, 3521 (1991).

[22] W. Beyer and J. Stuke, In *Amorphous and Liquid Semiconductors*, Proceedings of the Fifth International Conference on Amorphous and Liquid

Semiconductors, edited by J. Stuke and W. Brenig (Taylor & Francis, London, 1974) p. 251.

[23] J. H. Shin, J. S. Im, and H. A. Atwater, in *Phase Formation and Modification by Beam-Solid Interactions,* edited by G. S. Was, D. M. Follstaedt, and L. E. Rehn, Mat. Res. Soc. Symp. Proc. **235**, 21 (1992).

[24] A. L. Greer, in *Rapidly Solidified Alloys: Processes, Structures and Properties*, edited by H. H. Liebermann (Marcel Dekker, New York 1993) Ch. 10.

[25] K. Bothe and H. Neuhäuser, Script. Metall. **16**, 1053 (1982).

[26] P.A. Stolk, L. Calcagnile, S. Roorda, W. C. Sinke, A. J. M. Berntsen, Appl. Phys. Lett. **60** 1688 (1992).

[27] C. A. Volkert, private communication.

[28] O.S. Narayanaswamy, J. Am. Ceram. Soc. **61** 146 (1978).

[29] W. Primak, Phys. Rev. **100**, 1677 (1955).

[30] M. R. J. Gibbs, J. E. Evetts, and T.A. Leake, J. Mater. Sci. **18**, 278 (1983).

[31] L. de Wit, S. Roorda, W. C. Sinke, F. W. Saris, A. J. M. Berntsen, and W. F. van der Weg, in *Kinetics of Phase Transformations*, edited by M. M. Thompson, M. J. Aziz, and G. B. Stepheson, Mat. Res. Soc. Symp. Proc. **205**, 3 (1991).

# Chapter 2

# The Activation Energy Spectrum of Amorphous Silicon

## 2.1 Introduction

Although it is well established that the kinetics of structural relaxation of amorphous silicon (a-Si) is described by a spectrum of activation energies, so far no systematic investigation of the activation energy spectrum has been made. For instance, Roorda *et al.* [1] have shown, using differential isothermal calorimetry measurements, that defects with many different activation energies contribute to relaxation. However, due to the lack of an explicit understanding of the enthalpy released upon defect annihilation in a-Si, no quantitative analysis of the activation energy spectrum has been attempted.

On the other hand, theories for electrical conductivity of a-Si are well developed and supported by experimental data. It is also well established that the electrical conductivity of a-Si is sensitively dependent on the degree of relaxation [3, 4]. Furthermore, electrical conductivity also has the experimental advantages of accuracy and *in-situ* capability, allowing us to probe time and temperature regimes that have not been accessible to date. Therefore, by combining existing models of electrical conductivity of a-Si with the activation energy spectrum theory discussed in Chapter 1, we can for the first time quantitatively analyze the activation energy spectrum for structural relaxation in a-Si. The results of the analysis enables us to comment on the relationship between structural relaxation and the rate of solid phase epitaxy (SPE) of c-Si into a-Si, and on irradiation-enhanced nucleation of crystal silicon in an a-Si matrix.

Using electrical conductivity measurements, we only measure the structural relaxation kinetics of defects that are electrically active. Recently, however, Coffa and Poate [5] have shown that passivating ion-irradiated (i.e., unrelaxed) a-Si with hydrogen has the same effect on the diffusion of transition metals in a-Si as structural relaxation by annealing does. Hydrogen is well known to passivate electrically active defects in a-Si, and decrease the

electrical conductivity of a-Si by reducing the number of localized electronic states in the energy gap [6]. The fact that passivating such electrically active defects with hydrogen has the same effect on diffusion of transition metals as structural relaxation by annealing suggests that it is reasonable to suppose that the electrically active defects are representative of the defect population as a whole.

## 2.2 Electron Transport in Amorphous Semiconductors

Optical and electrical measurements have shown the Mott [7] theory of electron conduction in amorphous solids to be successful in explaining the observed electrical properties of pure (i.e., unhydrogenated), undoped, and tetrahedrally bonded amorphous semiconductors, such as a-Ge or a-Si [8, 9, 10]. Within this theory, the concepts of the electronic density of states $g(E)$ and the energy band gap are considered to be still conceptually valid and useful. The lack of long range order is thought to create a large density of localized states near the band edges, and electron mobilities in these localized band edge states are thought to be about three orders of magnitude smaller than the mobility in the extended states. Furthermore, other de-

fects inherent in amorphous solids are thought to create a band of localized electronic states near the middle of the energy gap which pin the Fermi level.

This picture is supported by experimental data. A recently estimated electronic density of states of amorphous silicon is shown in Fig. 2.1 [11]. The electronic density of states is estimated from optical measurements of the absorption coefficient $\alpha(h\nu)$, shown in Fig. 2.1a. Measurements in the photon energy range of 1.2 to 2.5 eV represent absolute measurements, while measurements in the photon energy range 0.6 to 1.0 eV were obtained by scaling absorption data from Photothermal Deflection Spectroscopy (PDS). Photothermal Deflection Spectroscopy measures the absorption coefficient by measuring the gradient of the index of refraction modulated by the gradient in the temperature of the medium, typically heated by a laser. More detailed description of PDS can be found elsewhere [12]. It must be noted, however, that the measured values for the density of electronic states is dependent on assumptions used in deriving them. Thus, Fig. 2.1b gives a reliable indication of the density of electronic states rather than a final determination. However, it is evident that the density of localized electron states near mid-gap decreases upon relaxation, which is consistent with our assertion that electrically active defects are representative of the defect population as a whole.

The apparent shift in the Fermi level upon relaxation of a-Si is an artifact of fixing the valence band edge to be zero, and the widening of the energy band gap upon relaxation due to annihilation of localized states near the band edges.

Conduction, then, is characterized by three different mechanisms, dependent upon the temperature. Conduction will occur through (a) phonon-assisted tunneling (hopping) of electrons near the Fermi level; (b) hopping conduction of electrons in the localized band tails; or (c) extended state (non-localized) conduction. At sufficiently high temperatures, enough electrons are excited to extended states to dominate the conduction process. In this case, the conductivity is given by

$$\sigma_{ext} = \sigma_o^x \exp[-(E_c - E_f)/kT], \tag{2.1}$$

where $E_c$ and $E_f$ are the conduction band edge and the Fermi level, respectively. At moderate temperatures, conductivity is thought to be dominated by localized state transport in the band tail states, and is treated in a way similar to the extended state conduction. That is,

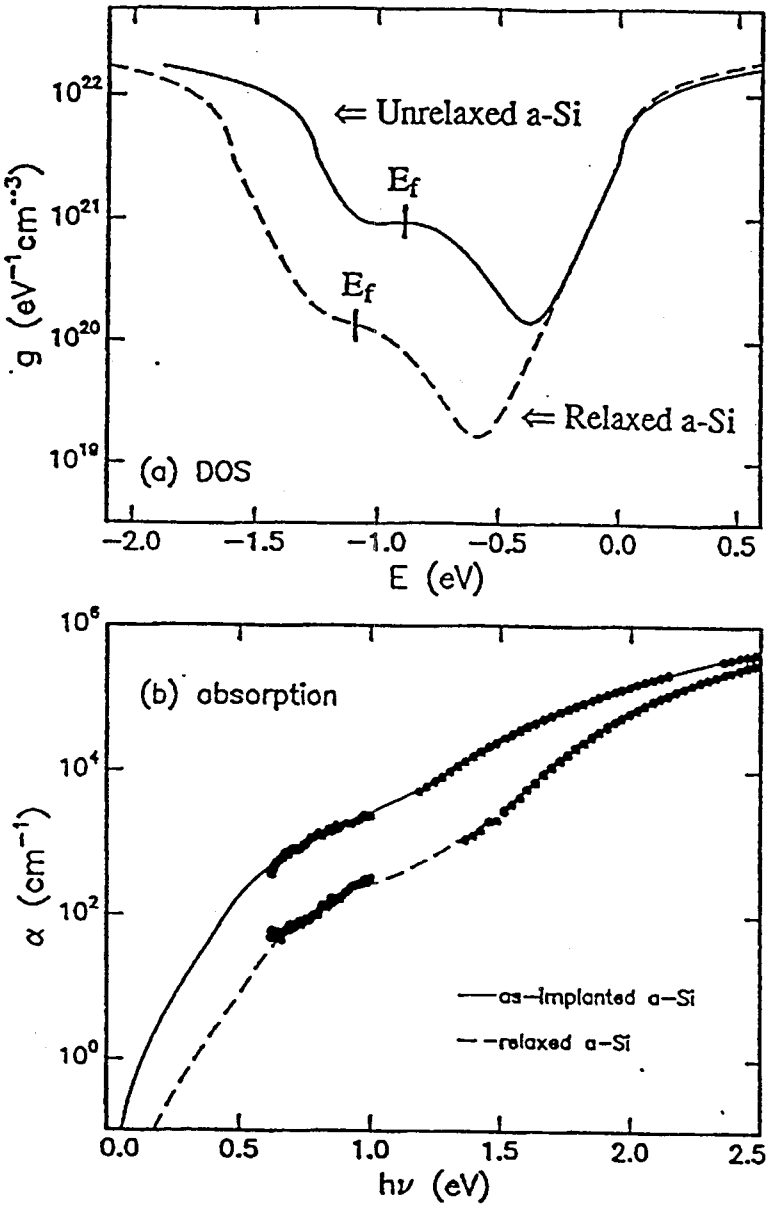


Figure 2.1: (a) Experimentally derived electronic density of states of amorphous silicon. It is found by fitting the optical data shown in (b). A Gaussian localized states distribution is assumed, and the Fermi level is assumed to be fixed in the center of the Gaussian peak.

$$\sigma_{tail} = \sigma_o^t \exp[-(E_c - E_f + W)/kT], \tag{2.2}$$

where $W$ is the activation energy for hopping. Like $\sigma_o^x$, $\sigma_o^t$ is difficult to estimate. However, it is expected to be at least three order of magnitude smaller than $\sigma_o^x$, since the mobility in localized states near the band edges is smaller by this factor. This supposed conduction due to hopping in the localized band tail states, however, is not observed for a-Si or a-Ge [3, 9, 10].

At low temperatures, conduction is expected to be dominated by the hopping (phonon-assisted tunneling) of electrons near the Fermi level from one localized state to another. The probability that an electron can tunnel from one localized state to another is given by

$$p_{tunnel} = \omega \exp(-2\alpha R - W/kT) \tag{2.3}$$

where $\omega$ is the attempt frequency of localized electrons, $\alpha^{-1}$ is the decay constant of the localized electron wavefunction, $R$ is the jump distance, and $W$ is the energy difference between the two localized states. The conduction will be dominated by a combination of the tunnel distance, $R$, and the energy difference, $W$, which minimizes the exponent in Eq. (2.3).

If the electronic density of states near the Fermi level is $g(E_f)$, the total number of electronic states with a energy difference $W$ within distance $R$ from a localized electronic state near the Fermi level is given by

$$\frac{4\pi}{3}R^3 g(E_f)W. \tag{2.4}$$

In order for a tunneling to be possible, the number of accessible state must be at least one, or

$$W = \frac{3}{4\pi R^3 g(E_f)}. \tag{2.5}$$

Substituting Eq. (2.5) in Eq. (2.3), we find

$$p_{tunnel} = \omega \exp(-2\alpha R - 3/4\pi R^3 g(E_f)kT). \tag{2.6}$$

And the value of $R$ which minimizes the exponent in Eq. (2.6) is

$$R = \left[\frac{9}{8\pi\alpha g(E_f)kT}\right]^{1/4}. \tag{2.7}$$

Using above equations, and Einstein's relation $\mu = eD/kT$, with $D =$

$(1/6)p_{tunnel}R^2$, Mott derived an expression for the hopping conduction. It is given by

$$\sigma_{hop} = \sigma_o^h \exp[-A/T^{1/4}]. \tag{2.8}$$

where

$$\sigma_o^h = \frac{e^2}{10}\omega\left[\frac{g(E_f)}{\alpha kT}\right]^{1/2} \tag{2.9}$$

$$A = 2.1\left[\frac{\alpha^3}{g(E_f)k}\right]^{1/4}, \tag{2.10}$$

This $\exp[-A/T^{1/4}]$ dependence of electrical conductivity on temperature is widely accepted and observed for amorphous semiconductors. We note, however, that the exact forms of $\sigma_o$ and $A$ are still somewhat controversial, and deviations from the simplifying assumptions used in obtaining Eqs. (2.10) and (2.10) will lead to slightly different results. We will assume Eqs. (2.10) and (2.10) to be accurate. However, it will be shown later in this chapter that for our purposes, it is sufficient to have the prefactor $\sigma_o^h$ to be only some weak function of $g(E_f)$, and the exponential factor $A$ to be proportional to $g(E_f)^{-1/4}$.

The importance of the electron transport in a-Si via hopping is twofold. First, conductivity is overwhelmingly dominated by those electronic states which lie very close to the Fermi level, of the order of few $kT$. This is true even though the most favorable energy difference for hopping, $W$, may be of the order of few tenths of an electron volt [8]. However, as we shall see later, the activation energies necessary to anneal out these electronically active defects near the Fermi level can vary by nearly 2 eV. This shows that there is very little correlation between the electronic energy of an electrically active defect and the activation energy necessary for its annihilation, and further supports our assumption that electrically active defects are representative of the defect population as a whole. Second, because the transport occurs via tunneling of electrons from one localized electronic state to another, the conductivity is fully controlled by localized states (presumably created by defects in a-Si), and not by some kind of resonant scattering of charge carriers. Therefore, the change in hopping conductivity accurately reflects the change in the localized electronic states near the Fermi level, and thus the defects which create them.

## 2.3 Experimental Procedure

Pure amorphous silicon films 450 nm thick were grown on thermally-oxidized Si substrates by ultrahigh vacuum electron-beam deposition. The oxide layer was 1.1 $\mu$m thick. Prior to loading into the deposition system, substrates were cleaned by immersion in a 5:1:1 solution of $H_2O : H_2O_2 : NH_4OH$ at 80°C, followed by a rinse in ultrahigh purity deionized $H_2O$. Prior to the deposition, the substrates were sputter cleaned by 100 eV Ar-ion bombardment, and the silicon evaporation source material was outgassed. The system base pressure was in the $10^{-10}$ Torr range, but the pressure rose to $5 \times 10^{-8}$ Torr during the deposition. The substrate temperature during the deposition was $\approx$ 400 K, and the deposition rate was 2 Åsec$^{-1}$. Immediately following the deposition, and prior to exposure to air, the films were heated in ultra high vacuum at 620 K for 1h to densify the a-Si film and to remove macroscopic voids which otherwise might lead to substantial trapping of oxygen and water vapor [13]. Following deposition, a-Si resistors were defined as mesas by photolithography and wet chemical etching. The photolithographic steps necessary for defining resistors and contact formation required samples to be annealed at 473 K. Aluminum contacts were evaporated for samples sub-

ject to temperatures less than 573 K during the conductivity measurements. Samples subject to temperatures higher than 573 K during the conductivity measurements employed sputter-deposited Ag contacts with amorphous Ti/Si/N diffusion barriers between the Ag contacts and a-Si. Amorphous Ti/Si/N diffusion barriers are known to be effective up to 900 K with crystallization temperatures in excess of 1273 K [14].

Conductivity measurements were made in a two-point probe configuration. The extremely high sample resistance made four-point probe measurements unnecessary, since the contact resistance was negligible compared to the sample resistance. For certainty, all contacts were verified to be Ohmic prior to use.

All anneals were performed in a high-vacuum furnace with a base pressure of $4 \times 10^{-6}$ Torr. All irradiations were performed with 600 KeV $Kr^{++}$ ions with total doses equal to or greater than one displacement per atom (dpa) as calculated by using the TRIM [15, 16, 17] collision cascade simulation program. A total dose of 1 dpa is known to be sufficient to completely unrelax a-Si [1]. The beam spot size was approximately 1 $cm^2$, and the beam was rastered across the sample in excess of 1 KHz.

For *in situ* conductivity measurements at elevated temperatures, samples

were clipped onto a resistively-heated metal hot stage. For *in situ* conductivity measurements at low temperatures, samples were glued onto a liquid cooled cold stage using heat conducting paste. For high temperature measurements, the sample temperature was measured by a thermocouple clipped onto the sample surface. This step was necessary, since temperature calibration showed that at elevated temperatures, the sample temperature and the stage temperature can differ by as much as 100 K. For low temperature experiments, the sample temperature was assumed to be equal to the stage temperature. A schematic of the experimental setup for *in situ* measurements is shown in Fig. 2.2. No effort was made to separate the contribution of ion beam current to the measured conductivity, since the ion beam current was much smaller than the sample current.

Simultaneous measurement of the ion beam current, the sample current, and the sample temperature proved to be difficult. Thus, for *in situ* experiments, ion beam current was measured indirectly by first stabilizing the beam at the desired dose rate, and then adjusting the accelerator controls during the actual irradiation so as to maintain a constant accelerating current and sample secondary electron current. The accuracy of dosimetry measurements made in this fashion was calibrated by Rutherford backscattering

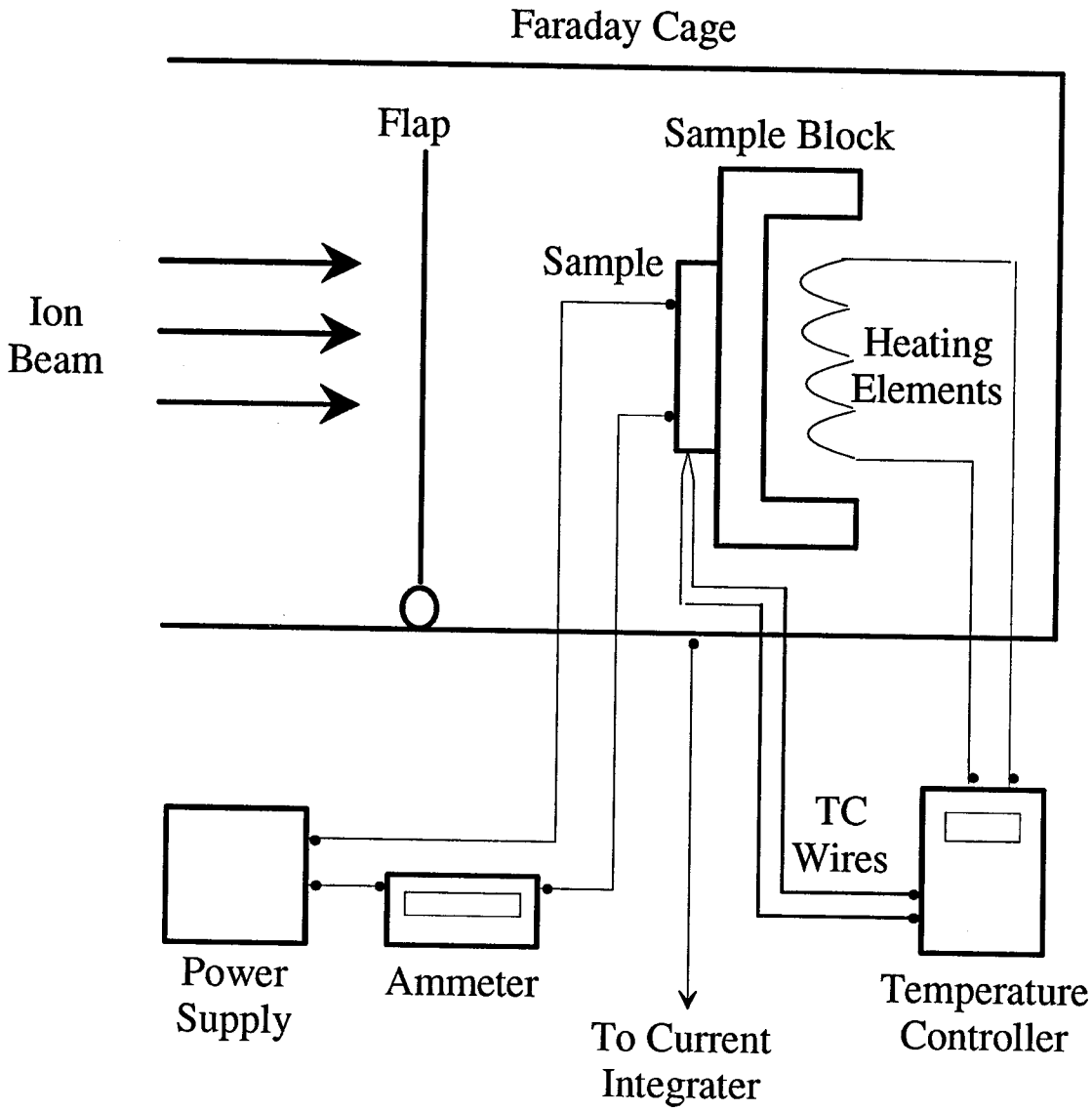


Figure 2.2: Schematic of the experimental setup used for *in situ* conductivity measurements.

spectroscopy (RBS) measurements to be within ± 15 %. This level of accuracy in dosimetry is acceptable, since the total irradiation dose in all cases greatly exceeded 1 dpa.

## 2.4 Experimental Conductivity Measurements

### 2.4.1 Temperature Dependent Conductivity of Relaxed Amorphous Silicon

The variation of electrical conductivity with measurement temperature for amorphous silicon that was relaxed by annealing at 873 K for 15 min prior to the conductivity measurement is illustrated in Fig. 2.3. The values obtained are in good agreement with previous reports of the conductivity of a-Si [3]. There is a clear change in the temperature dependence of the conductivity near 473K. For measurement temperatures greater than 473 K, the conductivity shows $\exp(-1/T)$ dependence. The solid line is a least-squares fit to a functional form of $\sigma_{rel} = \sigma_o \exp[-(E_c - E_f)/kT)]$. The values obtained for $\sigma_o$ and $(E_c - E_f)$ are $1.1 \times 10^4 \Omega^{-1}$ cm$^{-1}$ and 0.8 eV, respectively. For lower temperatures, Hause *et al.* have shown that the electrical conductivity of a-Si shows $\exp[-(1/T)^{1/4}]$ dependence up to room temperature [18], which was the highest temperature used in their experiments. We note that

previous work has indicated that the electrical conductivity of a-Ge, which has a band gap of about 0.6 eV and an activation energy for high temperature conductivity of 0.25 eV, also shows $\exp[-(1/T)^{1/4}]$ behavior up to room temperature [19]. Amorphous silicon has a band gap of about 1.4 eV and an activation energy for high-temperature conductivity of 0.8 eV. Therefore, it is reasonable to assume that hopping conduction must dominate to much higher temperatures in a-Si than in a-Ge. Consequently, a functional form of $\sigma = \sigma_o^h \exp[-A/T^{1/4}]$ was fitted, and was found to fit the data well. The values obtained for $\sigma_o^h$ and $A$ are $8.4 \times 10^5 \Omega^{-1}$ cm$^{-1}$ and $110\text{K}^{1/4}$, respectively.

### 2.4.2 Variation of Room Temperature Conductivity with Anneal Temperature

To discern the relationship between the extent of structural relaxation and the conductivity, samples were first fully unrelaxed by irradiation at room temperature to a total dose of 1 dpa and then partially relaxed by annealing at various temperatures for 15 min. Conductivities of the samples were then measured at room temperature. Since samples were stored at room temperature, the value of the conductivity after an anneal at room temperature is taken to be that which is measured 15 min after termination of ion

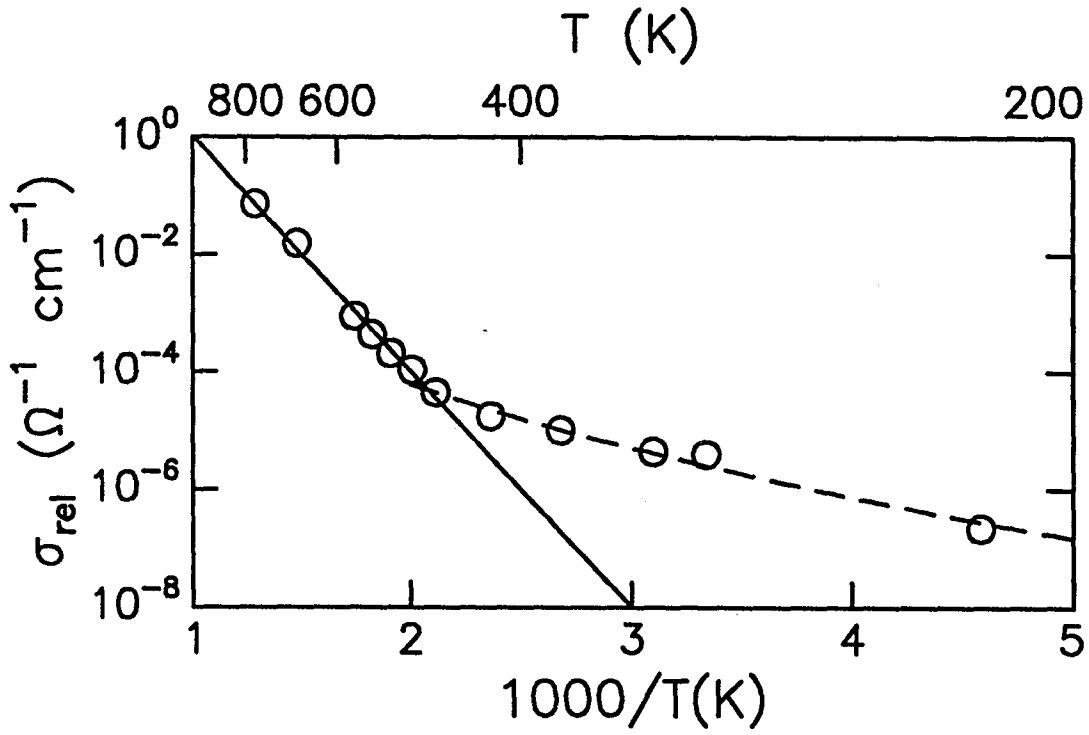


Figure 2.3: Temperature dependence of the electrical conductivity of a-Si relaxed by an 873 K anneal prior to measurement. The solid line is a fit to $\sigma \propto exp[-E/kT]$, and the dashed line is a fit to $\sigma \propto exp[-(A/kT)^{1/4}]$. The fits yield $E = 0.8$ eV, and $A = 110$ K$^{1/4}$.

irradiation at room temperature. For samples annealed at less than 473 K, Al contacts were applied prior to irradiation and post-irradiation annealing. For samples annealed at higher temperatures, contact evaporation was the last step prior to the measurement of the conductivity. Figure 2.4 illustrates the measured room temperature conductivity. The solid curve is a guide to the eye. The values of conductivity of two samples that were re-irradiated to 1dpa are shown as solid circles. Contact evaporation again required a prebake at 473 K. As indicated by Fig. 2.4, post-anneal irradiation causes the conductivity to revert back to the value of the original sample annealed at 473 K, represented by the broken line.

### 2.4.3 *In Situ* Measurements of Conductivity

Prior to the *in situ* conductivity measurements, samples were first relaxed by annealing at 873 K for 15 min. Figure 2.5 shows *in situ* conductivity measurements made before, during and after irradiation at various irradiation temperatures. Throughout the measurements, samples were held at the irradiation temperature. The dose rate was $7 \times 10^{11}$ Kr ions $cm^{-2}$ $sec^{-1}$, and the irradiation time was 30 min. Thus the total dose is calculated to be approximately 3 dpa. The conductivity is normalized to the value prior

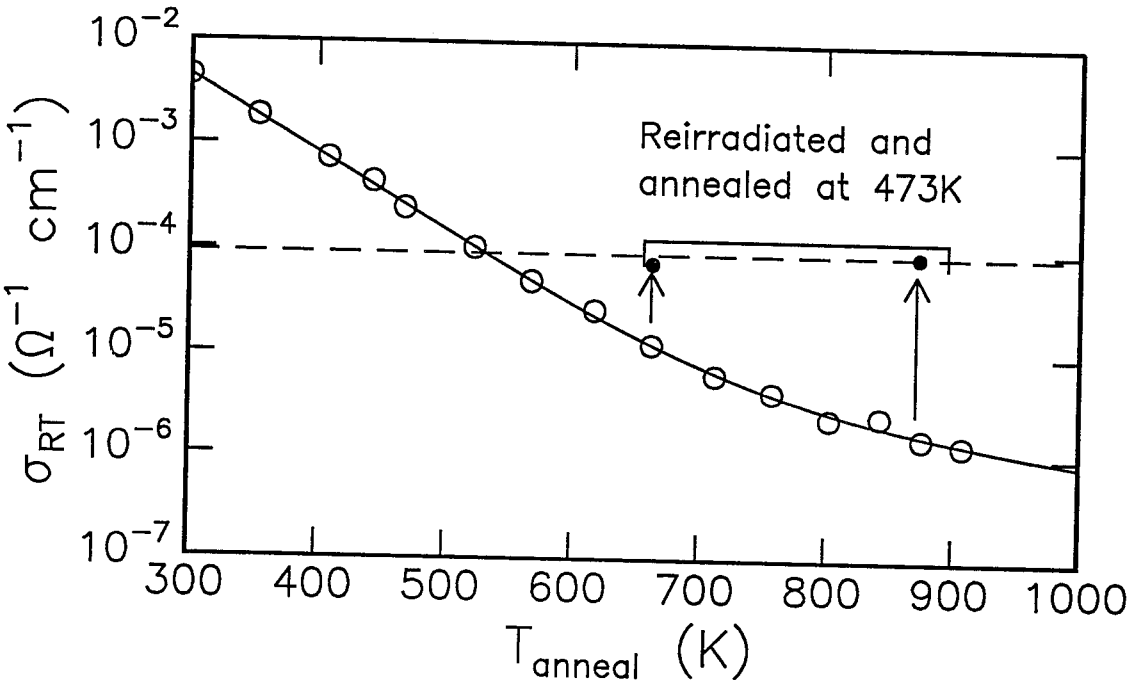


Figure 2.4: Room temperature conductivity of a-Si as a function of the anneal temperature. All samples were fully unrelaxed prior to anneals. The solid circles are values of the conductivity, after re-irradiation, of samples initially annealed at indicated temperatures. The solid line is a guide to the eye. The dashed line is the value of the conductivity of a-Si after initial relaxation by an anneal at 473K.

to irradiation. No data are given for the sample irradiated at 77 K because the conductivity was unmeasurably small prior to irradiation. However, the observed changes in the conductivity were similar to observed changes of the samples irradiated at higher temperatures. Note that the scale of the abscissa of Fig. 2.5 changes abruptly in order to show the extremely rapid and immediate increase in the conductivity upon the onset of irradiation. All curves show a rapid and immediate increase in the conductivity upon the onset of irradiation, and quick saturation to an apparent steady-state value. It is evident that lower implantation temperatures correspond to greater increases in the conductivity. The rapid conductivity decay in Fig. 2.5 marks the moment when ion irradiation was terminated. The conductivity decay transient after termination of irradiation is extremely rapid at first, but soon exhibits a slow decay, which continues even 45 min after the termination of irradiation.

For the sample irradiated at 773 K, however, the measured change in the conductivity is different, and is shown separately in Fig. 2.6. The conductivity rises rapidly with the onset of irradiation, and saturates to an apparent steady state value, as at other irradiation temperatures. But after $\sim$ 10 min, the conductivity starts to rise rapidly and linearly with time. Irradiation of

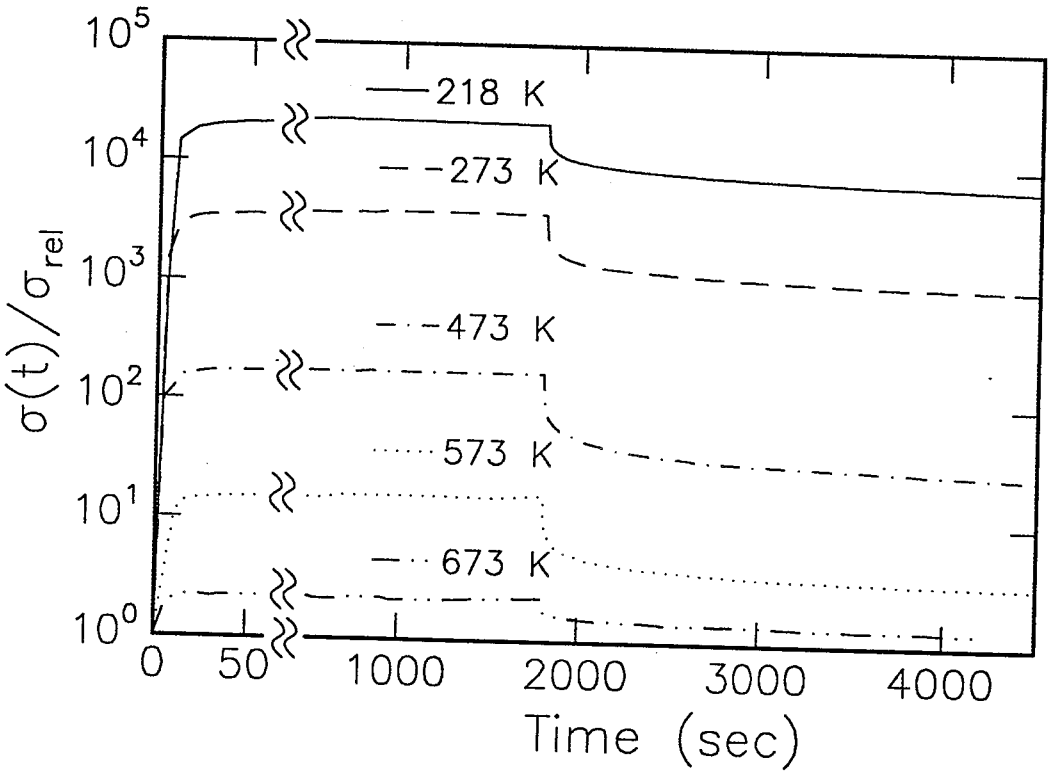


Figure 2.5: *In situ* measurement of the conductivity of initially relaxed a-Si during and after ion irradiation at indicated temperatures. The sharp drop in the conductivity marks the end of irradiation. The conductivities are normalized to the initial value at the irradiation temperature. Notice the change in the scale of the $x$ axis.

this sample was stopped earlier than other samples, but the total dose was still greater than 1dpa. The decrease in the conductivity following termination of irradiation is small, but measurable, and will be shown in more detail later in Fig. 2.7.

The most plausible explanation for the increase in conductivity during irradiation at 773 K after reaching an apparent steady-state value is the onset of crystal nucleation in a-Si. Since crystalline Si has much higher conductivity that a-Si, nucleation of crystalline silicon will irreversibly increase the sample conductivity. Ion irradiation is known to greatly enhance the rate of crystal nucleation in an a-Si matrix [20], and the irradiation parameters were such that the onset of crystal nucleation is anticipated. Indeed, the presence of crystal grains was later confirmed by x-ray diffraction. Furthermore, the observed change in the conductivity is consistent with crystallization exhibiting an incubation period followed by steady-state nucleation at a constant rate.

Part of the fluctuations in the conductivity both during and after irradiation, especially those observed for samples at high temperatures, is due to fluctuations in temperature, which could be maintained only to within $\pm$ 3 K for elevated temperatures. Part of the fluctuation in the conductivity during

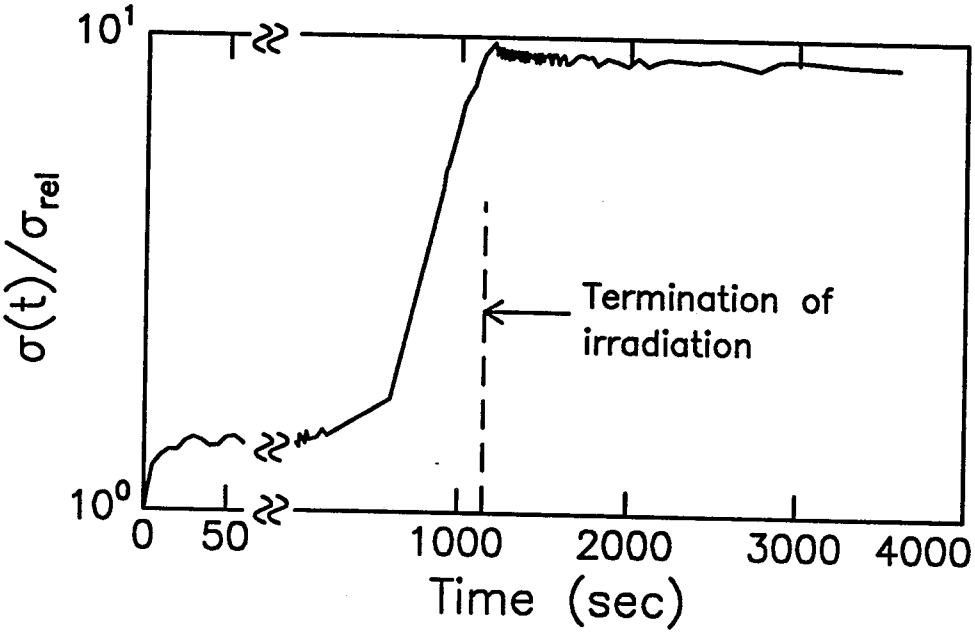


Figure 2.6: *In situ* measurement of the conductivity of initially relaxed a-Si during and after ion irradiation at 773 K. The scatter in data after termination of irradiation is due to fluctuations in temperature. The conductivity is normalized to the initial value at the irradiation temperature. Notice the change in the scale of the $x$ axis.

ion irradiation, however, was due to fluctuation in the ion flux. Indeed, it was observed that the conductivity increased when the ion flux increased. Finally, some samples were re-annealed at 873 K for 15 min following irradiation, and the room temperature conductivities of such samples were verified to revert to the pre-implanation value.

## 2.5 Activation Energy Spectrum

Both *in situ* and *ex situ* measurements suggest clearly that structural relaxation of a-Si is associated with a decrease in the conductivity. Eqs. (2.10) and (2.10) indicate that the change in the conductivity can arise either through change in $\alpha^{-1}$, the decay constant for electron wavefunction, or $g(E_f)$, the electronic density of states near the Fermi level. As Fig. 2.1 shows, however, structural relaxation of a-Si is associated with a decrease in $g(E_f)$. We will therefore make the assumption that $\alpha^{-1}$ remains relatively unchanged during structural relaxation, and that changes in electrical conductivity which accompany structural relaxation are due to changes in $g(E_f)$ alone. This seems reasonable since electronic energy of an electrically active defect and its activation energy for annihilation seem to be uncorrelated. Previous reports of the effect of ion irradiation on the conductivity of a-Ge and a-Si are

consistent with this interpretation [21].

Structural relaxation of a-Si, however, is associated with annihilation of point defects, whose activation energies form a continuous spectrum [1]. Since the localized electronic states near the Fermi level are presumed to have been created by defects, we define a function $E(Q)$, the density of defects with activation energy Q associated with the localized electron states near the Fermi level, such that

$$g(E_f) = \int E(Q)dQ. \tag{2.11}$$

Since we are assuming that these electrically active defects are representative of all defects (including those without any effect on $g(E_f)$), we further assume that $E(Q)$ is proportional to $N(Q)$, the overall density of defects in a-Si. In addition to $E(Q)$, we can also define $G(Q)$, the density of electrically active defect states. $G(Q)$ is analogous to $D(Q)$, the overall density of defect states. It is the saturation value of $E(Q)$, just as $D(Q)$ is the saturation value of $N(Q)$.

Information about the existence and qualitative features of the activation energy spectrum of electrically active defects can be obtained from the

*insitu* measurement of the electrical conductivity. It is important to note that as samples are being irradiated, they also undergo an unavoidable thermal anneal at the irradiation temperature $T_{ii}$. During irradiation, nearly all defects with activation energy $Q < kT_{ii}\ln(\nu t_i)$, where $t_i$ is the ion interarrival time, will recombine before the next ion arrives, while almost none of the defects with activation energy $Q > kT_{ii}\ln(\nu t_i)$ will recombine. These high activation energy defects will accumulate until they reach saturation density, $G(Q)$, and a steady-state defect concentration under irradiation will be established, as is observed from *in situ* measurements of the conductivity during ion irradiation. A quantitative analysis of conductivity measurements during irradiation is difficult, however, since no clear information exists about carriers generated by impinging ions.

Changes in the conductivity (after a short transient to ensure that both the excess carriers generated by irradiation and defects with low activation energies created just prior to termination of irradiation have all recombined) measured after termination of irradiation, however, will reflect the corresponding decrease in $g(E_f)$, the density of electronic states near the Fermi level. Since defects undergo thermal anneal during irradiation, a post-irradiation anneal is essentially a continuation of an anneal. Since $Q_\Theta$

of Eq. (1.8) depends logarithmically on total anneal time, $Q_\Theta$ will increase only slightly over the value $kT_{ii}\ln(\nu t_i)$ during the 45 min anneal following irradiation. Correspondingly, $g(E_f)$ will decrease only slightly, such that $\Delta g/g$ is small at all times.

In such cases, we can isolate changes in $g(E_f)$. Letting $g'(E_f) = g(E_f) - \Delta g(E_f)$, we can combine Eqs. (2.8) and (2.10) to obtain

$$\frac{\sigma'}{\sigma} = \frac{\sigma(g')}{\sigma(g)} = \frac{\sigma_o^h(g')}{\sigma_o^h(g)} \exp\left\{-2.1\left(\frac{\alpha^3}{gkT}\right)^{1/4}\left[\left(\frac{g}{g'}\right)^{1/4} - 1\right]\right\}. \tag{2.12}$$

Expanding $(g/g')^{1/4}$, and neglecting higher order terms,

$$\frac{\sigma'}{\sigma} = \frac{\sigma(g')}{\sigma(g)} = \frac{\sigma_o^h(g')}{\sigma_o^h(g)} \exp\left[-\frac{2.1}{4}\left(\frac{\alpha^3}{gkT}\right)^{1/4}\frac{\Delta g}{g}\right]. \tag{2.13}$$

If the prefactor $\sigma_o^h$ is some weak function of $g(E_f$ as in Eq. (2.10), then we can neglect it in comparison with the exponential when taking the logarithm of both sides. In such cases, we have

$$\ln(\frac{\sigma'}{\sigma}) = -\frac{2.1}{4}\left(\frac{\alpha^3}{gkT}\right)^{1/4}\frac{\Delta g}{g}. \tag{2.14}$$

Therefore, in the cases where the hopping conduction mechanism dominates, the logarithm of the normalized conductivity will be proportional to the

changes in $g(E_f)$, the density of electronic states near the Fermi level. Now the assumptions made in deriving Eq. (1.9), which predicted a $\ln(t)$ behavior, hold. If there exists a $G(Q)$, and if it is broad and slowly varying, then we expect the logarithm of the normalized conductivity to decrease as $\ln(t)$ after termination of irradiation. Note that this conclusion does not depend on the exact form of $A$ in Eq. (2.10).

Figure 2.7 illustrates the measured decay of the conductivity starting 5 sec after termination of irradiation, plotted against $\ln(t)$. For low temperatures where we expect hopping conduction to be the dominant conduction mechanism, $\ln(\sigma'/\sigma)$ is plotted; for high temperatures where we expect the extended state conduction to be dominant, $(\sigma'/\sigma)$ is plotted instead. Hopping conduction was assumed to be the dominant carrier transport mechanism for the sample irradiated at 573 K because previous reports suggested that unrelaxation tends to increase the temperature at which the transition from hopping conduction to extended state conduction occurs [3]. Indeed, the conductivity decrease after termination of irradiation at 573 K more closely resembles the one at 473 K than the one at 673 K. Thus it is deemed appropriate to assume hopping conduction at 573 K. Most curves display excellent linearity, and the rates of decay for the low-temperature relaxation ($\leq$ 573

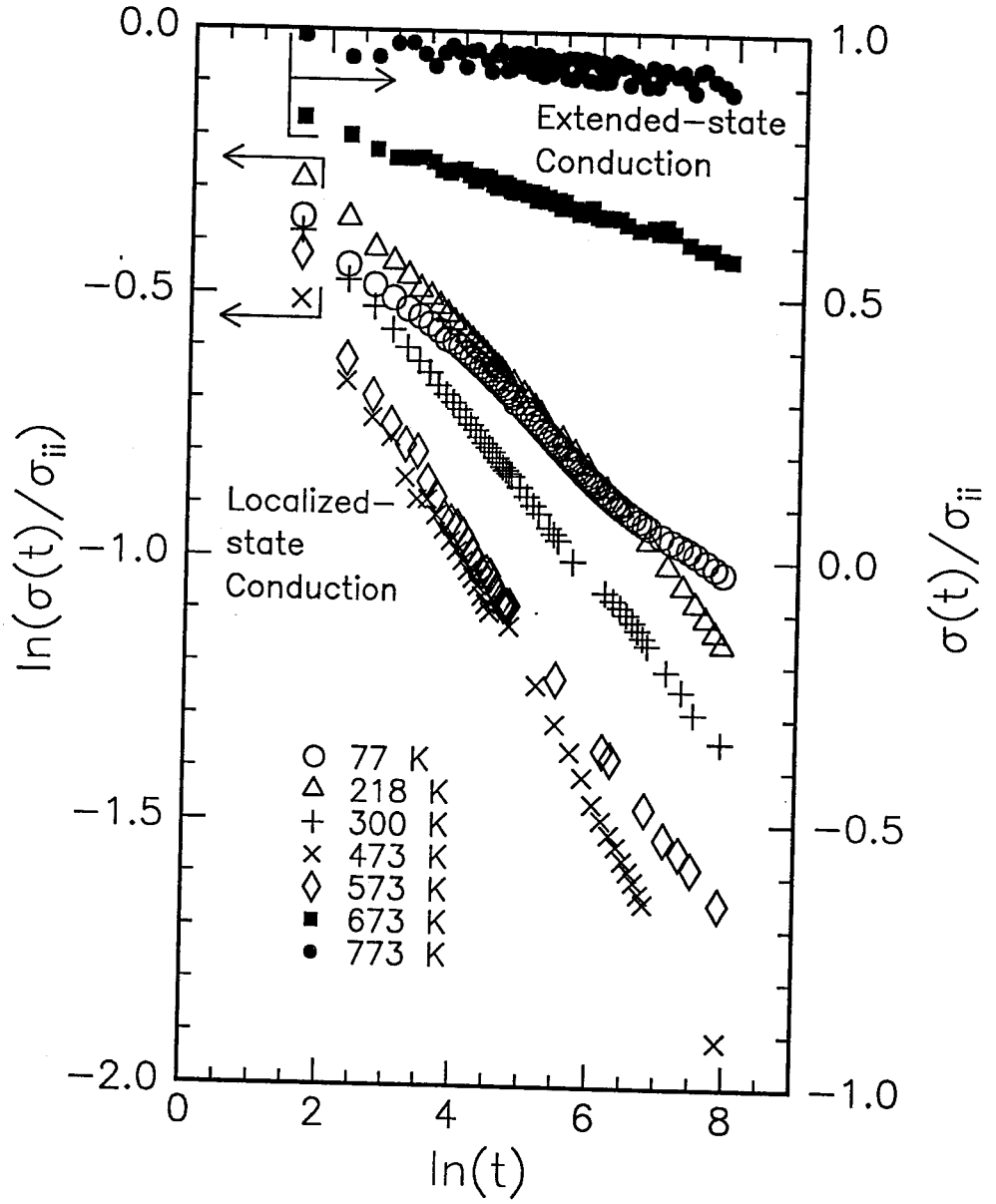


Figure 2.7: Conductivity transients for *in situ* measurements, plotted against $\ln(t)$. The left vertical axis is the logarithm of the conductivity normalized to the value of conductivity during irradiation. The right vertical axis is the value of the conductivity normalized to the value during irradiation.

K) are all similar. The two measurements made at below room temperatures deviate somewhat from the linear behavior, but the behavior can still be approximated by a straight line.

The observed $\ln(t)$ decay of the conductivity indicates clearly that the density of electronic states near the Fermi level $g(E_f)$ decreases as $\ln(t)$. This $\ln(t)$ decay and the similar rates of decay for different anneal temperatures indicate clearly that there indeed exists a $G(Q)$, the density of defect states with activation energy Q, associated with the localized electronic states near the Fermi level. Furthermore, the $\ln(t)$ behavior also indicates that $G(Q)$ is a slowly varying function that is nearly constant on a scale of a few tenths of an electron volt, the energy range spanned by the post irradiation anneal. The fact that the two samples irradiated and annealed at below room temperature deviate somewhat from the linear decay might be an indication of some features in the activation energy spectrum at low activation energies. However, the fact that they can be approximated by a straight line means that $G(Q)$, and also presumably $D(Q)$, the total density of defect states with activation energy $Q$, have non-zero values in the low $Q$ range, in this case below 0.23 eV. The high temperature ($\geq$ 573 K) data suggest that $G(Q)$ probably extends into high activation energy ranges as

well, although in such cases Eq. (2.14) is clearly invalid, since conduction at these high temperatures is dominated by the extended state conduction. It is possible that the onset of crystal nucleation has rendered the sample irradiated at 773 K a composite of amorphous and crystalline silicon whose conductivity is not amenable to a simple interpretation. Nonetheless, the fact that the conductivity does decrease during the post irradiation anneal is evidence that some post-irradiation structural relaxation occurs in a-Si even when irradiated at high temperatures, and that $G(Q)$ probably extends into high activation energy ranges.

A more quantitative insight into $G(Q)$ is possible from changes in the room temperature conductivity of a-Si that was initially fully unrelaxed by room temperature irradiation to doses greater than 1 dpa, then partially unrelaxed by 15 min isochronal anneals at different temperatures. We rewrite Eq. (2.11) as follows:

$$g(E_f) = g_o + \int_{Q_\Theta(T)}^{Q_\Theta^\circ} G(Q)dQ, \tag{2.15}$$

where $g_o$ is the electronic density of states at the Fermi level after 873 K anneal. The upper limit of integration is the value of $Q_\Theta$ after 873 K anneal,

and the lower limit is $Q_{\ominus}(T)$ after anneal for 15 min at temperature $T$. Note that we are integrating over the density of defect states, $G(Q)$, rather than the density of defects, $E(Q)$. This is because the samples were fully unrelaxed prior to 15 min anneals. Now we rewrite Eq. (2.12) as follows:

$$\frac{\sigma'}{\sigma} = \frac{\sigma_o^h(g')}{\sigma_o^h(g)} \exp\left\{-2.1\left(\frac{\alpha^3}{g_o kT}\right)^{1/4}\left[\left(\frac{g_o}{g_o + \int_{Q_{\ominus}(T)}^{Q_{\ominus}^o} G(Q)dQ}\right)^{1/4} - 1\right]\right\}. \tag{2.16}$$

From Fig. 2.3, we know the value of the factor $2.1(\alpha^3/g_o kT)^{1/4}$ to be 26.43 at room temperature. If we assume a reasonable value for $\alpha^{-1}$, we can calculate the value for $g_o$. Assuming $\alpha^{-1}$ to be $\approx$ 10 Å, we find that $g_o \approx 1.45 \times 10^{18}$ $\mathrm{eV}^{-1}$ $\mathrm{cm}^{-3}$. Taking the logarithm of both sides of Eq. (2.12), and again neglecting the prefactor in comparison to the exponent, we can isolate $G(Q)$:

$$\begin{aligned} G(Q') &= -\frac{d}{dQ'}\int_{Q_{\ominus}(T)}^{Q_{\ominus}^o} G(Q)dQ \\ &= -g_o\frac{d}{dQ}\left[1 - 0.038\ln\left(\frac{\sigma'}{\sigma_o}\right)\right]^{-4}. \end{aligned} \tag{2.17}$$

If a functional form of $A$ that is different from Eq. (2.10) is used, a slightly different form of Eq. (2.17) will result. However, the main conclusion of the analysis, again, is not affected.

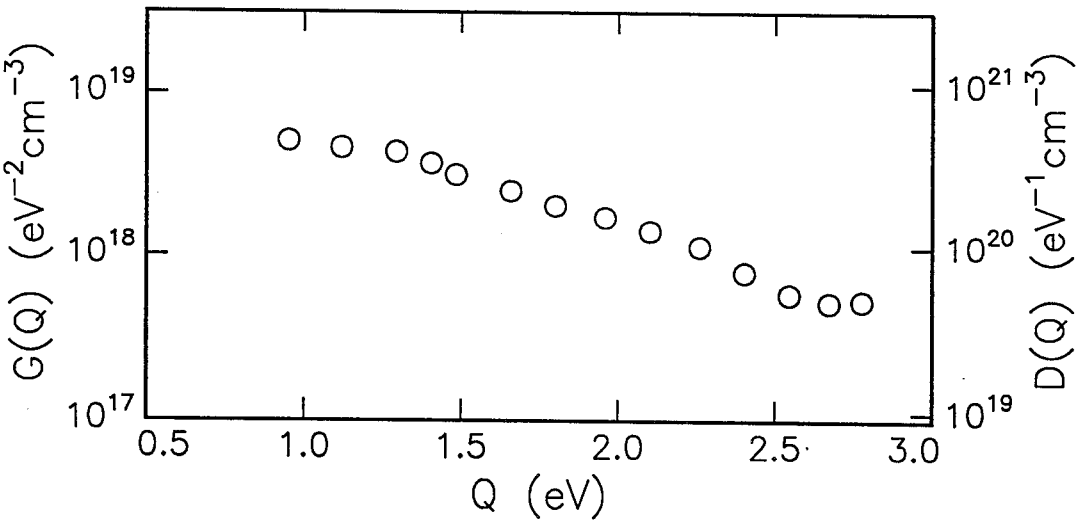


Figure 2.8: The density of the defect states of amorphous silicon. The left axis gives the density of electrically active defect states $G(Q)$ as derived from Fig. 2.4. The right axis gives the total density of defect states $D(Q)$, inferred from $G(Q)$.

In order to perform this differentiation, it is necessary to convert the abscissa of Fig. 2.4 from the anneal temperature to the activation energy $Q$. This requires an estimate of the reaction constant $\nu$. We assume $\nu$ to be of the order of the Debye frequency, or $10^{13}$ $\sec^{-1}$ for silicon. Similar values have been used previously for recombination of ion induced defects in a-Si [1, 27]. The result of the differentiation, using $10^{13}$ $\sec^{-1}$ for $\nu$, is illustrated in Fig. 2.8. *This is the central result of this chapter, an experimentally-measured density of defect states of amorphous silicon.* The left vertical axis shows $G(Q)$, the density of electrically active defects. The right vertical axis shows $D(Q)$, the overall density of defect states in a-Si. It is estimated by comparing the saturation value of $g(E_f)$, the density of electronic states near the Fermi level, with the estimated saturation density of defects in a-Si, which is found to be $\approx 1$ at. % [1, 22]. Assuming that one defect creates one electronic state, we find $D(Q) \approx 90$ eV $\times G(Q)$.

As expected, $G(Q)$ is broad, and extends from 0.9 eV to greater than 2.7 eV. It also seems to extend to lower values of the activation energy $Q$, corroborating the results of *in situ* measurements made below room temperature. It must be pointed out, however, that the activation energy range probed by the below-room-temperature irradiation and anneal lies outside

the region covered by the deduced activation energy spectrum in Fig. 2.8, and thus no quantitative conclusion can be drawn about the features of the density of defect states at low ($\leq$ 0.9 eV) activation energies. The density of defect states decreases slowly and monotonically with increasing activation energy, with no sharp features, thus justifying the approximation that we employed in deriving it. The lack of any discernible features in the density of relaxation states does not contradict the *in situ* low temperature measurements (which indicated the possibility of some features) since the range of activation energies covered in Fig. 2.8 does not extend to such low values.

## 2.6 Discussion

Care must be taken in interpreting Fig. 2.8, since rigorous conversion of the annealing temperature to the activation energy requires knowledge of the reaction constant $\nu$. But because $Q_\Theta$ depends only logarithmically on $\nu$, the conversion is fairly insensitive to errors in estimation. Indeed, $\Delta\nu$ would have to be much greater than one order of magnitude for there to be a significant shift in the activation energy scale. Even with such uncertainty in the absolute conversion of annealing temperature to activation energy, it is evident that the vast majority of defects in a-Si have low activation energies, and

that $D(Q)$ reaches small values at high ($Q \geq 2.5$ eV) activation energies. Such a preponderance of defects with low activation energies is consistent with previous experimental results. For instance, using Raman spectroscopy, de Wit *et al.*. [23] have shown that the rate of increase in the degree of structural relaxation decreases with increasing anneal temperature; and Roorda *et al.*, [1] have shown using differential isothermal calorimetry (DIC) that more stored enthalpy was released during annihilation of low activation energy defects than during annihilation of high activation energy defects. The relative dearth of relaxation processes with activation energies greater than 2.5 eV is tantalizing, since 2.7 eV is the activation energy of the rate of the solid phase epitaxy (SPE) of crystalline silicon into a-Si. Unlike other processes involving a-Si, the rate of SPE has been shown to be conspicuously independent of the degree of structural relaxation [24], and is characterized by a single activation energy ($Q = 2.7$ eV) over nearly ten orders of magnitude in the SPE rate [25]. The observed dearth of relaxation processes with activation energies greater than 2.5 eV is consistent with the notion that structural relaxation and solid phase epitaxy are controlled by different processes. Structural relaxation is by nature a bulk phenomenon, whereas there is strong evidence that solid phase epitaxy is limited by interface re-

arrangement kinetics [24, 26, 27]. Furthermore, the likeliest candidate for the controlling event in solid phase epitaxy is dangling bond rearrangement [24, 28], while recent reports suggest that structural relaxation is associated with the annihilation of vacancy-like defects in a-Si [29, 30].

One other remarkable consequence of this analysis, as evidenced by the presence of defects with high activation energies and the *in situ* measurements of relaxation at high irradiation temperatures, is the ability of irradiation to maintain an excess concentration of structural defects in a-Si during irradiation even when the irradiation temperature is high (573 - 773K). In other words, irradiation creates a substantial number of defects with relatively high activation energies and long lifetimes to measurably increase the steady-state defect concentration during irradiation at 773 K relative to the defect concentration following a 773 K anneal. This increased defect concentration has been demonstrated to substantially increase the defect enthalpy and thus the overall free energy of a-Si. In later chapters, we will discuss in more detail the implication of such an increase in the free energy for the possible mechanism responsible for the observed enhancement of nucleation of crystal silicon in an amorphous silicon matrix under irradiation at elevated temperatures.

Recently, Coffa *et al.*, using identical methods, have also measured the

density of defect states $D(Q)$, of a-Si [31]. Unlike the work presented in this chapter, they probed $D(Q)$ at low ($\leq 0.5$ eV) activation energies as well. The values of $D(Q)$ measured by Coffa *et al.* within the activation energy range covered in this thesis ($0.9$ eV $\leq Q \leq 2.8$ eV) differ from the values measured in this thesis, since he takes the decay length of electron wavefunction $\alpha^{-1}$ to be 3 Å. When corrected for this different value of $\alpha$, his values of $D(Q)$ and the values of $D(Q)$ derived in this thesis agree reasonably well, within $\pm \sim 3{\times}10^{19}$ eV$^{-1}$ cm$^{-3}$. A pronounced disagreement occurs near 1.5 eV, however, where they observe a pronounced dip in the density of defect states near 1.5 eV, something not observed in Fig. 2.8. However, the least square fit to his values of $D(Q)$ within the activation energy range covered in this thesis agrees very well with the least square fit to the values of $D(Q)$ measured in this thesis.

Such a dip in the density of defect states may be an artifact of the experimental procedure. It is interesting to note that the supposed dip in the density of defect states measured by Coffa *et al.* occurs right after the activation energy corresponding to a room temperature anneal. Since structural relaxation takes place indefinitely (albeit as $\ln(t)$), a prolonged storage at room temperature will sufficiently relax the samples that temperatures much

greater than room temperature are needed to further relax the material. In such cases, the electrical conductivity will change only a little with an intial increase in anneal temperature beyond room temperature, and the density of defect states will indeed display a dip after the activation energy corresponding to a room temperature anneal. On the other hand, the possibility that the fine details of the density of defect states of a-Si are dependent on the mode of production cannot be completely discounted. Coffa *et al.* have produced their a-Si film by low temperature chemical vapor depostion, unlike the a-Si films used in this chapter, which were produced by ultrahigh vacuum electron-beam deposition.

## 2.7 Conclusion

Through measurement of irradiation-induced conductivity changes, we have probed $G(Q)$, the density of relaxation states with localized electron states near the Fermi level, and thus $D(Q)$, the total density of relaxation states in a-Si. It is a function that decreases slowly with activation energy $Q$, ranging from below 0.9 eV (and probably below 0.23 eV) to beyond 2.6 eV. The dearth of defect states with activation energies greater than the activation energy for solid phase epitaxy is consistent with the notion that structural relaxation

and solid phase epitaxy are controlled by different processes, and may explain the observed independence of the rate of solid phase epitaxy on the extent of structural relaxation. *In situ* measurements of the conductivity show that $D(Q)$ decreases linearly with $\ln(t)$ following irradiation, consistent with the predictions of an activation energy spectrum model and further supports the conclusion that $D(Q)$ varies slowly over the energy range investigated. High temperature irradiation shows that even at elevated irradiation temperatures ($573K \leq T \leq 773K$) ion irradiation unrelaxes a-Si. Furthermore, under ion irradiation, the steady-state defect concentration (and thus the free energy of a-Si) is maintained at a level higher than that following an anneal at the irradiation temperature.

# Bibliography

[1] S. Roorda, W. C. Sinke, J. M. Poate, D. C. Jacobson, S. Dierker, B. S. Dennis, D. J. Eaglesham, F. Spaepen, and P. Fuoss, Phys. Rev. B **44** 3702 (1991).

[2] J. M. Poate, S. Coffa, D. C. Jacobson, A. Polman, J. A. Roth, G. L. Olson, S. Roorda, W. Sinke, J. S. Custer, M. O. Thompson, F. Spaepen, and E. Donovan, Nucl. Inst. Methods B **55** 533 (1991).

[3] W. Beyer and J. Stuke, in *Amorphous and Liquid Semiconductors*, Proceedings of the Fifth International Conference on Amorphous and Liquid Semiconductors, edited by J. Stuke and W. Brenig (Taylor & Francis, London, 1974) p. 251.

[4] J H. Shin, J. S. Im, and H. A. Atwater, in *Phase Formation and Modification by Beam-Solid Interactions,* edited by G. S. Was, D. M. Follstaedt, and L. E. Rehn, Mat. Res. Soc. Symp. Proc. **235**, 21 (1992).

[5] S. Coffa and J. M. Poate, Appl. Phys. Lett. **59**, 2296 (1991).

[6] M. H. Brodsky, in *Amorphous Semiconductors*, edited by M. H. Brodsky, 2nd. ed. (Springer-Verlag, New York, 1985) p. 3.

[7] N. F. Mott and E. A. Davis, *Electronic Processes in Non-Crystalline Materials,* (Clarendon, Oxford, 1971) p. 42.

[8] M. Pollak, M. L. Knotek, H. Kurtzman, and H. Glick, Phys. Rev. Lett. **30**, 856 (1973).

[9] M. L. Knotek, M. Pollak, and T. M. Donovan, Phys. Rev. Lett. **30**, 853 (1973).

[10] P. Nagels, in *Amorphous Semiconductors* (Ref. [6]) p. 113.

[11] Ph. D. thesis, FOM Instituut voor Atoom- en Mulecuulfysica, The Netherlands (1993), with help from A. J. M. Berntsen, G. Krötz and G. Müller.

[12] A.C. Boccara, D. Fournier, W. Jackson, and N. M. Amer, Optics Letters, **5**, 377 (1980).

[13] J. C. Bean and J. M. Poate, Appl. Phys. Lett. **36** 59 (1980).

[14] J. R. Reid, E. Kolawa, T. A. Stephens, J. S Chen, and M-A. Nicolet, in *Advanced Metallization for ULSI Applications,* edited by V. V. S. Rana, R. V. Joshi, and I. Ohdomari (Materials Research Society, Pittsburgh, 1992) pp. 285-291.

[15] J. F. Ziegler, J. P. Biersack, and U. Littmark, *The Stopping and Range of Ions in Solids* (Pergammon, New York, 1985).

[16] J. P. Biersack and L. J. Haggmark, Nucl. Instrum. Methods **174**, 257 (1980).

[17] Copyright J. F. Ziegler, 1990.

[18] J. J. Hauser, Phys. Rev. B **8** 3817 (1973).

[19] M. L. Knotek and T. M. Donovan, Phys. Rev. Lett. **30** 652 (1972).

[20] J. S. Im and Harry A. Atwater, Appl. Phys. Lett. **57**, 1766 (1990).

[21] N. Apsley, E. A. Davis, A. P. Troup, and A. D. Yoffe, in *Amorphous and Liquid Semiconductors:* Proceedings of the Seventh International Conference on Amorphous and Liquid semiconductors, edited by W. E. Spear (Centre for Industrial Consultancy & Liaison, University of Edinburgh, Edinburgh, 1977) p. 447.

[22] S. Coffa, J. M. Poate, D. C. Jacobson, W. Frank, and W. Gustin, Phys. Rev. B **45**, 15 8355 (1992)

[23] L. de Wit, S. Roorda, W. C. Sinke, F. W. Saris, A. J. M. Berntsen, and W. F. van der Weg, in *Kinetics of Phase Transformations*, edited by M. M. Thompson, M. J. Aziz, and G. B. Stepheson, Mat. Res. Soc. Symp. Proc. **205**, 3 (1991).

[24] G. Q. Lu, Eric Nygren, and M. Aziz, J. Appl. Phys. **70**, 5323 (1991).

[25] G. L. Olson and J. A. Roth, Mater. Sci. Reports, **3** 1 (1988).

[26] J. S. Custer, A. Battaglia, M. Saggio, and F. Priolo, Phys. Rev. Lett. **69** 780 (1992).

[27] K. A. Jackson, J. Mater. Res. **3**, 1218 (1988).

[28] J. A. Roth, G. L. Olson, D.C. Jacobson, and J. M. Poate, Appl. Phys. Lett. **57** 1340 (1990).

[29] S. Roorda, R. A. Hakvoort, A. van Veen, P. A. Stolk, and F. W. Saris, in *Phase Formation and Modification by Beam-Solid Interactions,* edited by G. S. Was, D. M. Follstaedt, and L. E. Rehn, Mat. Res. Soc. Symp. Proc. **235**, 39 (1992).

[30] G. N Vandehoven, A. N. Liang, L. Niesen, and J. S. Custer, Phys. Rev. Lett.. **68** 3714 (1992).

[31] S. Coffa, F. Priolo, and A. Battaglia, Phys. Rev. Lett. **70** 3756 (1993).

# Chapter 3

# Generalized Activation Energy Spectrum Theory

## 3.1 Introduction

Using the activation energy spectrum theory as formulated by Gibbs *et al.*, [1] we were able to quantitatively measure $D(Q)$, the density of defect states responsible for structural relaxation in a-Si. However, as mentioned often in Chapter 2, the simple theory relies on several approximations and implicit assumptions that render the theory inappropriate for an accurate, quantitative description of defect kinetics under many circumstances. One of these is the approximation of the annealing function $f(Q,T,t)$, by a step function. Since this approximation is valid for both first and second order defect recombination kinetics, we cannot distinguish between them using the simple theory.

Also, no mechanism is provided for unrelaxation, thus preventing the theory from being applicable to both creation and annihilation of defects. The ability to address both defect creation and annihilation, however, is essential for a quantitative description of defect kinetics under ion irradiation.

A more serious shortcoming of the simple theory is the *ad hoc* assumption that defects with different activation energies are independent of each other. Such an assumption might be justified in the case of unimolecular recombination of defects with fixed sink sites, especially if defects are isolated point defects. In the case of bimolecular recombination, it is unphysical to assume that defects in amorphous solids somehow do not interact with each other if their activation energies differ by an amount $dQ$.

It is therefore the aim of this chapter to develop a new, more physically reasonable theory, hereafter referred to as the generalized activation energy spectrum theory, which takes into account the possibility that defect dynamics may depend on other defects with different activation energies. To test and compare the generalized theory with the simple theory, models of defect creation and annihilation of a-Si based on the simple and on the generalized theory will be developed, and compared against experimental data.

## 3.2 Generalized Activation Energy Spectrum Theory

As written in Chapter 1, the kinetics of defect annihilation is described by the simple theory as

$$\frac{dN(Q)}{dt} = -\nu_o \exp\left(\frac{-Q}{kT}\right) N(Q)^n, \tag{3.1}$$

where $\nu_o$ is the reaction constant, and $n$ is the order of the reaction. In essence, we have a continuum of independent equations for all possible values of $Q$.

The main difference between the simple and the generalized theory is the interaction between defects with different activation energies. This can be achieved by rewriting Eq. (3.1) as

$$\frac{dN(Q)}{dt} = -\frac{\nu_o N(Q)}{2}\left[\exp\left(\frac{-Q}{kT}\right)\int \sigma_1(Q,Q')N(Q')dQ' + \int \exp\left(\frac{-Q'}{kT}\right)\sigma_2(Q,Q')N(Q')dQ'\right]. \tag{3.2}$$

The function $\sigma_1(Q,Q')$ and $\sigma_2(Q,Q')$ are generalized reaction cross sections appropriate to the relaxation dynamics considered. For bimolecular recombination kinetics, they represent reaction cross sections between defects with

activation energies $Q$ and $Q'$. The physical meaning of Eq. (3.2) becomes more clear if the terms are considered separately. The first term on the right,

$$\nu_o N(Q) \left[ \exp\left(\frac{-Q}{kT}\right) \int \sigma_1(Q,Q') N(Q') dQ' \right], \tag{3.3}$$

is the rate at which a defect with activation energy $Q$ annihilates other defects with activation energy $Q'$. The second term on the right,

$$\nu_o N(Q) \left[ \int \exp\left(\frac{-Q}{kT}\right) \sigma_1(Q,Q') N(Q') dQ' \right], \tag{3.4}$$

is the rate at which a defect with activation energy $Q$ is annihilated by other defects with activation energy $Q'$. The factor of $1/2$ is needed because we are counting each defect recombination event twice. Although Eq. (3.2) is cast in a form of bimolecular recombination kinetics, by choosing suitable forms for $\sigma_1(Q,Q')$ and $\sigma_2(Q,Q')$, we can transform Eq. (3.2) to represent other recombination kinetics. For example, if

$$\sigma_1(Q,Q') = \sigma_2(Q,Q') = \delta(Q,Q'), \tag{3.5}$$

we recover the simple theory. If we let

$$\sigma_1(Q,Q') = 2S_o\delta(Q')/N(Q'), \sigma_2(Q,Q') = 0, \tag{3.6}$$

we recover the unimolecular recombination kinetics, provided we have $S_o =$ density of fixed sinks. The generalized theory can also be employed to model defect recombination kinetics in phases other than the amorphous phase. For example, the defect dynamics of crystalline solids may be modelled by having the defect density $D(Q)$ consist of one or more sharp peaks. It is also possible that a form of $D(Q)$ intermediate between the crystalline and amorphous forms may be used to describe the defect dynamics of heavily damaged crystals.

## 3.3 Defect Dynamics of Amorphous Silicon: Modelling and Experiments

### 3.3.1 Modelling Defect Dynamics

In order to test the generalized theory, the defect dynamics of ion-irradiated a-Si is modelled, and the results are compared with experimental data and with the simple activation energy spectrum theory. To model the evolution of defect population in a-Si during ion irradiation and anneal, we make the following assumptions. First, we assume that an impinging ion creates

defects with different activation energies with equal probabilities. Second, we assume that annihilation occurs via bimolecular recombination, which is consistent with previous experimental observations [2, 3]. Finally, we assume that $\sigma_1(Q,Q') = \sigma_2(Q.Q') =$ constant; that is, defects with different activation energies recombine with equal cross section. We then write

$$\frac{dN(Q)}{dt} = g\dot{\phi}\left(1-\frac{N(Q)}{D(Q)}\right) - \frac{\nu_o N(Q)}{2}\left[\exp\left(\frac{-Q}{kT}\right)\int N(Q')dQ' + \int \exp\left(\frac{-Q'}{kT}\right)N(Q')dQ'\right] \tag{3.7}$$

where $g$ and $\dot{\phi}$ are defects/flux and ion flux, respectively. The first term on the right side of Eq. (3.7) is the defect generation term. It ensures that the defect population saturates at $D(Q)$. A similar form for generation of defects in a-Si by irradiation has been used successfully in the past [8]. If we use the simple theory [1], we can write

$$\frac{dN(Q)}{dt} = g\dot{\phi}\left(1-\frac{N(Q)}{D(Q)}\right) - \nu_o \exp\left(\frac{-Q}{kT}\right)N(Q)^2 \tag{3.8}$$

With Eq. (3.8) and (3.7), the time evolution of defects in a-Si during both irradiation and the subsequent anneal can be solved. In both cases, we have $g$ and $\nu_o$ as fitting parameters to be determined.

The assumption underlying the interaction of defects with different activation energies is that the defects are of similar kinds (presumably point defects), and differ only in their activation energies. The activation energies are unlikely to be that of self-diffusion, since the activation energy for self-diffusion in a-Si is between 0.13 and 0.22 eV [9]. Most likely, the activation energies are that of some rate-limiting step to defect migration, possibly that of the transition states necessary for the defects to become mobile.

For Eq. (3.8) for the simple theory, an analytical solution can be found. It is given by [4]

$$N(t,T,Q,\dot{\phi}) = \frac{\left[\Omega \tanh\left[\frac{\Omega t + 2D(Q)\tanh^{-1}(g\dot{\phi}/\Omega)}{2D(Q)}\right] - g\dot{\phi}\right]}{2\nu_o \exp(-Q/kT)D(Q)} \quad (3.9)$$

where

$$\Omega = \sqrt{\left(g\dot{\phi}\right)^2 + 4\nu_o \exp(-Q/kT)g\dot{\phi}D(Q)^2}. \quad (3.10)$$

For Eq. (3.7), however, no analytical solution could be found. Therefore, it was solved by computer simulation. To ensure an accurate comparison between the results of the two theories, Eq. (3.8) was also solved by computer simulation. The simulation of the defect dynamics during irradiation and

anneal consisted of calculating $dN/dt$ using either Eq. (3.7) or Eq. (3.8), and then altering $N(Q)$ such that $N(Q, t + \delta t) = N(Q, t) + \delta t(dN/dt)$. This step was repeated for the desired length of time. One implicit result of this simulation is the approximation of the defect generation as a steady stream. Under real conditions, defects are more likely to be generated as pulses corresponding to the collision cascades produced by impinging ions. For both theories, the range of activation energy $Q$ covered in the simulations was from 0.6 eV to 2.8 eV. A minimum value of 0.6 eV was chosen for two reasons. First, $D(Q)$, the density of relaxation states, from Chapter 2 extends only down to 0.9 eV. Therefore, we introduce more uncertainty as the lower limit is lowered, especially since $D(Q)$ increases exponentially with decreasing $Q$. Second, the time step required for accurate simulation becomes unpractically short as the lower limit is lowered. The value of 0.6 eV was a compromise between the practicability of simulation and the need to consider as much of $N(Q)$ as possible. For the simulation of irradiation, the value of $\delta t$ was $2 \times 10^{-5}$ sec. This value was chosen because it is much less than the expected lifetime of the defects with activation energy 0.6 eV, as evidenced by the fact that further decrease in $\delta t$ did not result in any changes in the final results. For simulations of defect dynamics during an anneal, the value

of $\delta t$ was adapted during calculation to be 1/10 of the lifetime of most mobile defects that were still present in significant numbers, defined to be $1 \times 10^{-30}$ $cm^{-3}$. At this concentration, the recombination rates of even the most mobile defects are negligible compared with others. Finally, the numerical solutions to Eq. (3.8) were compared with the analytical results, and found to agree very well, thus confirming the validity of the simulation.

By explicitly solving the equations for the defect dynamics, we remove the step function approximation of the annealing function. Therefore, the solutions of Eq. (3.8), whether numerical or analytical, are already a great improvement over the results derived using the existing simple theory. Henceforth, the simple theory without the step function approximation will be referred to as the modified simple theory. The three different theories discussed in this chapter, and the assumptions associated with them are summarized in table 3.1.

### 3.3.2 Experiments

In all experiments described in this chapter, same a-Si resistors as described in Chapter 2 were used. The anneal protocol was identical to that described in Chapter 2. All irradiation was performed at room temperature. However,

| Theories | Assumptions |
|---|---|
| Simple theory | Constant reaction cross section |
| | Bimolecular recombination |
| | Step function approximation |
| | No interaction between defects with different $Q$ |
| Modified simple theory | Constant reaction cross section |
| | Bimolecular recombination |
| | No interaction between defects with different $Q$ |
| Generalized theory | Constant reaction cross section |
| | Bimolecular recombination |

Table 3.1: Theories discussed in this paper, along with significant assumptions associated with them.

since accurate measurement of dose and dose rate was critical, no *in situ* measurements of the conductivity during irradiations were attempted. Instead, the conductivity was measured *in situ* immediately after irradiation. A schematic of the experimental setup for the *in situ* measurements is shown in Fig. 3.1.

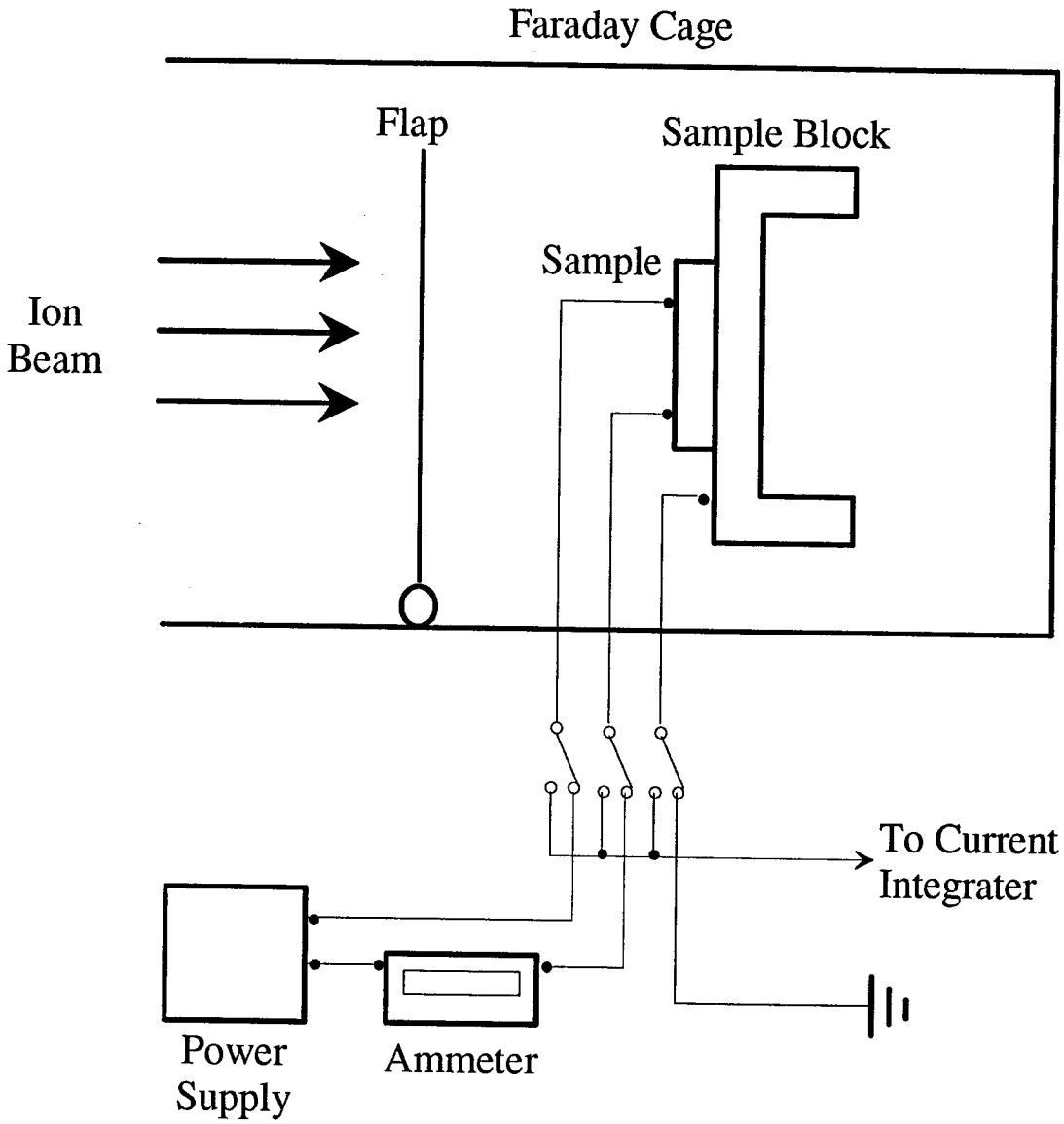


Figure 3.1: Schematic of the experimental setup used for the second sets of *in situ* conductivity measurements. Note that, ion current is measured directly from the sample.

## 3.4 Results and Discussion

In all experiments, the quantity actually measured was the electrical conductivity of a-Si. However, using values obtained in Chapter 2, we can obtain the total defect density. Therefore, we will hereafter discuss structural relaxation of a-Si in terms of an experimentally determined defect density without explicit reference to the measured conductivity.

### 3.4.1 Evolution of Defect Density vs. Irradiation Dose

Figure 3.2 shows the defect density of a-Si, measured 15 minutes after termination of irradiation, as a function of the dose. Prior to irradiation, samples were relaxed by a 15 min anneal at 900 K. The symbols are experimental data. The ions used were 600 KeV $Kr^{++}$, 350 KeV $Ar^{++}$, 250 KeV $Si^{+}$, and 190 KeV $Ne^{+}$. These energies were chosen to confine the damage distribution within the a-Si film. As expected, the evolution of defect density with irradiation dose depends strongly on the irradiating ion, with heavy ions being much more efficient in unrelaxing a-Si. However, the evolution of the defect density follows the same sigmoidal curve regardless of the ion species. Furthermore, the saturation level of the defect density is independent of irradiating ion.

Figure 3.3 shows the defect population vs. irradiating dose, but this time

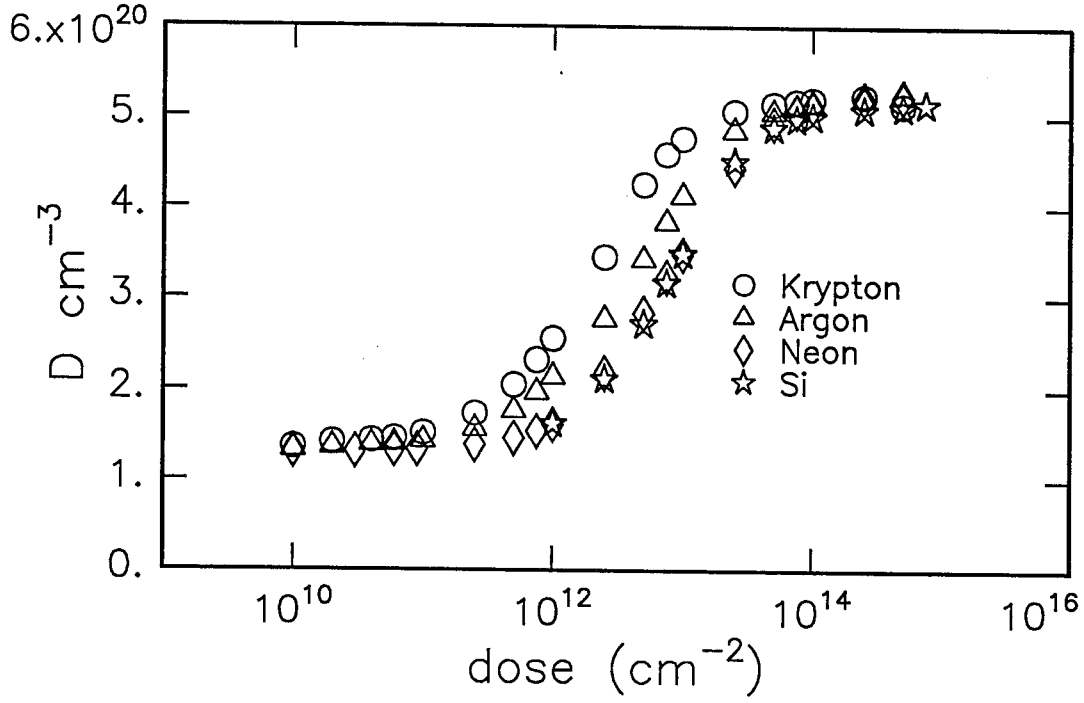


Figure 3.2: Experimentally measured defect population, plotted vs. irradiating dose. The ions used were 600 KeV $Kr^{++}$, 350 KeV $Ar^{++}$, 250 KeV $Si^{+}$, and 190 KeV $Ne^{+}$.

the dose is normalized to the displacement per atom (dpa) as calculated by the TRIM simulation program [5, 6, 7]. Again, the symbols are experimental data. The solid curve in Fig. 3.3 is the result of fitting the generalized theory, and the dashed curve is the result of fitting the modified simple theory. Both theories give an excellent fit to the data, and they are nearly indistinguishable from each other. The values of $g$ and $\nu_o$ used to fit the data are $4.1\text{x}10^{22}\,\text{cm}^{-3}\text{dpa}^{-1}$ and $1.7\text{x}10^{-10}\,\text{cm}^3\text{sec}^{-1}$ for the generalized activation energy theory, and $4.1\text{x}10^{22}\,\text{cm}^{-3}\text{dpa}^{-1}$ and $5.1\text{x}10^{-8}\,\text{cm}^3\text{sec}^{-1}$ for the modified simple theory. The same values of $g$ and $\nu_o$ are used in all of the following figures. *Since there are no more adjustable parameters, the results which follow are the results of calculation, not a fit to the data.* It needs to be remarked that the value of the reaction constant for the generalized activation energy theory depends on the lower limit of activation energy used. However, the conclusions that can be drawn from the analysis are not significantly affected, provided that the same values of $\nu_o$ and the lower limit of activation energy are used consistently.

It is clear that once scaled to dpa, the evolution of defect population shows a universal behavior. Therefore, we will discuss unrelaxation in terms of dpa without making specific reference to the irradiating ion. The defect

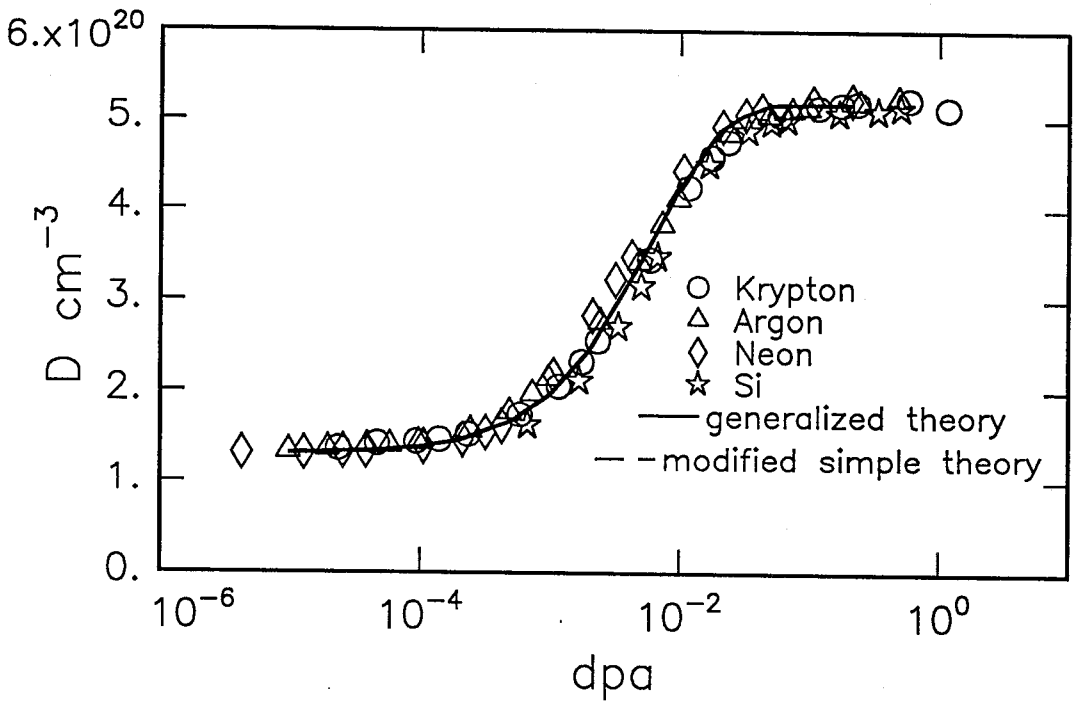


Figure 3.3: Experimentally measured defect population, plotted vs. dpa, as calculated from TRIM. Symbols are experimental data. The solid line is the result of fitting the results of calculations based on the generalized activation energy theory. The dashed line is the result of fitting the results of calculations based on the modified simple theory.

population starts to saturate near the dose of 0.02 dpa, in agreement with results obtained by others using different methods [2, 8]. However, the defect density continues to increase with increasing dose, albeit very slowly and slightly. One important implication of Fig. 3.3 is the irrelevance of cascade structure to structural unrelaxation. A 600 KeV $Kr^{++}$ ion is expected to create a dense, compact cascade, while a 190 KeV $Ne^{+}$ ion is expected to create widely scattered regions of high defect density. TRIM simulations of cascade created by an Ne ion and a Xe ion are shown in Figs. 3.4 and 3.5, respectively. The fact that it is possible to scale such disparate ion damages by such a simple quantity as dpa indicates that a heavy ion does not completely unrelax a-Si within its cascade. Rather, unrelaxation of a-Si seems to be controlled by point defects that have lifetimes that are much longer than that of a typical cascade, and thus diffuse out from cascade regions to the surrounding matrix. This is in contrast to ion damage in crystal silicon, in which a heavy ion such as Kr creates small regions that are very heavily defective or even amorphous.

With the values of $g$ and $\nu_o$ fixed, we can follow the time evolution of $N(Q)$, the defect population as a function of the activation energy, during irradiation. Figure 3.6 a) shows the results of calculations using the gener-

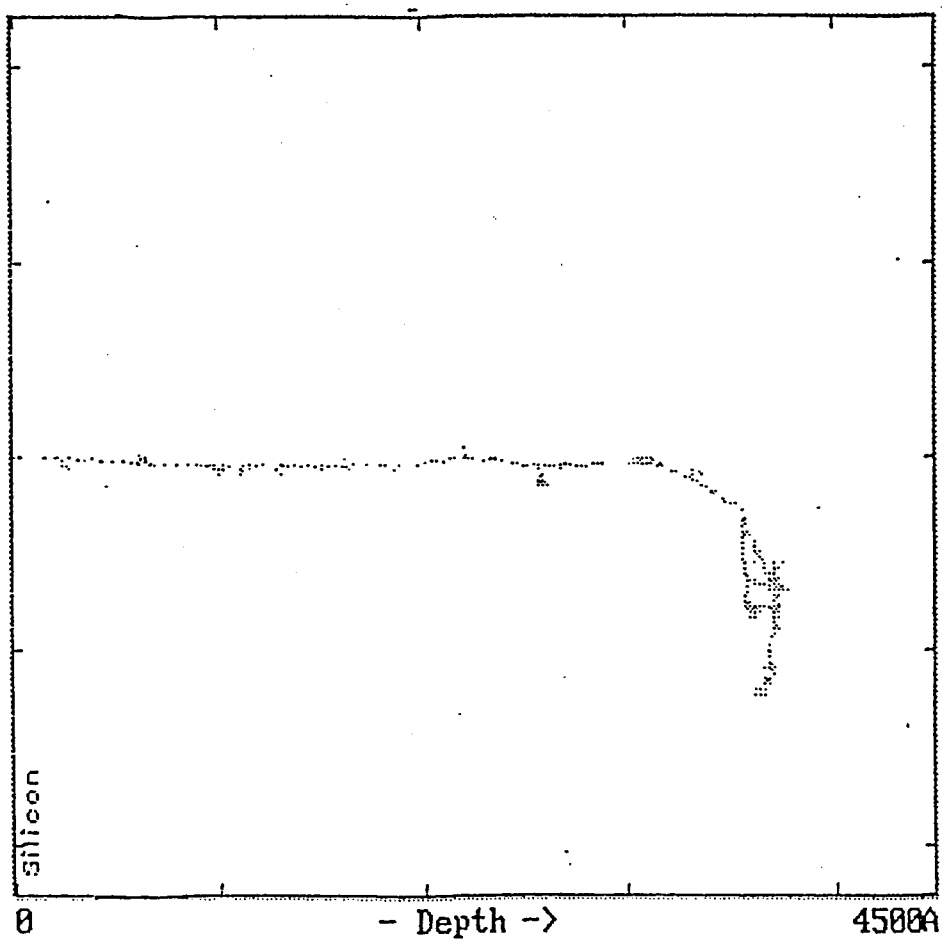


Figure 3.4: Cascade generated by a 190 KeV Ne ion.

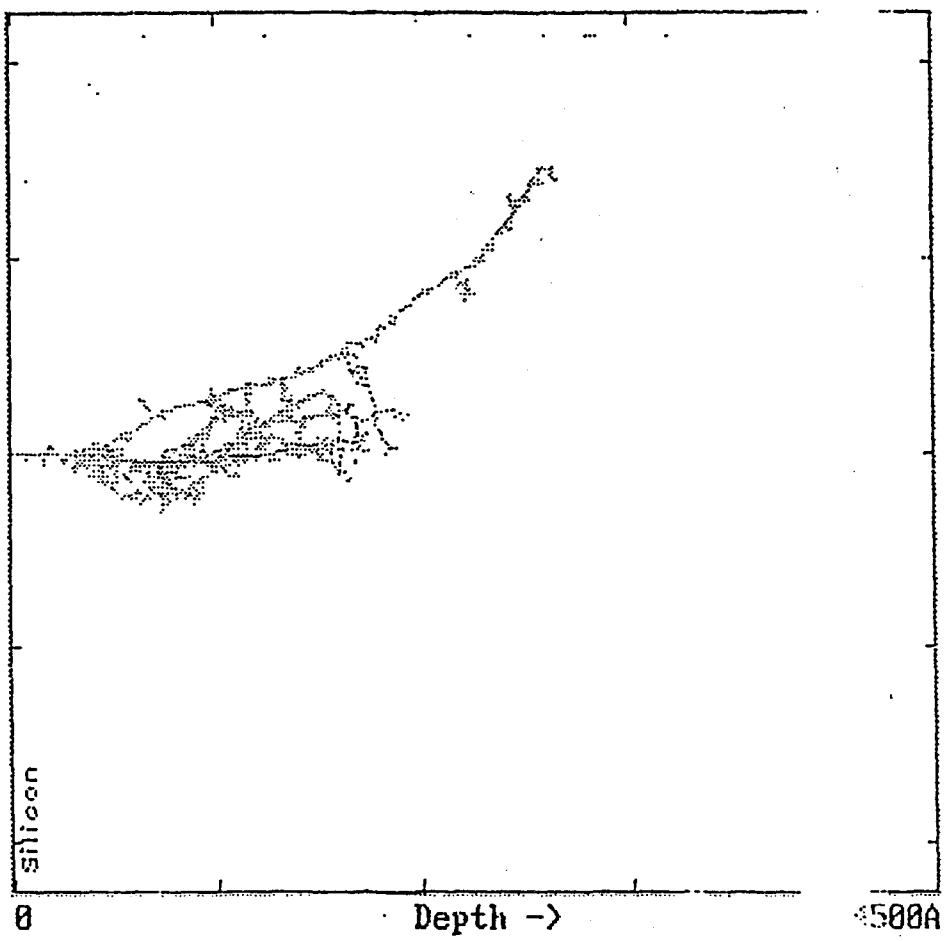


Figure 3.5: Cascade generated by a 600 KeV Xe ion.

alized activation energy theory, and Fig. 3.6 b) shows the results of calculations using the modified simple theory. The doses were 0.001, 0.002, 0.005, 0.01, 0.02, and 0.05 dpa. The symbols are $D(Q)$ as calculated in Chapter 2. The results are qualitatively very similar. However, Fig. 3.6 highlights a crucial difference between the two theories. As shown in Fig. 3.6 b), the modified simple theory predicts that the defect population increases monotonically with increasing dose for all activation energies. The generalized theory predicts a quite different and unexpected result that the population of low-activation energy defects will first increase with increasing dose, then actually *decrease* with further increases in the dose. Figure 3.7 shows this difference more clearly. This counterintuitive prediction is due to the ability of low activation energy defects to recombine with defects across the entire activation energy spectrum. As the total defect density increases, so does the recombination rate of low activation energy defects. After a critical dose, the recombination rates of low activation energy defects exceed the generation rate, which is assumed to be independent of the activation energy. The defect population of *low activation energy* defects then *decreases* with further increases in the dose, although the *total* defect population *increases.*

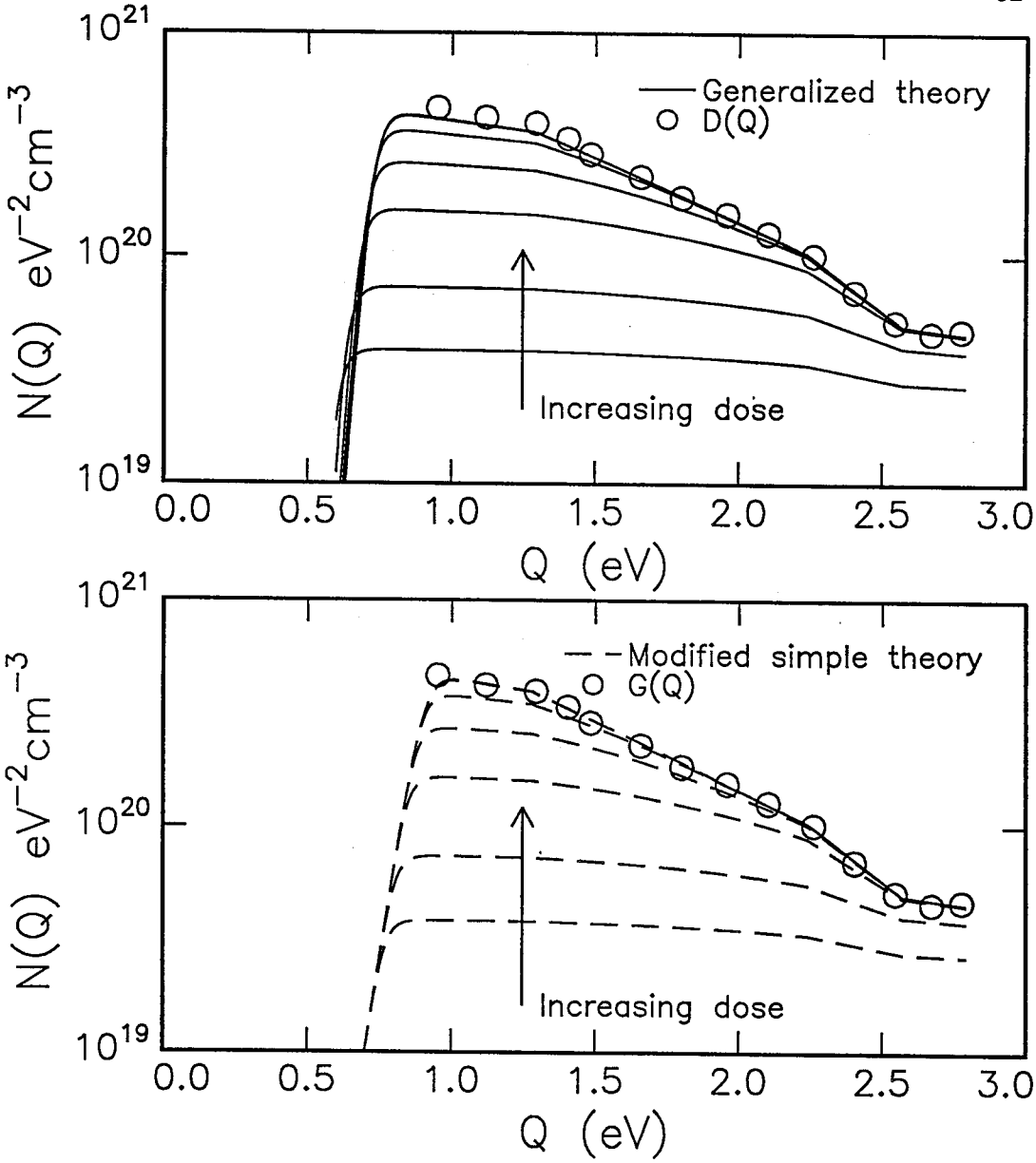


Figure 3.6: Time evolution of the defect population. Figure a) shows the results of generalized theory, and b) shows the results of the modified simple theory. The symbols are $D(Q)$ from Chapter 2. The doses are 0.001, 0.002, 0.005, 0.01, 0.02, and 0.05 dpa.

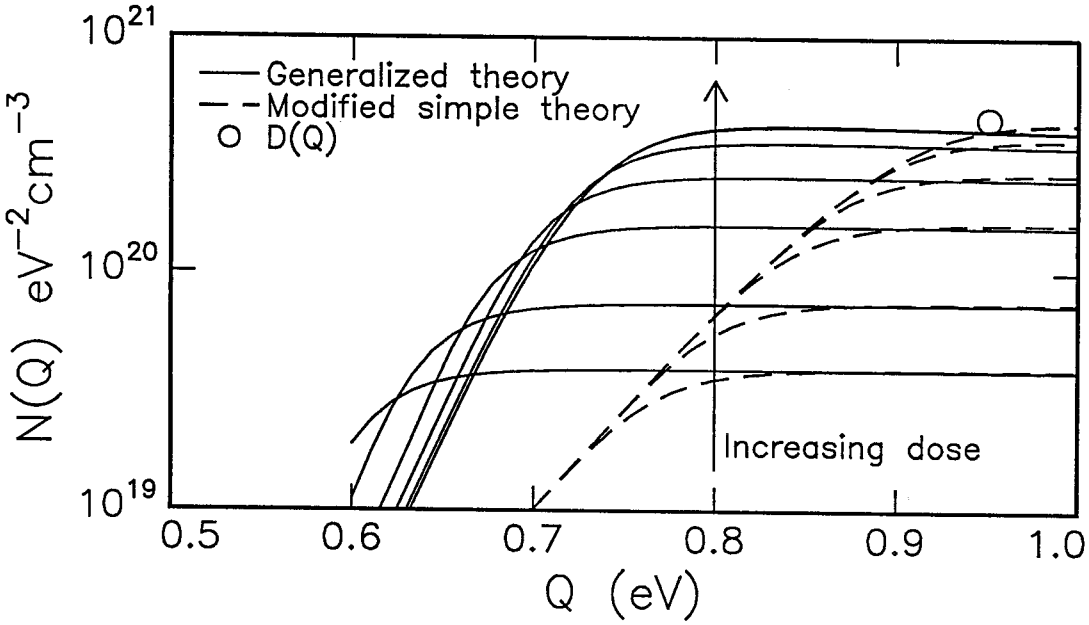


Figure 3.7: Time evolution of the low activation energy defect population. Solid curves are the results of the generalized theory, and dashed curves are the results of the modified simple theory. The doses are 0.001, 0.002, 0.005, 0.01, 0.02, and 0.05 dpa.

### 3.4.2 Evolution of Defect Density During Anneal

The ability of low activation energy defects to annihilate defects across the entire activation energy spectrum is much more readily apparent when the defect dynamics during an anneal are calculated, and the resulting change in the defect population compared. Figure 3.8 shows the $N(Q)$, the defect density as function of the activation energy $Q$, for a-Si irradiated to saturation and then annealed for 15 min at different temperatures. The symbol is $D(Q)$ from Chapter 2. The solid curves are the results of calculations using the generalized theory, and the dashed curves are the results of calculations using the modified simple theory. Also included are the results of the simple theory, with its step function approximation.

Within the modified simple theory, it is evident that there really does exist an activation energy $Q_\Theta$ such that most of the defects with $Q \lesssim Q_\Theta$ have recombined after an anneal at a temperature $T_{anl}$ for an anneal time $t_{anl}$, while most of the defects with $Q \gtrsim Q_\Theta$ have not. However, Fig. 3.8 shows clearly that the step function approximation of $f(Q,T,t)$ made in the simple theory is inaccurate, especially for high temperature anneals. Therefore, the simple theory will not be discussed further. Within the generalized theory,

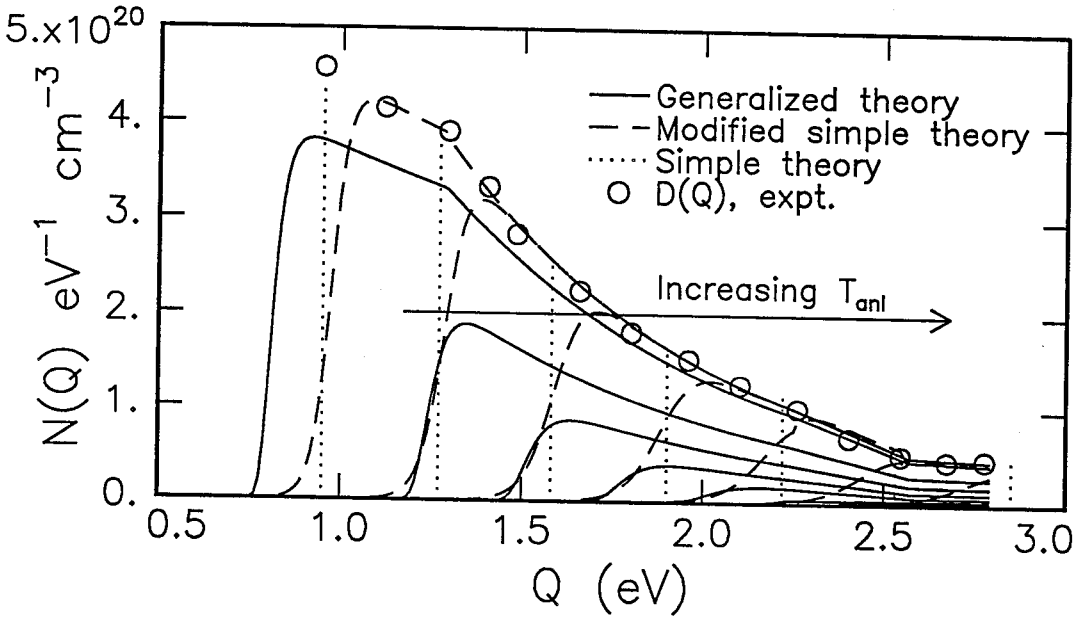


Figure 3.8: $N(Q)$ after isochronal anneals, for samples irradiated to saturation prior to anneals. Symbols are $D(Q)$ from Chapter 2. Solid curves are the results of calculations using the generalized theory, and dashed curves are results of calculations using the modified simple theory. Dotted curves are the results of calculations using thesimple theory.

however, $Q_\Theta$ does not have a real meaning. The generalized theory predicts that after an anneal, even some of the defects with highest activation energies will have been annihilated by the low activation energy defects.

When the total integrated defect density is compared with the experimental data, this annihilation of the high activation energy defects even after an anneal at low to moderate temperatures is found to be essential to achieve good agreement between the experimental data and the theoretical predictions, as shown in Fig. 3.9. Symbols are the experimental data. For accuracy in dosimetry, low-, medium-, and saturation dose irradiations were performed with 250 KeV $Si^+$, 190 KeV $Ne^+$, and 600 KeV $Kr^{++}$, respectively. Solid curves are the results of calculation using the generalized theory, and the dashed curves are the results of the modified simple theory. For calculations using the generalized theory, it was necessary to take into account the fact that the samples were stored at room temperature after irradiation and prior to the anneals. No such precaution was necessary for the modified simple theory.

Neither the generalized theory nor the modified simple theory results in exact agreement with the experimental data, nor is such exact agreement expected, since the results shown in Fig. 3.9 are direct predictions based on

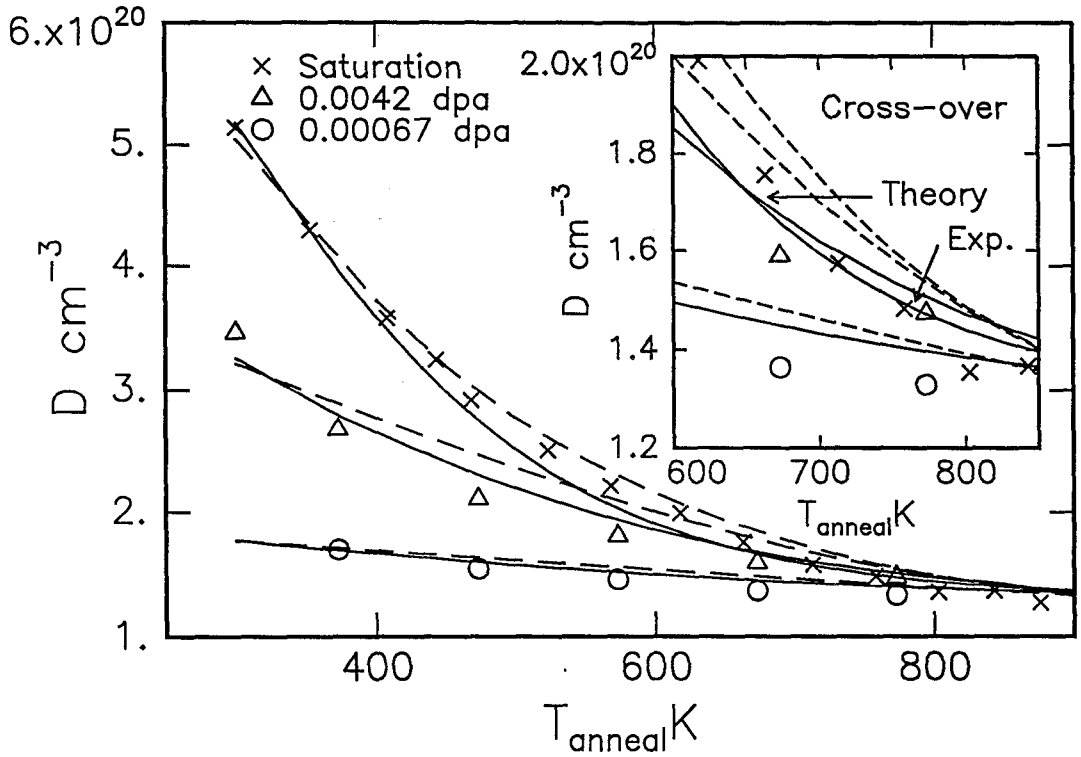


Figure 3.9: Integrated defect density after isochronal anneals. Symbols are experimental data. Solid curves are the results of calculations using the generalized theory, and dashed curves are the results of calculations using modified simple theory. The inset shows the "cross-over" effect in more detail.

parameters derived by fitting the experimental data of Fig. 3.3. It is possible that a better fit could be achieved, should an attempt be made to do so. Yet it is clear that the values predicted by the generalized theory are in better agreement with the experimental data than the values predicted by the modified simple theory, especially for low- and medium dose irradiated samples. For such samples, the modified simple theory predicts a decay in the defect density that is nearly linear with annealing temperature, which is not observed. Even for low dose irradiated samples, experimental data show that the decrease in defect concentration exhibits a pronounced concave curvature. Such curvature, however, is correctly predicted by the generalized theory. This disparity between the two theories comes about because $Q_\Theta$ still plays an important role in the modified simple theory. At doses below saturation, $N(Q)$ is nearly constant and is independent of the activation energy $Q$, as can be seen in Fig. 3.6. For constant $N(Q)$, the decrease in the defect concentration is solely determined by $Q_\Theta$. Since $Q_\Theta \propto T_{anl}$, the defect concentration in such cases will indeed decrease linearly with increasing anneal temperature. Within the generalized theory, however, even some of the defects with activation energies so high that they are immobile at the given anneal temperature are annihilated during an anneal by the low acti-

vation energy defects. Therefore, the defect density decreases more rapidly than linearly with an initial increase in the anneal temperature even when $N(Q)$ is constant, and thus predicts the concave curvature that is observed experimentally.

Furthermore, as the inset in Fig. 3.9 shows, the generalized theory predicts an experimentally observed "cross-over" effect. That is, for a certain combination of irradiation dose and anneal temperature, samples irradiated to a higher dose have a lower defect density after an anneal, since they initially contain more mobile (low-activation energy) defects to annihilate defects that are immobile (i.e., have high activation energies). This "cross-over" effect *cannot* occur in the simple and modified simple theories. The prediction of the experimentally observed "cross-over" effect by the generalized theory thus represents a substantial step in understanding the defect dynamics of a-Si, more important than a simple improvement in accuracy.

### 3.4.3 *In Situ* Measurements of Conductivity

Figure 3.10 shows the defect density immediately following termination of irradiation to same doses but at different fluxes, plotted against ln(t). The symbols are the experimental data measured *in situ*, and lines are results of

calculations using either the modified simple or the generalized theory. The ion used for irradiations was 600 KeV $Kr^{++}$, and the total irradiation dose for all samples was 0.23 dpa, well past the saturation dose. Again, no attempt was made to fit the data in Fig. 3.10. The results are predictions using the parameters derived from Fig. 3.3.

It is clear from Fig. 3.10 that the results of the generalized theory and the experimental data converge quickly to the same values within experimental resolution. Furthermore, the generalized theory again predicts the observed "cross-over" effect, shown more clearly in Fig. 3.11. The reason for this "cross-over" effect is this: with higher flux, more mobile defects are available immediately after termination of irradiation to annihilate the defects that are immobile. This "cross-over" effect, however, need not always be present. Other investigations into the defect dynamics of a-Si failed to observe this effect [10]. However, it was verified by calculation that if the defect generation rate is small enough, as was the case in Ref. [10], there will not be enough low activation energy defects to produce the "cross-over" effect. The "cross-over" effect will never occur, however, if defects of different activation energies are independent of each other, as is assumed in the modified simple theory. Therefore, the observed "cross-over" effect in the decay transient of defect

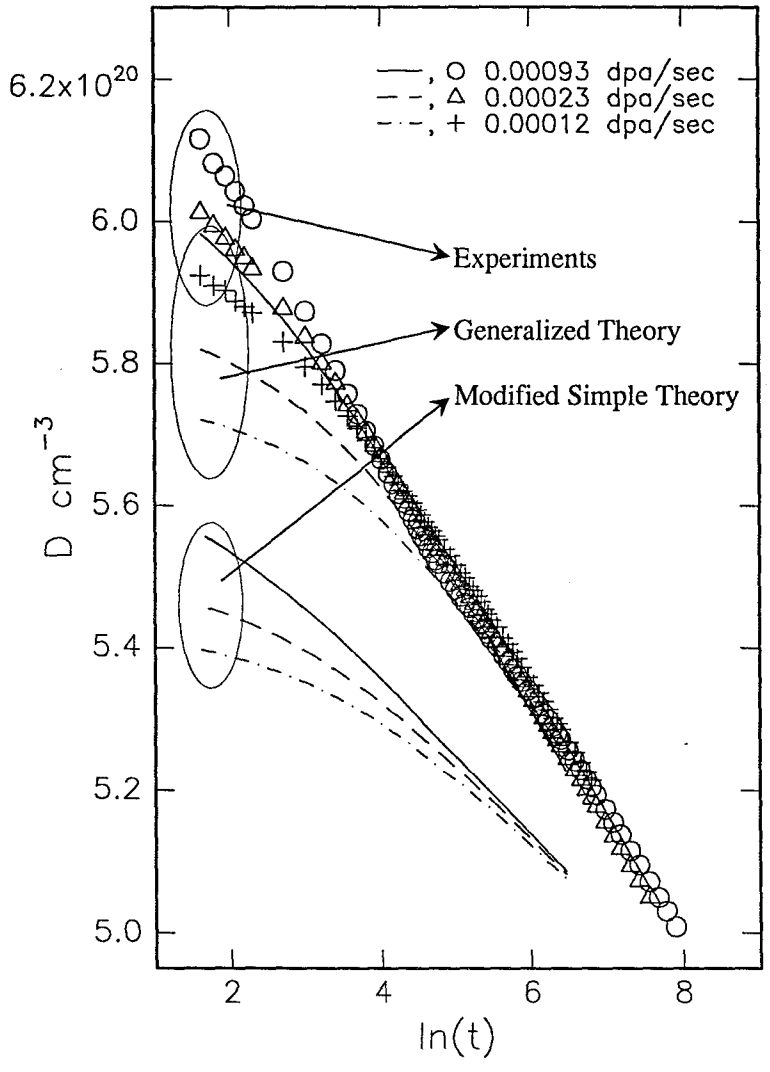


Figure 3.10: *In situ* measurement of decay transient following irradiations at different ion fluxes. The symbols are the experimental data. The lines are results of calculation using either the modified simple or the generalized theory.

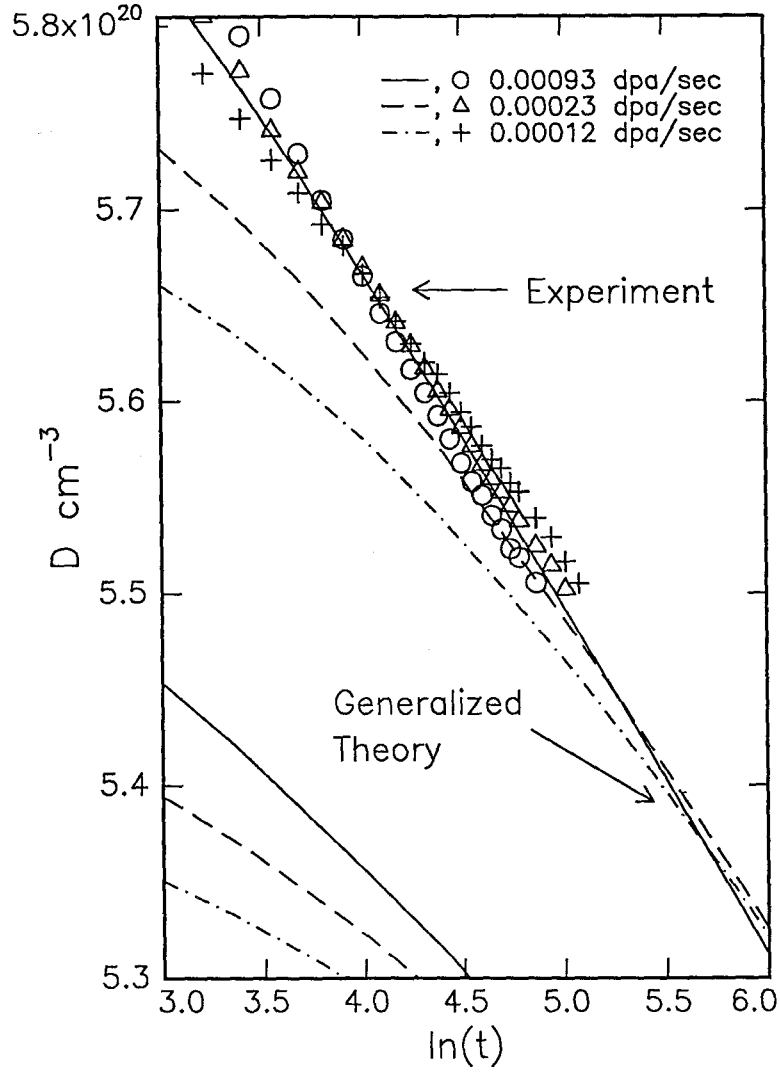


Figure 3.11: The *in situ* measurements of "cross-over" effect is shown in detail, marked by arrows. The symbols are the experimental data. The lines are results of calculation using either the modified simple or the generalized theory.

concentration is strong evidence supporting generalized activation energy spectrum theory.

Such independence of defects with different activation energies might be reasonable, however, if defect recombination were to occur via unimolecular recombination of locally isolated defects (such as isolated point defects) at fixed sinks. Therefore, the existence of a "cross-over" effect may be interpreted as a strong evidence for the bimolecular recombination of defects with different activation energies in a-Si.

## 3.5 Conclusion

In conclusion, a generalized theory is presented to describe the structural relaxation dynamics of amorphous solids. It is specifically designed to allow for interactions between defects with different activation energies. Furthermore, other forms of defect recombination dynamics may by modelled by suitable choices of parameters, although such modelling is not attempted here. Applied to structural relaxation dynamics of a-Si, the generalized theory is found to be needed for an accurate description of the relaxation dynamics. The results also suggest that defects in a-Si annihilate via bimolecular recombination. The success of the generalized theory does not obviate the need for

the simple theory, however. After all, $D(Q)$, the density of defect states in a-Si, was derived in Chapter 2 using the simple theory. The simple theory is still valid for a quick, qualitative description of relaxation dynamics. The generalized theory is necessary when an accurate, quantitative description of the relaxation dynamics is needed.

# Bibliography

[1] M. R. J. Gibbs, J. E. Evetts, and T.A. Leake, J. Mater. Sci. **18**, 278 (1983).

[2] S. Roorda, W. C. Sinke, J. M. Poate, D. C. Jacobson, S. Dierker, B. S. Dennis, D. J. Eaglesham, F. Spaepen, and P. Fuoss, Phys. Rev. B **44** 3702 (1991).

[3] C. A. Volkert, J. Appl. Phys. **70**, 3521 (1991).

[4] J. H. Shin and H. A. Atwater, in *Thermodynamics and Kinetics of Phase Transformation in Thin Films*, edited by M. Atzmon, A. Greer, J. Harper, and M. Libera, Mat. Res. Soc. Symp. Proc. **311**.

[5] J. F. Ziegler, J. P. Biersack, and U. Littmark, *The Stopping and Range of Ions in Solids* (Pergammon, New York, 1985).

[6] J. P. Biersack and L. J. Haggmark, Nucl. Instrum. Methods **174**, 257 (1980).

[7] Copyright J. F. Ziegler, (1990).

[8] P.A. Stolk, L. Calcagnile, S. Roorda, W. C. Sinke, A. J. M. Berntsen, Appl. Phys. Lett. **60** 1688 (1992).

[9] B. Park and F. Spaepen, J. Appl. Phys. **68** 4556 (1990)

[10] S. Coffa, F. Priolo, and A. Battaglia, Phys. Rev. Lett. **70** 3756 (1993).

# Chapter 4

# Modification of Crystallization Dynamics of Amorphous Silicon by Irradiation

## 4.1 Introduction

Amorphous silicon is thermodynamically unstable with respect to crystal silicon, as is evidenced by the highly non-equilibrium methods necessary to produce it. At elevated temperatures, a-Si will inevitably crystallize. If a single crystal template is present, single crystal silicon will grow epitaxially into a-Si. This process is known as solid phase epitaxy (SPE), and begins to proceed at measurable rates from $\approx$ 700 K. SPE is a thermally activated process, with a single activation energy of 2.7 eV over 10 orders of magnitude in SPE rate, and temperature range in the excess of 1300 K [1]. If no crys-

tal template is present, a-Si crystalizes via random nucleation and growth (RNG). That is, small crystal grains nucleate randomly in the a-Si matrix and grow in size, until the a-Si is transformed into polycrystalline silicon [2]. If steps are taken to ensure a clean environment, nucleation of crystal silicon occurs homogenously within the a-Si matrix rather than heterogeneously [3, 4]. In explaining the observed nucleatin dynamics of c-Si, the classical theory of nucleation is often invoked [2, 3, 5, 6].

This random nucleation and growth of crystal silicon in an amorphous matrix is of a great technological interest, since large grained polycrystalline silicon films for thin film transistor applications with high ( $\geq 100$ $cm^2$ /V s) channel mobility can be produced this way. [7]. Random nucleation of crystal grains ahead of the advancing epitaxial crystal growth interface is also one of the fundamental limiting steps in the production of single crystal silicon on insulator films [8]. Therefore, a thorough understanding of nucleation kinetics is needed to obtain more control over these technologically important processes.

Furthermore, since the crystallization of amorphous silicon occurs in a homogeneous, single component system, and no significant volumetric or morphological change occurs during nucleation, crystallization of amorphous

silicon is an ideal candidate to study the phenomenon of nucleation and growth in general. Nucleation and growth is the path taken by many phase transformations, and has been the subject of intense theoretical studies for more than 50 years since first treated by Volmer and Weber [10-17]. However, the theory of nucleation is by no means settled, and arbitrary control of nucleation kinetics is still out of reach.

One of the reasons for the inability to control the evolution of microstructure (e.g., grain size and grain size distribution) during nucleation is the fact that the relative rates of nucleation and growth are usually coupled via thermally activated interface kinetic processes, usually making it impossible to increase (or decrease) one without affecting the other. Another fundamental limit in most nucleation processes is the inability to observe the basic events in nucleation, since the critically sized clusters, which control nucleation, are usually very small. In the crystallization of amorphous silicon, for example, the critical size is comparable to or smaller than the minimum observable size. This inability to directly observe the clusters that control nucleation has to date prevented the direct experimental characterization of the evolution of the subcritical and critical cluster size distribution during nucleation. As a consequence, many critical parameters that characterize nucleation (such

as the time lag for steady state nucleation to be established) can only be inferred by observing the much larger visible clusters. Unfortunately, it has been shown [15] that the values obtained by such inferences depend on experimental and observational conditions, making quantitative comparison of different experiments very difficult.

Ion irradiation is well known to greatly increase the rate of SPE at elevated temperatures [18, 19]. At low temperatures, ion irradiation can reverse the motion of an a-Si/c-Si interface, and amorphize crystal silicon in a layer by layer fashion [20]. Ion irradiation is also known to greatly enhance the crystal nucleation kinetics [22, 4, 5]. No clear understanding yet exists for the dependence of these phenomena on ion irradiation. A widely accepted model for irradiation enhanced SPE exists [23, 24], but it is only phenomenological. Similarly, the mechanism behind this enhancement remains neither well defined nor understood, although the classical theory of nucleation is often invoked to explain the ion enhanced nucleation of crystal silicon.

With ion irradiation, it is possible to allow the ratio of the nucleation rate to the growth rate to be varied much more widely than is possible under purely thermal conditions, and thus gain a greater control over nucleation. Jackson's model, [23], for example, predicts that at high temperatures and

low irradiation rates, the growth rate will be purely thermal. Nucleation, on the other hand, is known to be affected even under such conditions [25]. With *in situ* observation of crystal nucleation under irradiation, it is possible to eliminate many experimental difficulties associated with the study of nucleation, and thus isolate the effect of ion irradiation. By continuously observing the entire transformation of one area, many variables that affect the final analysis can be eliminated, and the observed changes correlated to the changes in irradiation conditions. In this chapter, we will use *in situ* observation of nucleation under irradiation to obtain information on the evolution of the cluster size distribution, and on the role the irradiation plays in the modification of the nucleation rate.

## 4.2 Classical Theory of Nucleation

### 4.2.1 Formulation of the Theory

The classical theory of nucleation envisions the nucleation and growth process as the result of a series of small, bimolecular reactions between the growing cluster and the atoms of the metastable phase [26, 27]. The driving force for the transformation is the free energy difference between the metastable phase and the nucleating phase. The free energy of formation, $\Delta G_n$, of a

cluster of size $n$, however, initially rises with increasing size due to the large number of atoms that are on the surface. Only for large clusters does the free energy of formation decrease with increasing size. The maximum value of the free energy of formation is the free energy barrier to nucleation, and is denoted by $\Delta G_c$. The value of $n$ at which $\Delta G_c$ occurs is the critical size, and is denoted by $n_c$. As we shall see later, $\Delta G_c$ and $n_c$ play determining roles in controlling the nucleation kinetics.

Two of the important quantities in the characterization of the nucleation dynamics are the nucleation rate $I$, and the time lag for establishment of steady state nucleation $\tau$, also known as the incubation time. These are determined by the time evolution of clusters and by the time evolution of the cluster size distribution, $C_n$, respectively. Within the classical theory of nucleation, the net rate of flux between clusters of size $n$ and $(n+1)$ is given by

$$I_{n,t} = C_{n,t}k_n^+ - C_{n+1,t}k_{n+1}^-, \tag{4.1}$$

where $k_n^+$ and $k_n^-$ are the rate of addition and deletion of one atom for a cluster of size $n$, respectively. The subscript $t$ is a reminder that the flux

is, in general, time dependent. For solid phase nucleation which does not involve long range diffusion or compositional changes, Turnbull and Fisher [12] have shown that $k_n^+$ can be written as

$$\begin{aligned} k_n^+ &= O_n \gamma_n^+, \\ \gamma_n^+ &= \gamma \exp[-(\Delta G_{n+1} - \Delta G_n)/2kT], \end{aligned} \tag{4.2}$$

and

$$\begin{aligned} k_{n+1}^- &= O_{n+1} \gamma_{n+1}^-, \\ \gamma_{n+1}^- &= \gamma \exp[(\Delta G_{n+1} - \Delta G_n)/2kT]. \end{aligned} \tag{4.3}$$

$O_n$ is the number of possible attachment sites of a cluster of size $n$. For most atomic configurations, it can be approximated by $4n^{2/3}$ [15]. $\gamma$ is the term that governs the rearrangement kinetics at the interface of growing nuclei. For the crystallization of a-Si, it is simply related to the rate of movement of a-Si/c-Si interface, as shown more explicitly in Appendix A. Notice that

$$k_n^+ < k_n^- \quad \text{for} \quad n < n_c,$$

$$k_n^+ > k_n^- \quad \text{for} \quad n > n_c. \tag{4.4}$$

A cluster of a size less than the critical size will tend to shrink, while a cluster with a size greater than the critical size will tend to grow.

In the case of thermal equilibrium, the cluster size distribution would simply be

$$C_n^e = C_o \exp(-\Delta G_n/kT), \tag{4.5}$$

where $C_o$ is the number of atoms in the initial phase. At such thermal equilibrium, however, the net rate of nucleation, $I$, would be zero. In other words,

$$I_n^e = C_n^e k_n^+ - C_{n+1}^e k_{n+1}^- = 0. \tag{4.6}$$

The "equilibrium" cluster size distribution $C_n^e$, which yields a zero nucleation rate, is very useful in the classical theory of nucleation. In fact, some authors [16, 17] have changed the order of definition, and defined $C_n^e$ to be the cluster distribution which satisfies Eq. 4.6. $\Delta G_n$ is then defined as the free energy which yields $C_n^e$, with no physical connection to the free energy of formation.

Combining Eqs. (4.6) and (4.1), we can express the time-dependent nucleation rate as

$$I_{n,t} = C_n^e k_n^+ \left[ \frac{C_{n,t}}{C_n^e} - \frac{C_{n+1,t}}{C_{n+1}^e} \right]. \tag{4.7}$$

The time evolution of the cluster size distribution is given by

$$\frac{\partial C_{n,t}}{\partial t} = I_{n-1,t} - I_{n,t}. \tag{4.8}$$

The entire problem of the classical theory of nucleation, then, is reduced to solving the above set of coupled difference equations, subject to the appropriate boundary conditions.

Finally, the incubation time is defined in terms of the numbers of nucleated grains. At long times, the steady state nucleation rate, $I^s$, is reached, and the number of nucleated grains is given by

$$\text{Number of grains} = I^s(t - \tau) \qquad , t \gg \tau. \tag{4.9}$$

Equation (4.9) defines the incubation time, $\tau$. An equivalent definition that allows for the calculation of $\tau$ is given by [15, 17]

$$\tau = \int_0^\infty \left[1 - \frac{I_{n_c,t}}{I^t}\right] dt. \tag{4.10}$$

Equation (4.11), however, gives the time lag it takes for the nucleation rate to reach the steady state value at the critical size, which may not be visible. A more general definition of the incubation time as a function of the cluster size is given by [17]

$$\tau_n = \int_0^\infty \left[1 - \frac{I_{n,t}}{I^t}\right] dt. \tag{4.11}$$

### 4.2.2 Solutions to the Problem

Equations (4.7) and (4.8) can be solved in its discrete form [16]. The results, however, are given in forms of summations and integrals, and are unwieldy. More compact forms can be obtained by replacing Eq. (4.8) by its continuum approximation, and solving the resulting partial differential equation. The differential form of Eq. (4.8) is

$$\frac{\partial C_{n,t}}{\partial t} = \frac{\partial}{\partial n}\left[k_n^+ C_n^e \frac{\partial}{\partial n}\left(\frac{C_{n,t}}{C_n^e}\right)\right]. \tag{4.12}$$

This is also known as the Zeldovich-Frenkel [14, 28] equation, and is formally equivalent to the diffusion of clusters in the size space, with $k_n^+$ and $C_n, t$ as the diffusion coefficient and the concentration, respectively.

The accuracy of above continuum approximation has been estimated by Wu [16]. He has found that it is accurate to a few percent, and that a more accurate approximation can be obtained by using a slightly different form of $k_n^+ C_n^e$. A more significant problem is the assumption that nucleation proceeds by addition or deletion of single atoms of the metastable phase. In reality, nucleation may proceed by bursts; that is, more than one atom may be added to or deleted from a cluster at one time. In the case of a-Si, there is evidence which suggests that solid phase epitaxy proceeds by the addition of more than one atom at a time [29]. Such possibility has been examined before. Wu, for example, has obtained expressions for Eq. (4.12) and the incubation time in such cases [16, 17]. However, no closed expressions for the nucleation rate and incubation time are given. On the other hand, no complications would arise if nucleation proceeds by the addition of a fixed number of atoms, since we could simply scale everything in terms of the number of atoms added (or deleted) at one time.

Much more significant problem lies with $\Delta G_n$. It is the most important

factor in determining the dynamics of nucleation, since it controls both the nucleation rate and the time evolution of the cluster size distribution. Traditionally, it has been identified with the the free energy of formation[26]. Yet as Wu has pointed out, such identification is neither necessary nor wholly justified. Even if we do identify $\Delta G_n$ with the free energy of formation of a cluster of size $n$, the exact functional form of $\Delta G_n$ remains controversial. In the case of solid state nucleation, where the entropy due to movement and rotation of clusters can be neglected, many authors [11, 12, 15, 26] have used the form

$$\Delta G_n = -\Delta G n + \Lambda \sigma n^{2/3}, \tag{4.13}$$

where $\Delta G$ is the difference in Gibbs free energy per atom between the phases, $n$ the number of atoms in a cluster, $\Lambda$ a geometrical factor for the surface area, and $\sigma$ is the free energy associated with the interface between the crystal and the surrounding matrix.

Equation (4.13), however, is hard to justfy physically. It is not clear whether it is physical to assign a mathematical surface to a cluster that contains only a few atoms, especially when the width of the transition region

between the cluster and the surrounding matrix may be of the same order as the diameter of the cluster. Similarly, it is also not clear whether it is physical to assign a surface free energy to such a "surface". In the case of solid state nucleation, it may also be possible that the possible strain contribution to the volume free energy difference may be dependent on the cluster size, making $\Delta G$ be a non-trivial function of $n$.

In the classical theory of nucleation, however, such difficulties are ignored, and bulk values of $\Delta G$ and $\sigma$ are used. In this thesis, the classical theory of nucleation will be assumed to be accurate, and Eq. (4.13) will be used for all of the analysis. Furthermore, we will assume that nucleation occurs as the result of the addition and deletion of single atoms. Doing so allows us to use compact, closed expressions for the nucleation rate, the incubation time, and the cluster size distribution. To its justification, we note that despite its lack of firm physical justification, the classical theory of nucleation with these simplifications has been used successfully many times to describe the observed kinetics of nucleation. [2, 5, 30]. Assuming Eq. (4.13) to be accurate, the free energy barrier to nucleation, $\Delta G_c$, and the critical cluster $n_c$, may now be explictly calculated. They are

$$\Delta G_c = \frac{4\Lambda^3\sigma^3}{27\Delta G^2} \tag{4.14}$$

$$n_c = \left[\frac{2\Lambda\sigma}{3\Delta G}\right]^3. \tag{4.15}$$

In the case of amorphous silicon, assuming spherical clusters, $\Delta G$ and $\sigma$ are 0.1 eV and 0.32 J m$^{-2}$, respectively [21]. The critical size, $n_c$, is then 110 atoms. Figure 4.1 shows the calculated values of $\Delta G_n$ for silicon.

Boundary conditions are required in order to solve Eq. (4.7). For the steady state, it is usually assumed that as $n \to 0, C_n^s \to C_n^e$, and as $n \to \infty, C_n^s \to 0$. In such case, we can sum Eq. (4.1) to obtain

$$I^s \sum_u^v \frac{1}{C_n^e k_n^+} = \frac{C_u^s}{C_u^e} - \frac{C_v^s}{C_v^e} = 1 \tag{4.16}$$

where the limits of summation $u$ and $v$ are such that $u \ll n_c \ll v$. The sum is evaluated by approximating it by an integral, expanding the integrand with a Taylor expansion around $n_c$, and then dropping the higher order terms. Such an approximation is possible because near $n_c$, $\Delta G_n$ is at its maximum, and is slowly varying. Given these assumptions, most authors [11, 13, 12, 16] have obtained a steady state nucleation rate of the form

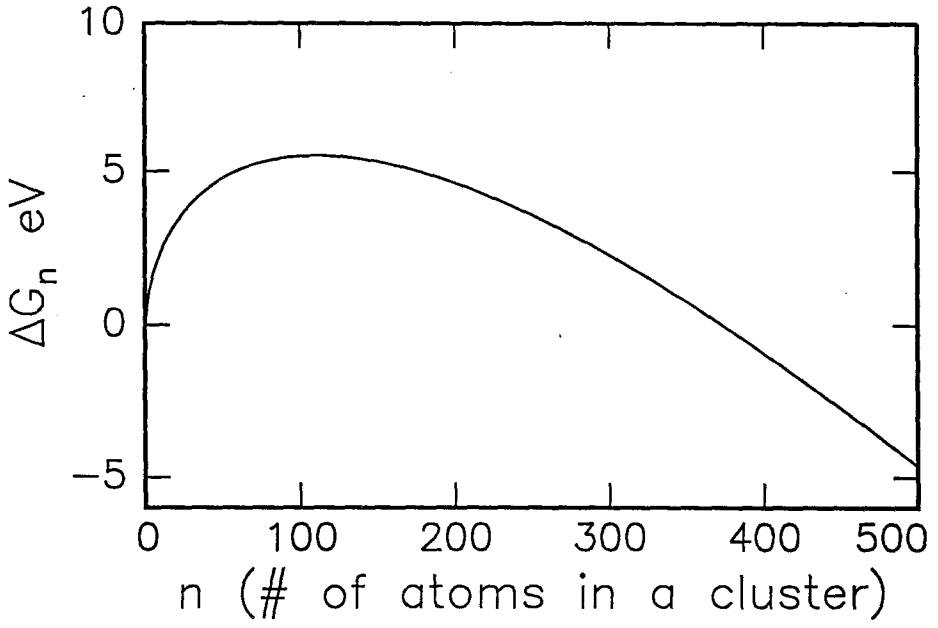


Figure 4.1: Free energy of formation for silicon.

$$\begin{aligned} I^s &= Zk^+_{n_c}C^{eq}_n \\ &= C_o O_{n_c}\gamma Z \exp\left(\frac{-\Delta G_c}{kT}\right), \end{aligned} \tag{4.17}$$

where $Z$ is the Zeldovich factor, given by

$$Z = \sqrt{\left(\frac{\Delta G}{6\pi kTn_c}\right)}. \tag{4.18}$$

Some controversy exists on the steady state cluster size distribution, and the incubation time however. Depending on the approximation used, many authors have derived somewhat different forms of $C^s_n$. Solving Eq. (4.12) numerically, Kelton *et al.* [15] have proposed that the expression derived by Kashchiev to be the most accurate. Recently, however, Wu [17] has shown that the agreement to be a fortuitous one, and proposed a new set of expressions. In this thesis, the expressions derived by Wu will be used exclusively. According to Wu, the steady state cluster size distribution near $n_c$ is given by

$$C^s_n = \frac{1}{2}\mathrm{erfc}[\sqrt{\pi}Z(n-n_c)]C^e_n. \tag{4.19}$$

The incubation time, assuming no prior cluster size distribution, is given by

$$\begin{aligned} \tau &= \frac{L}{2\pi Z^2 k_{n^c}^+} = \frac{L}{8\pi n_c^{2/3} \gamma Z^2}, \\ L &= \ln(\sqrt{\pi} Z n_c) + 0.3. \end{aligned} \tag{4.20}$$

Notice that the incubation time is inversely proportional to $\gamma$, which we stated to be simply related to the growth velocity. Although the Zeldovich factor and the prefactor, $L$, both depend on temperature, they do so only weakly. In the case of amorphous silicon, the deviation of incubation time from Arrhenius behavior in the temperature range of 700K to 1000K is very small. Therefore, the incubation time has nearly Arrhenius behaviour within this limited temperature range. Therefore, the absolute value of the apparent activation energy of incubation time within the temperature range should be equal to the absolute value of activation energy of growth velocity. This is indeed found to be the case, for both thermal and irradiation enhanced cases [2, 6], and shows the validity of identifying $\gamma$ with the growth velocity.

## 4.3 Experiments

The experiments consisted of two parts. In both parts, the samples used were 100 nm thick a-Si films on $SiO_2$ free of supercritical clusters created by implanting chemical vapor deposited Si films with 70 KeV Si to a dose of $1 \times 10^{15}$ ions $cm^2$ at 77 K. In the first part, performed at Caltech, the nucleation and the growth rates of crystal silicon were investigated at high temperatures and low dose rates to confirm that the growth rate is unaffected by the ion beam under such conditions, but the nucleation rate is. The samples were irradiated with 600 KeV $Xe^+$+ ions at a dose rate of $2 \times 10^{10}$ ions $cm^{-2}$ $sec^{-1}$ at an irradiation temperature range of $873K < T_{irr} < 903K$. Since the accurate control of the temperature is critical, a specially designed heating stage was used. Figure 4.2 shows a schematic of the experimental setup used for the nucleation experiments performed at Caltech. At these high temperatures, it was impossible to measure the beam current directly off the sample due to electrons emitted from the heating elements. Therefore, the dose rate was maintained by first stabilizing the beam at the desired dose rate, and then maintaining a constant accelerating current and secondary electron current. The ion beam was also periodically interrupted briefly

to ensure that the dose rate was constant within $\pm$ 10 %. The samples were then analyzed *ex situ* by transmission electron microscope (TEM). The growth rate was determined by measuring the average of the square roots of the areas of the ten largest grains in each micrograph, and following the time evolution. Presumably, the largest grains were the first ones to nucleate in each samples, all around the same time into irradiation.

In the second part, nucleation of crystal silicon under irradiation was measured *in situ* at the High Voltage Electron Microscope/Tandem Accelerator facility at Argonne National Laboratory [31]. The HVEM/Tandem facility consists of a 2 MeV tandem accelerator interfaced to a high voltage electron microscope, with continuous video data-image acquisition during irradiation. Free standing a-Si films created by back etching the substrate were irradiated with 600 KeV $Xe^+$ ions at a constant dose rate of $4 \times 10^{10}$ ions$^{-2}$ sec$^{-1}$ at $T_{irr} = 903K$. In the second part, only the total irradiation dose was varied between different samples. In both parts, TEM images were digitized using a frame grabber, and analyzed with the aid of an image analysis program [32]. For time-resolved analysis of nucleation rates, the time evolution of each individual grain was followed to ensure accuracy of counting.

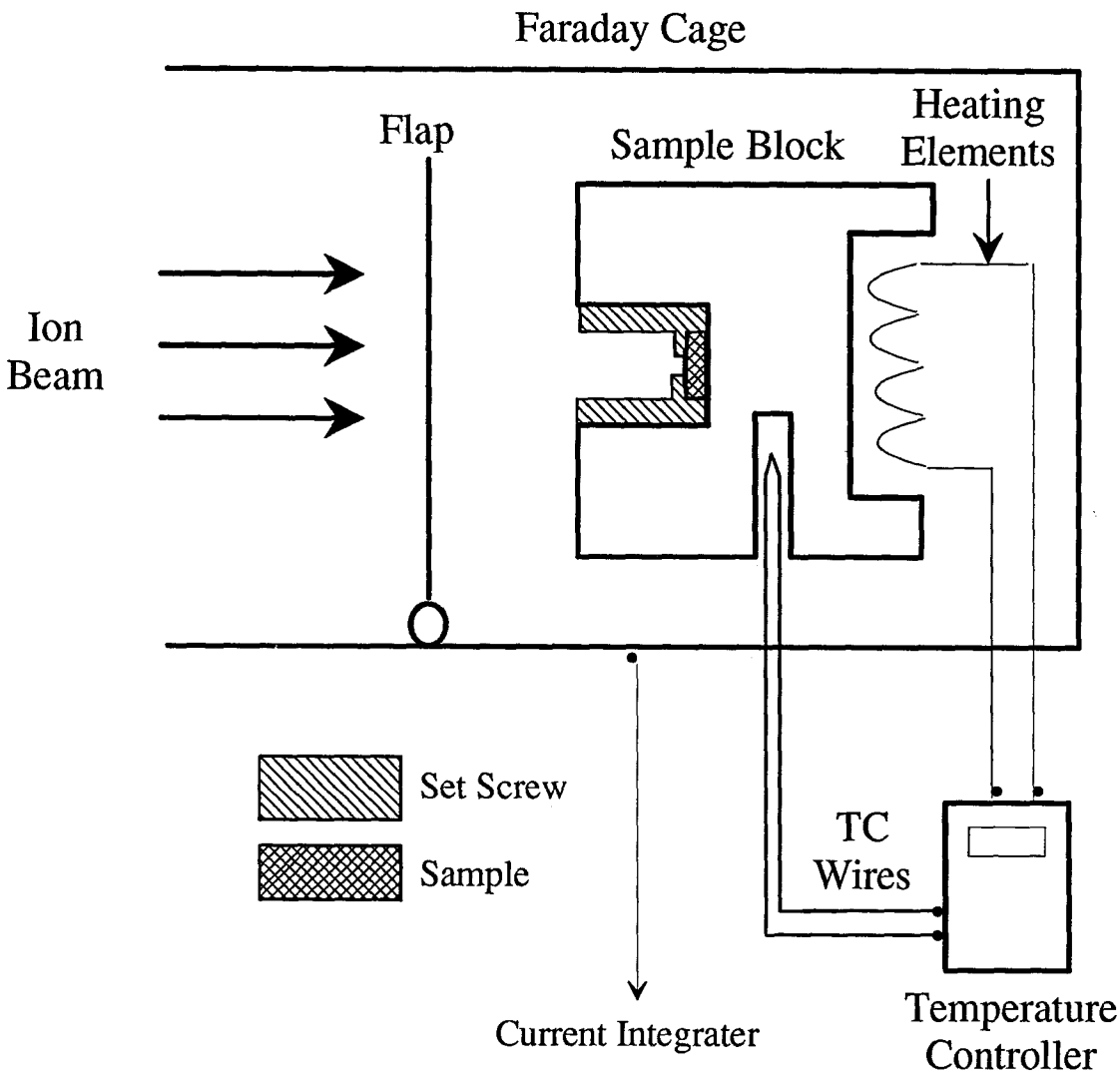


Figure 4.2: Experimental setup for the irradiation enhanced nucleation in the high temperature, low ion flux regime, perfomed at Caltech.

## 4.4 Results and Discussion

Results from the first part of experiments are shown in Figs. 4.4 and 4.5. Table 4.4 shows the measured nucleation rate and incubation time under irradiation, and the expected values for purely thermal transformations from Iverson *et al.* [2]. The incubation time was obtained by subtracting the estimated time needed for nucleated clusters to grow to observable size from the intercept of plots of variation of grain density with time. Quantitative comparison of thermal and irradiation-enhanced values is inappropriate, since the measurement conditions were not identical. Nonetheless, it is evident that both the nucleation rate and the incubation time are significantly affected by irradiation. However, as Fig. 4.5 shows, the growth rate of nucleated clusters is not affected by irradiation, as predicted by Jackson [23]. The solid line in Fig. 4.5 is not a fit to the data, but the expected SPE rate for the [111] orientation [1, 33]. The morphologies of the nucleated grains were irregular, heavily twinned, and in many cases elongated. This is typical of thermally grown grains, but is in contrast to round, isotropic shapes characteristic of grains whose growth is enhanced by irradiation, as shown in Fig. 4.3. These results are in agreement with previous reports [2, 34] which showed that

the growth rate of nucleated grains seems to be limited by movement of the [111] planes, and demonstrate convincingly that the growth rate, and thus the interfacial rearrangement rate of nucleated grains, were only thermally activated, and had no irradiation-enhanced component.

| T(K) | Nucleation rate (grains $cm^{-3}$ $sec^{-1}$) | | Incubation time (sec) | |
|---|---|---|---|---|
| | Under irradiation | Thermal anneal | Under irradiation | Thermal anneal |
| 873 | $1.1 \times 10^{13}$ | $3.8 \times 10^{7}$ | $1.4 \times 10^{3}$ | $3.6 \times 10^{4}$ |
| 888 | $2.1 \times 10^{13}$ | $1.2 \times 10^{8}$ | $1.1 \times 10^{3}$ | $2.0 \times 10^{4}$ |
| 903 | $2.1 \times 10^{13}$ | $3.6 \times 10^{8}$ | $7.2 \times 10^{2}$ | $1.1 \times 10^{4}$ |

Table 4.1: Comparison of the irradiation enhanced and the thermal values of the nucleation rate and the incubation time. The irradiation enhanced values were measured from experiments performed at Caltech.

The nucleation rate is, as Eq. (4.17) shows, linearly dependent on the interfacial rearrangement rate and exponentially dependent on the free energy barrier to nucleation. The incubation time is also dependent on the free energy barrier, although not as strongly as is the nucleation rate. The observed enhancement in the nucleation rate and the incubation time in the absence of enhancement in the interfacial rearrangement rate, as evidenced by the thermal rate of growth for the nucleated grains, strongly suggests that ion irradiation modifies the thermodynamic component of the nucleation. The

a) Irradiation-enhanced growth regime

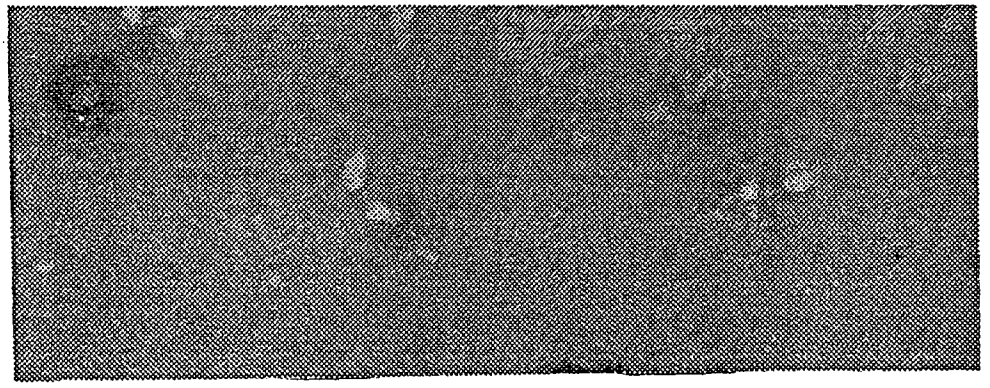


b) Thermal growth regime.

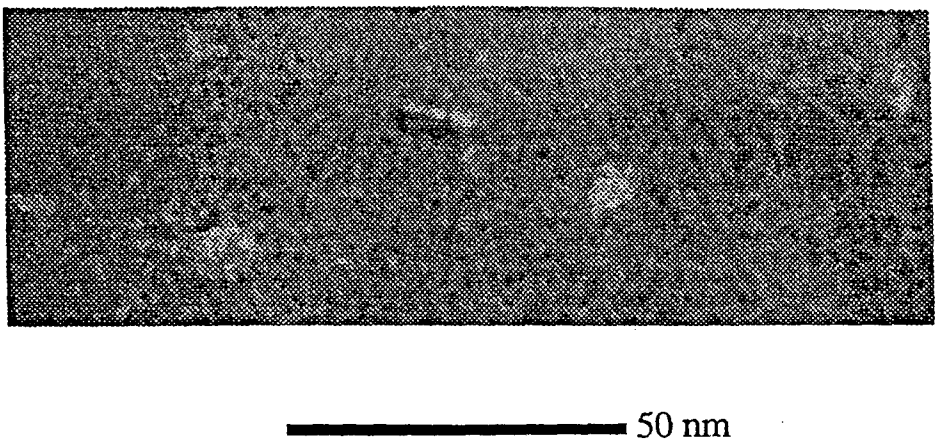


Figure 4.3: Comparison of grain morphology of grains grown under thermal and irradiation-enhanced growth conditions

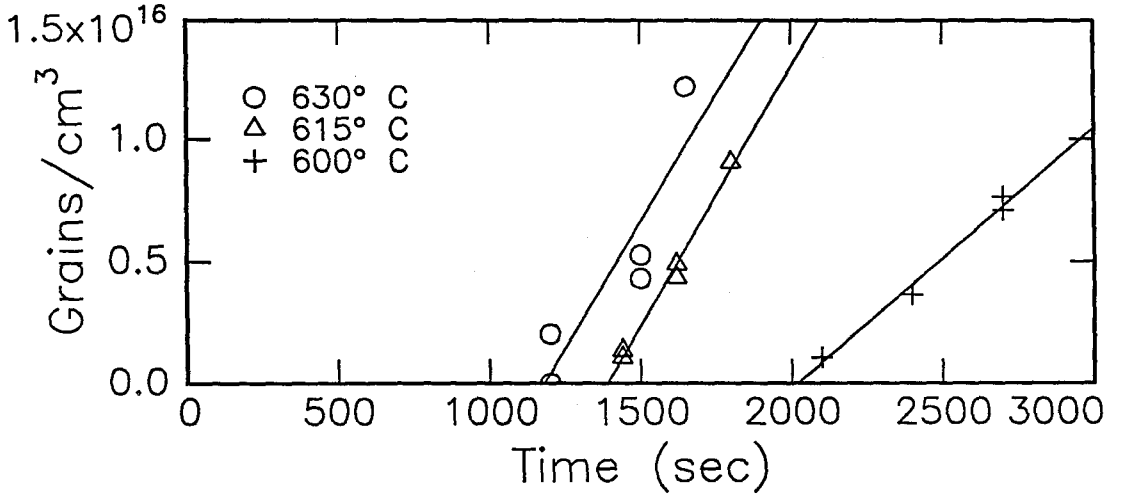


Figure 4.4: Measured grain density, corrected for the crystal fraction, of samples irradiated at Caltech with 600 KeV $Xe^{++}$ ions at a flux of $2 \times 10^{10}$ ions $cm^{-2}$ $sec^{-1}$ at the indicated temperatures. The solid lines are least square fits to the data.

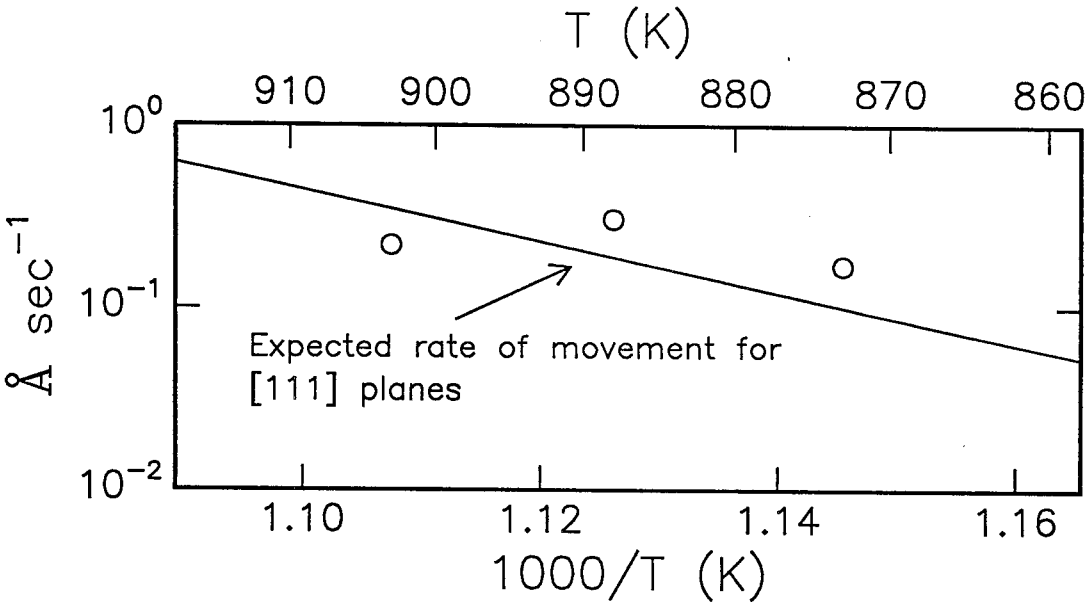


Figure 4.5: Measured growth rate of the nucleated grains under irradiation. The solid line is the expected SPE rate of the [111] planes from refs. [1, 33].

relatively minor effect of irradiation on the incubation time compared with the nucleation rate is also consistent with this conclusion.

Results of *in situ* measurements of the nucleation rate during irradiation are shown in Figs. 4.6 and 4.7. Under continuous irradiation, the number of grains rises linearly with time, indicating a steady state nucleation, as shown in Fig. 4.6. The steady state nucleation rate under irradiation is found to be $2.9 \times 10^{12}$ grains$^{-3}$ sec$^{-1}$. A control sample which was annealed at 903 K under identical conditions but without ion irradiation did not show any nucleation of crystal grains until after approximately 2 hrs of annealing. Interestingly, when the irradiation is terminated after steady state nucleation is observed, we do not observe any drastic changes in nucleation kinetics following termination of irradiation. The arrow marks the moment when the irradiation is terminated, at the dose of $8 \times 10^{13}$ ions cm$^{-2}$. Indeed, after termination of irradiation, nucleation seems to continue for a few minutes at the same rate as under irradiation, followed by a gradual decrease at later times.

Figure 4.7 shows the nucleation kinetics of samples for which irradiation was terminated prior to establishment of steady state nucleation under irradiation. The arrows mark the times at which the ion irradiation was ter-

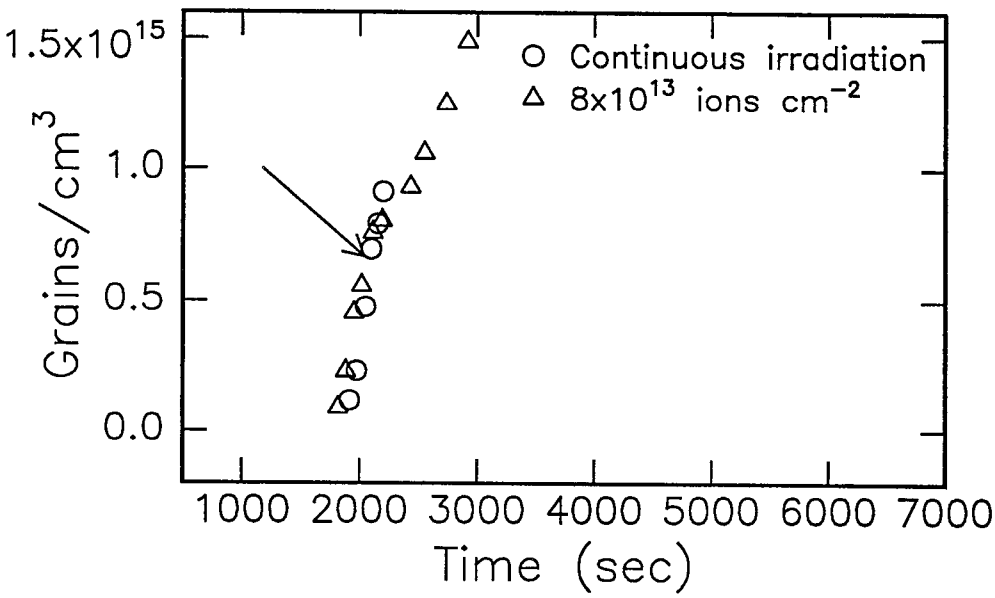


Figure 4.6: *In situ* measurements of the nucleation rate for samples for which steady state nucleation under irradiation is observed.

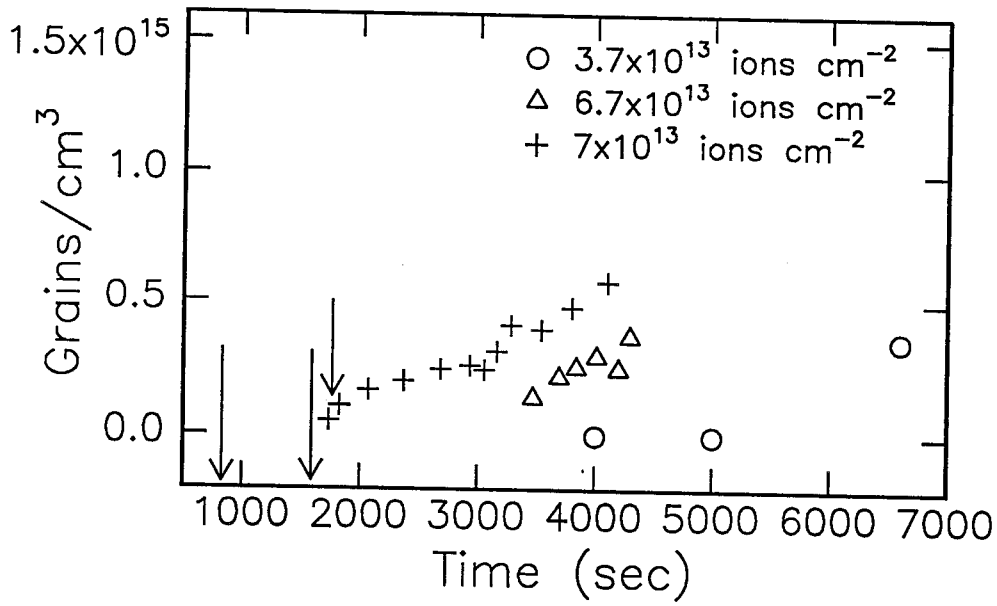


Figure 4.7: *In situ* measurements of the nucleation rate for samples for which irradiation is terminated before steady state nucleation under irradiation is observed.

minated. The doses were, in the increasing order, 3.7, 6.7, and 7 $\times 10^{13}$ ions $cm^{-2}$ . For the smallest dose,the crystallization kinetics were similar to that of purely thermally induced crystallization, except for one very important difference. A few ($< 1 \times 10^{14}$ $cm^{-3}$) grains nucleated early, and grew to large ($> 1000\mathring{A}$) sizes with no further nucleation of crystal grains. Only later, at a time comparable to thermal incubation time, did nucleation of crystal silicon occur again. Similar transformation kinetics characterize other samples for which irradiation was terminated before steady state nucleation under irradiation is observed. After an incubation time, a few grains nucleate initially, followed by a characteristic "quiescent" time period during which negligible nucleation occurs. Subsequently, nucleation begins again and reaches a steady-state rate of $2 \pm 0.5 \times 10^{11}$ grains $cm^{-3}$ $sec^{-1}$, which is one order of magnitude slower than the steady state nucleation rate under irradiation. With increasing dose, we find that more grains nucleate initially, and that the "quiescent" period is shortened. However, the nucleation rate following the quiescent period remains unchanged.

The observed dynamics of nucleation rate upon termination of irradiation at various doses can be explained in the context of classical nucleation theory, if we assume that during the quiescent period, the free energy of formation

and the cluster distribution evolves from values modified by irradiation to thermal values. Defect injection into a-Si is known to significantly increase its stored enthalpy [9]. Moreover, as we have shown in Chapter 2, ion irradiation can maintain excess defect population in a-Si, even when the irradiation temperature is high. It is not clear whether irradiation injected defects affect $\Delta G$, the free energy difference between a-Si and c-Si, or $\sigma$, the interfacial free energy of a crystalline cluster, or possibly both. However, as will be shown later, the modification of either parameter by irradiation affects the nucleation rate in a similar manner.

Assuming that the second nucleation regime following the quiescent period corresponds to the onset of thermal nucleation, and using Eq. (4.17), one can readily estimate the changes in: i) the free energy barrier to nucleation, $\Delta G_c$; ii) the critical cluster size; iii) the change in the free energy difference between a-Si and c-Si $\Delta G$, assuming that change in $\Delta G_c$ occurs through change in $\Delta G$ only; iv) the change in the interfacial free energy $\sigma$, assuming that change in $\Delta G_c$ occurs through change in $\sigma$ only. The results are summarized in table 4.4. From the values given in table 4.4, we can also calculate the free energy of formation, $\Delta G_n$, the steady state cluster distribution, $C_n^s$, and its gradient, $dC_n^s/dn$. The results of these calculations are

illustrated in Figs. 4.8, 4.9, and 4.10.

| | Under irradiation | Under thermal conditions |
|---|---|---|
| $\Delta G_c$ | 5.31 eV | 5.5 eV |
| $n_c$ | 104 atoms | 111 atoms |
| $\Delta G$ | 0.102 atom$^{-1}$ | 0.1 atom$^{-1}$ |
| $\sigma$ | 0.316 J m$^{-2}$ | 0.32 J m$^{-2}$ |

Table 4.2: Calculated changes in thermodynamic parameters controlling nucleation.

It is clear from Figs. 4.9 and 4.10 that the changes in the cluster size distribution and its gradient under irradiation are generally similar, whether change in $\Delta G_c$ occurs through change in free energy difference $\Delta G$ or a change in the interfacial free energy $\sigma$. In both cases, the critical cluster size is smaller during irradiation than during a purely thermal treatment. The cluster size distribution is also much larger, and much steeper during irradiation than during a purely thermal treatment. This similarity means that we cannot tell which effect is more dominant, however. In either case, when irradiation is terminated, the cluster size distribution becomes too large and steep to be able to be supported by new, thermal values of the free energy of formation, $\Delta G_n$. This now unstable cluster size distribution has to

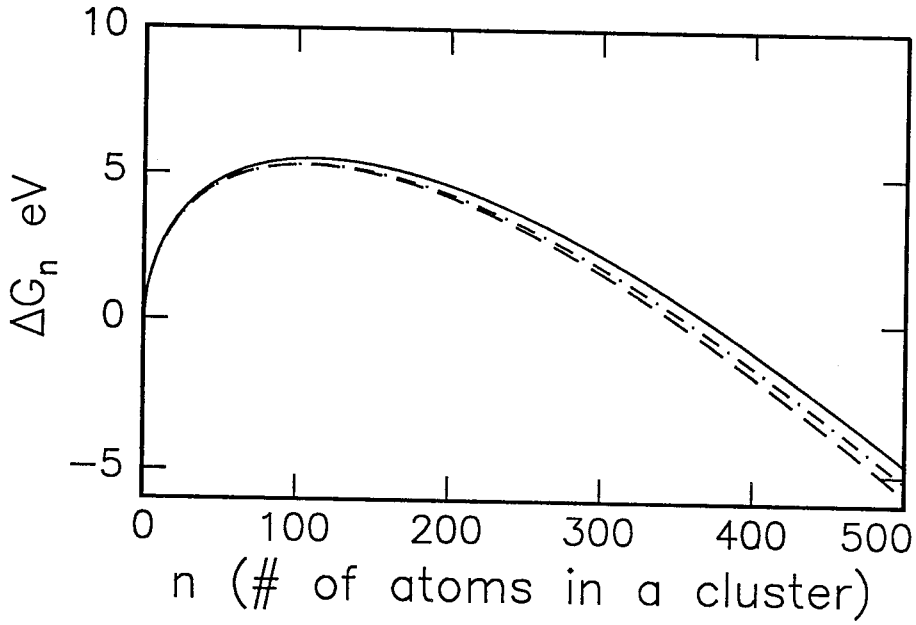


Figure 4.8: Comparison of the free energies of formation, for thermal and irradiation-enhanced cases. The solid line is the free energy of formation during thermal anneal. The free energy of formation under irradiation is calculated assuming assuming i) modification of the free energy difference only (dashed curve), and ii) assuming modification of amorphous-crystal interface free energy only (dash-dot curve).

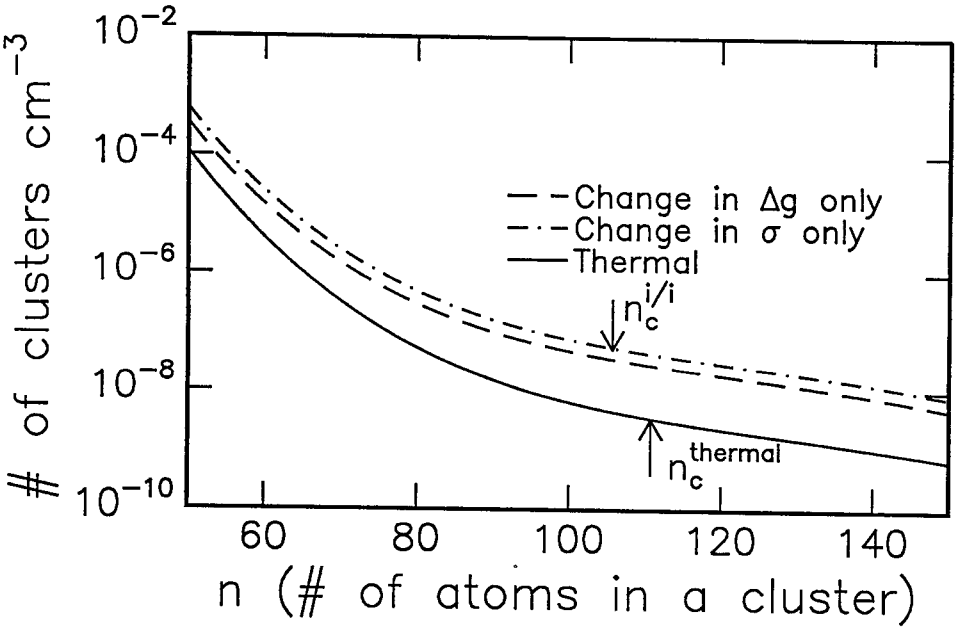


Figure 4.9: Comparison of the calculated cluster size distribution, $C_n^s$ according to Eq. (4.21). The solid curve is the cluster size distribution under purely thermal conditions. Estimates of $C_n^s$ under irradiation were made assuming i) modification of the free energy difference only (dashed curve), and ii) assuming modification of amorphous-crystal interface free energy only (dash-dot curve). The critical cluster sizes under irradiation and under thermal conditions are indicated.

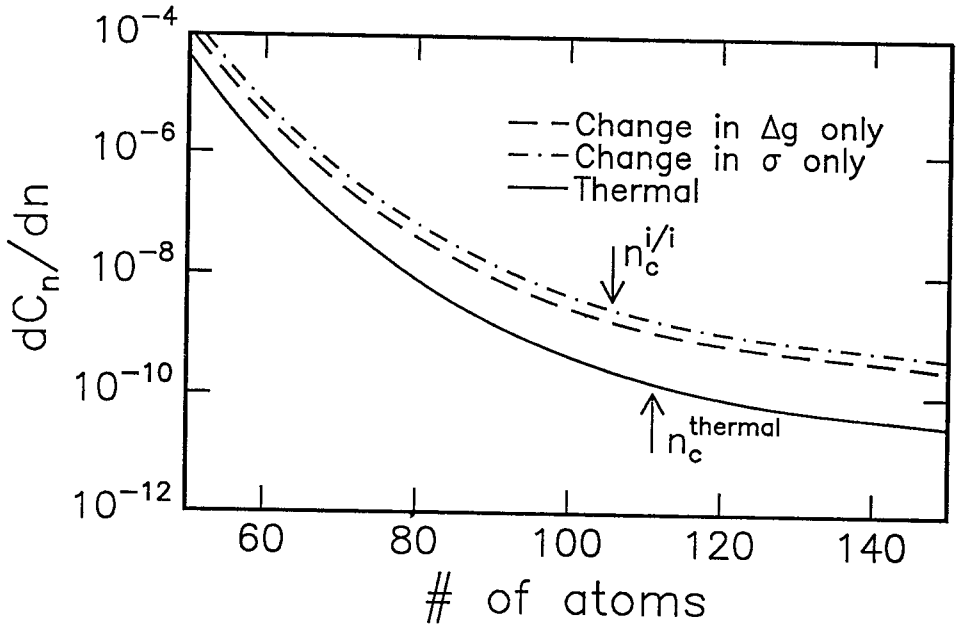


Figure 4.10: Comparison of the gradient of calculated cluster size distribution, $dC_n^s/dn$ according to Eq. (4.21). The solid curve is the expected values under purely thermal conditions. Estimates of $dC_n^s/dn$ under irradiation were made assuming i) modification of the free energy difference only (dashed curve), and ii) assuming modification of the amorphous-crystal interface free energy only (dash-dot curve). The critical cluster sizes under irradiation and under thermal conditions are indicated.

evolve toward the thermal steady state distribution. One possible scenario is a burst of nucleation, caused by the growth of all the excess clusters near the critical region. Such a burst, however, is not observed. Furthermore, the thermal critical cluster size is larger than the critical cluster size under irradiation, which implies that some clusters that would have grown under irradiation now tend to shrink. Taken together, it is much more likely that the cluster size distribution "crashes" toward thermal values. The net result of such changes in cluster size distribution is a *net backward flow of clusters in size space.* Thus when irradiation is terminated, nucleation will cease until the thermal cluster distribution is established, which is consistent with observations. When the steady state under irradiation is already observed, however, it implies that there are already many clusters that are supercritical but still unobservable. Therefore, termination of irradiation in this case will yield a smaller and much more gradual change in nucleation rate, since the supercritical yet unobservable cluster population will continue to contribute to the observed nucleation rate. These evolution of clusters size distribution upon termination of irradiation is shown schematically in Figs. 4.11 and 4.12.

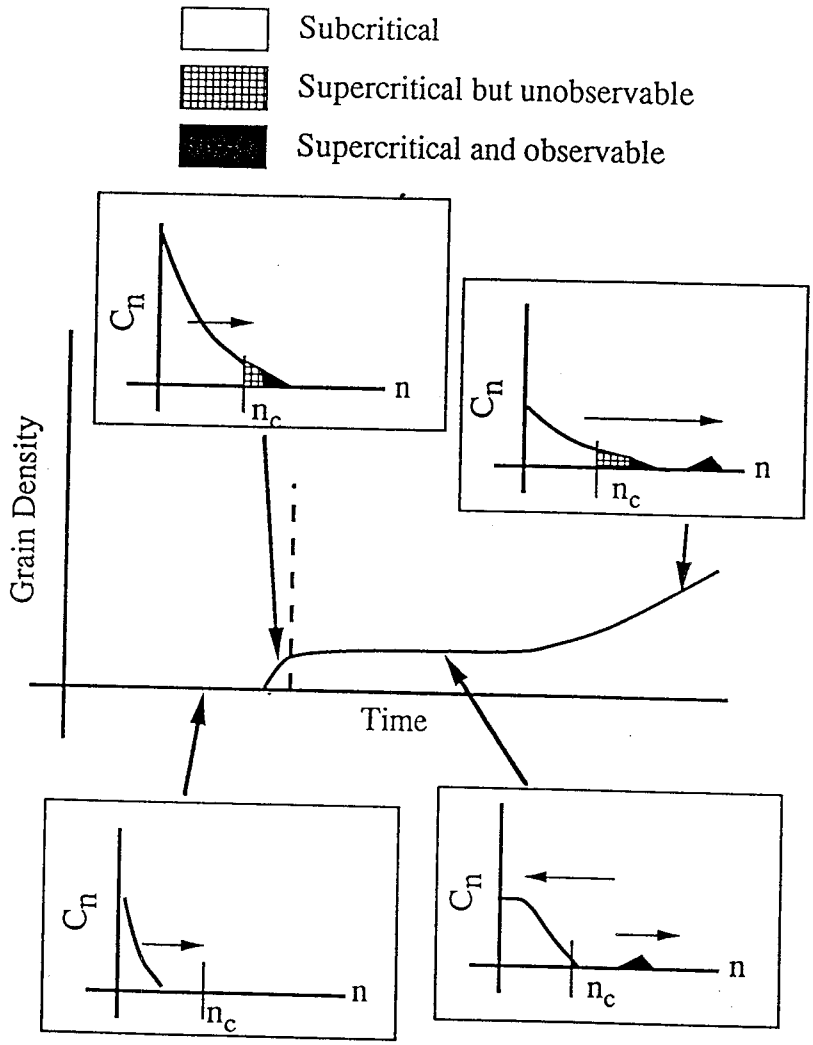


Figure 4.11: Schematic description of evolution of the cluster size distribution function and the nucleation rate for samples for which steady state nucleation under irradiation is not observed.

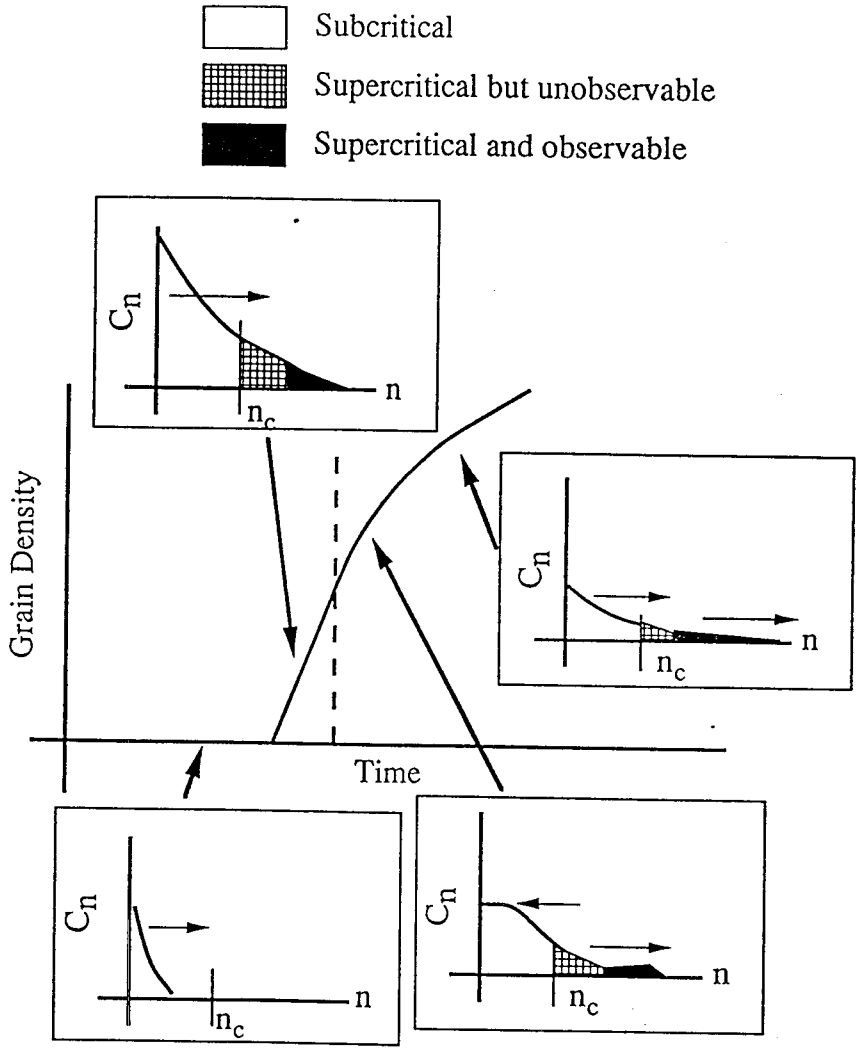


Figure 4.12: Schematic description of evolution of the cluster size distribution function and the nucleation rate for samples for which steady state nucleation under irradiation is observed.

## 4.5 Conclusion

We have demonstrated that ion irradiation greatly enhances the crystal nucleation rate in an amorphous silicon matrix, even when irradiation conditions were such that the crystal growth rate is unchanged by irradiation. *In situ* observation of crystal nucleation has indicated that termination of irradiation during the transient stage of nucleation produces changes in nucleation rate that is best explained by assuming that irradiation affects the thermodynamic quantities that control nucleation process, presumably through defect injection into a-Si matrix. The results suggest clearly that irradiation can be used to independently control thermodynamic and kinetic quantities that control irradiation induced phase transformations.

# Bibliography

[1] G. L. Olson and J. A. Roth, Mater. Sci. Reports, **3** 1 (1988).

[2] R. B. Iverson and R. Reif, J. Appl. Phys., **62** 1675 (1987).

[3] S. Roorda, Ph.D. dissertation, FOM, Netherlands (1990).

[4] Tomonori Yamaoka, Keiji Oyoshi, Takashi Tagami, Yasunori Arima, Ken Yamashita, and Shuhei Tanaka, Appl. Phys. Lett., **57** 1970 (1990).

[5] C. Spinella, A. Battaglia, F. Priolo and S. U. Campisano, Europhys. Lett., **16** 313 (1991)

[6] J. S. Im and Harry A. Atwater, Nucl. Inst. Meth. B, **59** 422 (1992)

[7] T. Ohshima, T. Noguchi, and H. Hayashi, Jpn. J. Appl. Phys., **25** L291 (1986).

[8] H. Ishiwara, A. Tamba, and S. Furukawa, Appl. Phys. Lett., **48**, 773 (1986).

[9] S. Roorda, W. C. Sinke, J. M. Poate, D. C. Jacobson, S. Dierker, B. S. Dennis, D. J. Eaglesham, F. Spaepen, and P. Fuoss, Phys. Rev. B **44** 3702 (1991).

[10] M. Volmer and A. Weber, Z. Phys. Chem. **119**, 227 (1926).

[11] R. Becker and W. Döring, Ann. Phys. **24** 719 (1935).

[12] D. Turnbull and J. C. Fisher, J. Chem. Phys. **36** 2080 (1949).

[13] D. Kashchiev, Suf. Sci. **14** 209 (1969).

[14] J. B. Zeldovich, Acta Physicochim. URSS **18** 1 (1943).

[15] K. F. Kelton, A. L. Greer, and C. V. Thompson, J. Chem. Phys. **79** 6162 (1983).

[16] David T. Wu, J. Chem. Phys. **97**, 1922 (1992).

[17] David T. Wu, J. Chem. Phys. **97**, 2644 (1992).

[18] J. Linnross, G. Holmen and B. Svennson, Phys. Rev. B **32** 227 (1985).

[19] J. Linnross, R. G. Ellliman and W. L. Brown, J. Mater. Res. **3** 1209 (1988)

[20] W. L. Brown, R. G. Elliman, R. V. Knoel, A. Lieberich, J. Linnross, and J. S. Williams, in *Microscopy of Semiconductor Materials*,edited by A. G. Cullis (Institute of Physics, London, 1987) p. 61.

[21] K. N. Tu, Appl. Phys. A **53**, 32 (1991).

[22] J. S. Im and Harry A. Atwater, Appl. Phys. Lett. **57**, 1766 (1990)

[23] K. A. Jackson, J. Mater. Sci. **51** 1218 (1988)

[24] J. S. Custer, A. Battaglia, M. Saggio, and F. Priolo, Phys. Rev. Lett. **69** 780 (1992)

[25] J. S. Im, Jung H. Shin and Harry A. Atwater, presented at Fall '91 Materials Research Society Conference.

[26] A good introduction to the classical theory of nucleation can be found in J. W. Christian, *The Theory of Transformation in Metals and Alloys*, 2nd. ed. (Pergammon, Oxford, 1975) pp. 442-448.

[27] K. Binder and D. Stauffer, Adv. in Physics, **25** 343 (1976).

[28] J. Frenkel, *Kinetic Theory of Liquids* (Oxford University, Oxford 1946).

[29] G. Q. Lu, Eric Nygren, and M. Aziz, J. Appl. Phys. **70**, 5323 (1991).

[30] K. F. Kelton and A. L. Greer, Phys. Rev. B **38** 10089 (1988).

[31] A. Taylor, C. W. Allen and E. D. Ryan, Nucl. Inst. Meth. B **24** 598 (1987).

[32] A public domain image analyzer by NIH.

[33] L. Csespregi, E. F. Kennedy, J. W. Mayer and T. W. Sigmon, J. Appl. Phys. **49** 3906 (1978).

[34] C. Spinella, S. Lombardo and S. U. Campisano, Appl. Phys. Lett. **57** 554 (1990).

[35] F. Spaepen, Acta Metall. **26** 1167 (1978).

# Chapter 5

# Estimate of Change in the Free Energy of Crystallization Using Generalized Activation Energy Theory

## 5.1 Introduction

In Chapter 4, we explained the observed enhancement in kinetics of nucleation under irradiation in the absence of the enhancement in the interfacial rearrangement rate by postulating that defects generated by irradiation affect the thermodynamic quantities that control nucleation. With the generalized activation energy theory developed in Chapter 3, it is possible to follow the time evolution of the defect population under irradiation conditions employed in the nucleation experiments. From previous work that relates the

degree of structural unrelaxation (defect density) with excess enthalpy [1, 2], this allows us to estimate the change in the free energy difference between amorphous and crystal silicon during irradiation, and to compare with experimental data obtained in Chapter 4. It is true that by doing so, we are neglecting the effect of irradiation on the surface free energy. However, there are no good estimates of the effect of defect generation on the interfacial free energy. Thus, no attempt will be made to include this effect.

## 5.2 Estimates of Change in the Free Energy

### 5.2.1 Estimating the Defect Population

Although it would be straightforward to directly simulate the defect population during irradiation at high (903 K) temperature, it is not very practical. At such high temperatures, the defects are very mobile; i.e. they have a very short lifetime. At 903 K, the lifetime of a defect with activation energy of 0.6 eV is expected to be less than $1 \times 10^{-6}$ sec. For an accurate simulation, the timestep taken during simulation would have to be of the order of $1 \times 10^{-7}$ sec. This would require computation time in the excess of 4000 hrs on IBM RISC System/6000$^{TM}$. Computation time could be shortened by using an activation energy greater than 0.6 eV as the lower limit for the activation

energy. Doing so, however, renders the results inaccurate, since the reaction constant $\nu_o$ is dependent on the lower limit of activation energy used.

Such dependence of results on the time step taken and the lower limit for activation energy is actually beneficial, since they can be used to put upper and lower limits on the defect concentration during irradiation without having to resort to excessively long computations. The lower limit on the defect concentration was determined by simulating the evolution of defect population with timesteps that are longer than the estimated defect lifetime. This is equivalent to letting defects continue to annihilate even after they are already annihilated, and results in an underestimate of the defect population. By doing several simulations with 0.6 eV as the lower limit for activation energy, but employing successively shorter (but still practical) timesteps, a good estimate for lower limit for defect population can be made. The upper limit on defect concentration during irradiation was determined by simulating the evolution of defect population with a lower limit of activation energy that is greater than 0.6 eV. The defects with low activation energies are very mobile, and exert controlling influence on the total defect density by annihilating all defects, regardless of their activation energies. Therefore, using a lower limit of activation energy that is higher than 0.6 eV is equivalent to neglecting

their dominant contribution to defect annihilation, and results in an overestimate of the defect population. To ensure that the timesteps were long enough, two simulations were performed, with two different timesteps but with the same lower limit on activation energy. Simulations were performed with a successively lower limit on the activation energy until the results of the two simulation diverged by more than 0.1 %.

| $Q_{min}$ (eV) | Defect Concentration ($cm^{-3}$) |
|---|---|
| 1.7 | $5.65 \times 10^{19}$ |
| 1.4 | $4.23 \times 10^{19}$ |
| 1.1 | $2.95 \times 10^{19}$ |
| 0.85 | $2.05 \times 10^{19}$ |

Table 5.1: Effect of changing $Q_{min}$ on steady state defect concentration under irradiation.

| Timestep (sec) | Defect Concentration ($cm^{-3}$) |
|---|---|
| 0.0002 | $3.17 \times 10^{18}$ |
| 0.00005 | $7.28 \times 10^{18}$ |
| 0.00002 | $1.06 \times 10^{19}$ |

Table 5.2: Effect of changing timestep on steady state defect concentration under irradiation. $Q_{min} = 0.6$ eV.

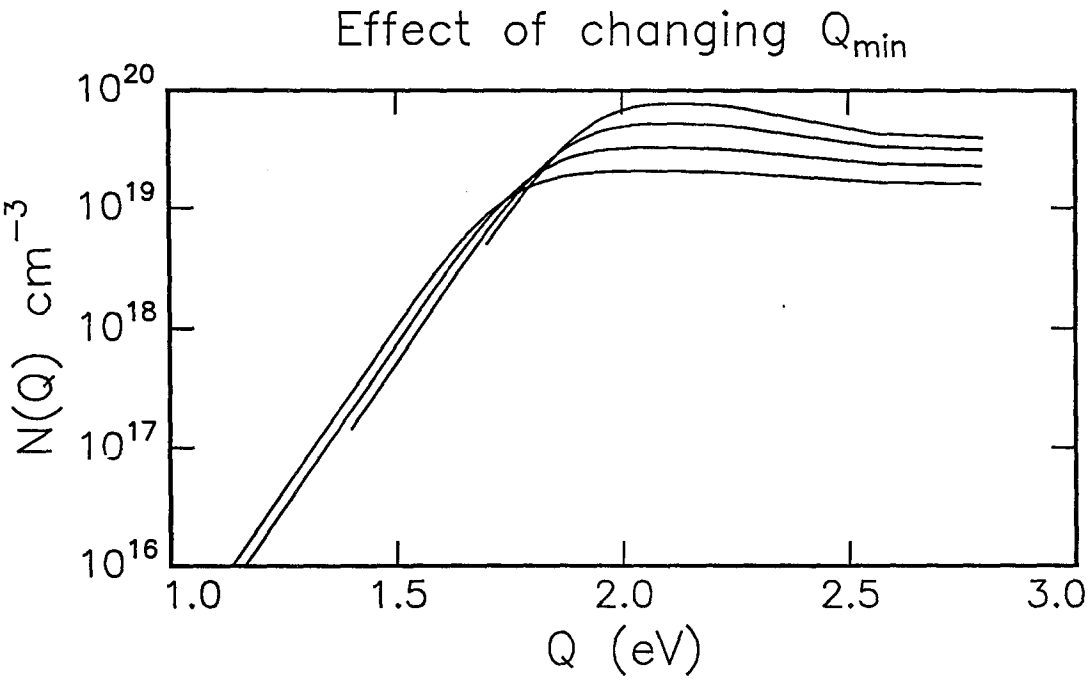


Figure 5.1: Effect of changing $Q_{min}$ on steady state defect concentration under irradiation.

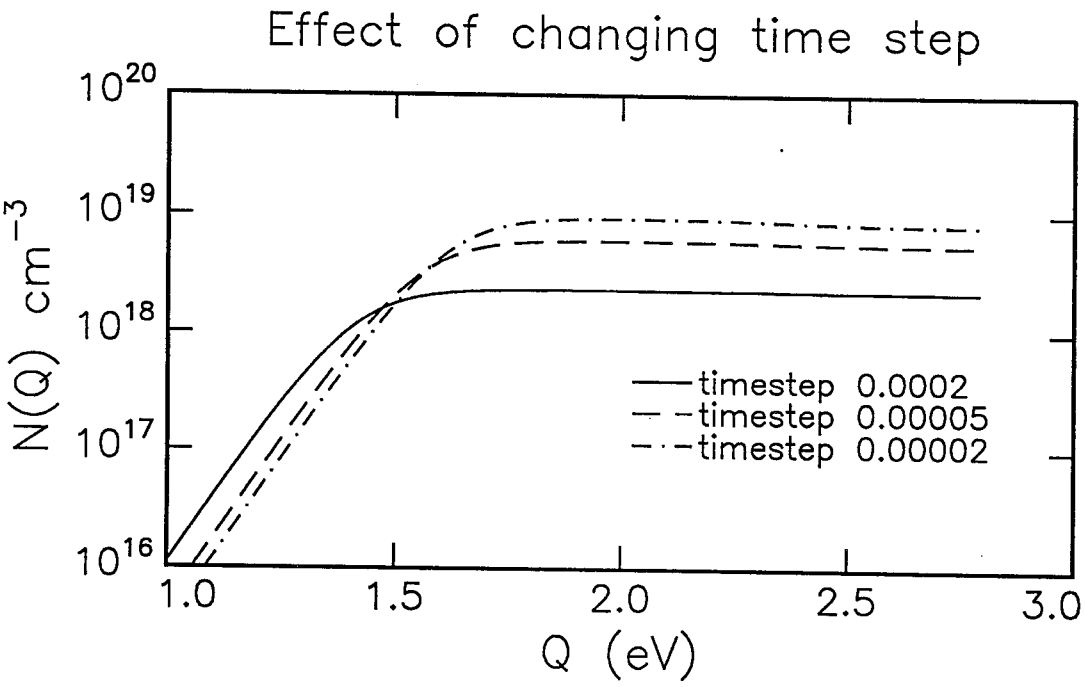


Figure 5.2: Effect of changing the time step on steady state defect concentration under irradiation. $Q_{min} = 0.6$ eV.

The results are shown in Figs. 5.1 and 5.2, and summarized in tables 5.2.1 and 5.2.1 As the timestep is decreased, the total defect population increases, as expected. As the lower limit of activation energy is decreased, the defect density decreases, as expected. Both calculations seem to converge to a value near $1.5 \times 10^{19}$ defects cm$^{-3}$. The lower and upper limits to steady state defect concentrations are $1.06 \times 10^{19}$ defects cm$^{-3}$ and $2.05 \times 10^{19}$ defects cm$^{-3}$, respectively. These limits on increase in the defect concentration under irradiation can be scaled to limits in the increase in the free energy difference, if we assume that the each defect contributes equally to stored enthalpy of unrelaxed a-Si. From previous Chapters, we know that increase in defect density by $3.55 \times 10^{20}$ defects cm$^{-3}$ results in increase in enthalpy of a-Si by $5.28 \times 10^{-2}$ eV atom$^{-1}$. Scaling, we find the limits on increase in free energy to be

$$0.00158 \text{ eV/atom} < \Delta(\Delta G) < 0.00305 \text{ eV/atom}. \qquad (5.1)$$

These limits are in excellent agreement with the experimentally derived change in the free energy from Chapter 4, which showed change in free energy of 0.002 eV/atom. Such an excellent agreement is not to be taken literally,

for it is likely to be fortuitous. Rather, it should be considered only to show the validity of the idea that excess defects generated by irradiation affect the thermodynamic quantities which control nucleation.

## 5.3 Conclusion

Using the generalized activation energy spectrum theory developed for structural relaxation of a-Si, we were for the first time able to quantitatively estimate the role that irradiation plays in affecting the thermodynamic factors which control nucleation. The estimated values are in excellent agreement with experimentally derived values. This structural unrelaxation approach towards the effects of irradiation on nucleation may be extended to investigate other effects. For example, Spinella *et al.* have shown that the nucleation rate under irradiation depends non-linearly with irradiating ion flux [3]. Such a non-linear effects would be a natural consequence of generalized activation energy theory, since with increasing dose rate, the dynamic annealing effects will be more pronounced, resulting in a non-linear increase in the defect density with increasing dose rate.

# Bibliography

[1] E. P. Donovan, F. Spaepen, J. M. Poate, and D. C. Jacobson, Appl. Phys. Lett. **55** 1516 (1989).

[2] S. Roorda, W. C. Sinke, J. M. Poate, D. C. Jacobson, S. Dierker, B. S. Dennis, D. J. Eaglesham, F. Spaepen, and P. Fuoss, Phys. Rev. B **44** 3702 (1991).

[3] C. Spinella, A. Battaglia, F. Priolo and S. U. Campisano, Europhys. Lett. **16** 313 (1991).

# Conclusion

This thesis consisted of two parts. The first part investigated the dynamics of defect creation (structural unrelaxation) and annihilation (structural relaxation) in amorphous silicon, while the second part investigated the enhancement of nucleation of crystal silicon in amorphous matrix by irradiation.

In the first part, using electrical conductivity as the probe, We have shown that the density of defect states, $D(Q)$, exists, and that the standard simple activation energy spectrum theory for structural relaxation is applicable to structural relaxation of amorphous silicon. Using the standard theory of structural relaxation, we have measured the value of the density of defect states, $D(Q)$, for amorphous silicon. We also developed the generalized activation energy spectrum theory, which was shown to be a more accurate, and more physically reasonable description of defect reaction kinetics during structural relaxation of amorphous silicon than the standard, simple theory of structural relaxation.

In the second part, we have shown that ion irradiation greatly enhances the crystal nucleation rate in an amorphous silicon matrix, even when irradiation conditions were such that the crystal growth rate is unchanged by

irradiation. *In situ* observation of crystal nucleation has indicated that defect injected by irradiation affect the thermodynamic quantities that control nucleation process, presumably through defect injection into a-Si matrix.

Finally, the two parts are brought together by using the generalized activation energy spectrum theory developed for structural relaxation of a-Si to estimate the modification of the thermodynamic factors which control nucleation by irradiation. The estimated and experimentally measured values are in excellent agreement with each other, and confirms the validity of the overall picture of the role of the defects in amorphous silicon developed in this thesis.

# Appendix A

# Growth Rate and Interface Rearrangement

In Chapter 4, we stated that the interfacial rearrangement frequency, $\gamma$, of Eq. 4.2 is simply related to the growth rate of large clusters. Here we show this explicitly, starting with Eqs. 4.2 and 4.3. These equations, respectively, give the rate at which an atom attaches to or detaches from a cluster of size $n$. Now, imagine a large cluster (such as the substrate), with $n \gg n_c$. In such a case, the rate at which the size of that particular cluster changes is given by

$$\begin{aligned} \frac{dn}{dt} &= k_n^+ - k_n^- \\ &= O_n\gamma\left(\exp\left[-\frac{(\Delta G_{n+1} - \Delta G_n)}{2kT}\right] - \exp\left[\frac{(\Delta G_{n+1} - \Delta G_n)}{2kT}\right]\right) \end{aligned} \quad \text{(A.1)}$$

For a large cluster, $\Delta G_{n+1} - \Delta G_n$ is simply $-\Delta G$. We can therefore simplify the above equation to

$$\begin{aligned} \frac{dn}{dt} &= k_n^+ - k_n^- \\ &= O_n \gamma \exp\left(\frac{\Delta G}{2kT}\right)\left[1 - \exp\left(-\frac{\Delta G}{kT}\right)\right]. \end{aligned} \tag{A.2}$$

To convert $dn/dt$ to a growth velocity, we note that $O_n \propto n^{2/3}$. Since the radius of a cluster, $r$, is proportional to $\mathrm{n}^{1/3}$, we can find the growth velocity $= dr/dt$.

$$\frac{dr}{dt} \propto \gamma \exp\left(\frac{\Delta G}{2kT}\right)\left[1 - \exp\left(-\frac{\Delta G}{kT}\right)\right]. \tag{A.3}$$

If we assume that $\gamma$ is thermally activated, we find

$$\frac{dr}{dt} \propto \gamma_o \exp\left(-\frac{(E - \Delta G/2)}{kT}\right)\left[1 - \exp\left(-\frac{\Delta G}{kT}\right)\right], \tag{A.4}$$

where $E$ is the activation energy for an interfacial jump. We immediately recognize this equation as the equation for velocity of planar crystallization front [1]. The $\exp(-\Delta G/2kT)$ term arises because of the way $E$ is defined in Turnbull-Fisher theory, as shown in fig. A.1. A more conventional definition

of the activation energy for an interfacial jump would define the activation energy as $E'$ in fig. A.1, which is simply $E - \Delta G/2$, in agreement with Eq. A.4. This shows that $\gamma$ is related simply to the rate of SPE.

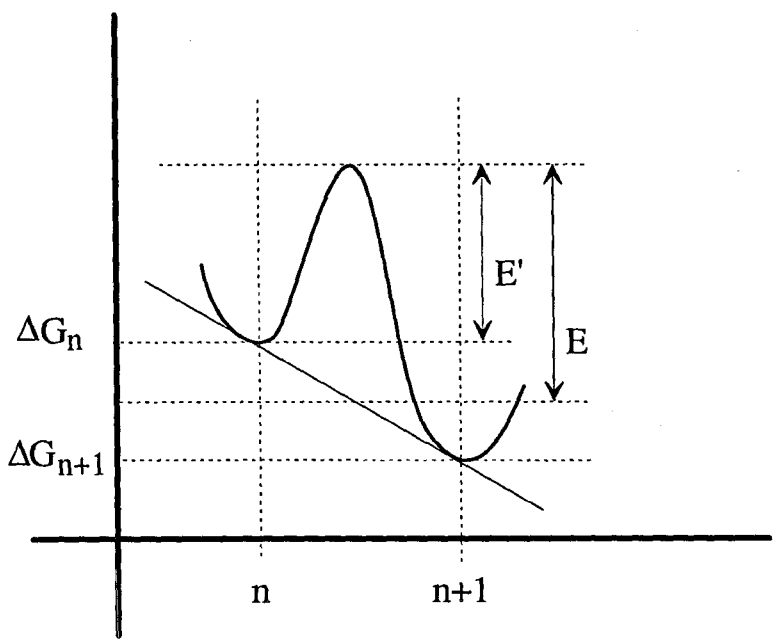


Figure A.1: Schematic of activation energy for interfacial jump

# Bibliography

[1] F. Spaepen and D. Turnbull, Materials, in *Laser Annealing of Semiconductors,* edited by J. M. Poate, J. W. Mayer (Academic Press, New York 1982) pp. 15-42.

[2] G. L. Olson and J. A. Roth, Mater. Sci. Reports, **3** 1 (1988).

# Appendix B

# Code for Simulation of Thermal Anneal

The following is the computer code for simulating defect dynamics during an anneal, using the generalized activation energy theory of Chapter 3. The code is written in C. The code assumes presence of a file named "list.anl", which contains the names of data files. The data file is assumed to contain a header line, then the values of anneal temperature, anneal time, and the reaction constant, all in one line. The next 200 lines of the data files are assumed to be the values of activation energies and the values of $N(Q)$ prior to anneal.

The time evolution of the defects is simulated by letting

$$N(Q, t + \delta t) \;=\; N(Q, t) + \delta t \times \frac{dN(Q, t)}{dt},$$

where $\delta t$ is the time step. The value of time step is not fixed, but is changed throughout the simulation to be 1/10th of the lifetime of the most mobile (i.e., with lowest activation energy) defect that is still in siginificant number. Integration is performed by simply trapezoidal approximation. Since the functions to be integrated are smoothly varying, the error in integration is estimated to be small. The simulation stops when the total anneal time exceeds the anneal time read in from the data file. The results are then written to a file named "name of data file.anl".

```
/*  Program for calculating time evolution of N(Q) */
/* upon annealing. It reads in data from files listed */
/* in 'list.anl'.  It uses adaptive time */
/* scaling to facilitate calculation */

#include <stdio.h>
#include <math.h>

/* Minimum population for defects */
#define min_population 1e-30

/* Bin size of activation energies */
#define Q_bin 200

/* Boltzmann constant */
```

```
#define k .0000862

#define max_list 20
#define name_length 15

double N_integrate(double NQ[]);
double N_eQ_integrate(double NQ[]);
double find_t(double NQ[],double integral_1,double integral_2);
void change_name(char f_list[]);

double v,g,T;
double Q[Q_bin];

main()
{

*/ Variables.  v = reaction constant, g=generation term */
*/ T = anneal temperature * NQ[] are arrays of data */

extern double v,g,T;
extern double Q[Q_bin];
double integral_1,integral_2,annl_time,newN,
tot_time,t_interval;
double NQ_1[Q_bin], NQ_2[Q_bin];
char comments[80], name[name_length];
char f_list[max_list][name_length];
register unsigned long int i;
int j,l,str_length;
FILE *fp;

/* initialize f_list so that they are all EOF's */

for (l=0;l<max_list;l++)
f_list[l][0]='\0';


/* Read the the list of files to read */
```

```
fp=fopen("list.anl","r");
fgets(comments, 80, fp);
l=0;
do
{
fgets(name,name_length,fp);
str_length = strlen(name)-1;
name[str_length]='\0';
strcpy(f_list[l],name);
l++;
}
while ((l<max_list)&&(f_list[l-1][0]!='\0')&&
(f_list[l-1][0]!='\n'));

fclose(fp);


/* Read in the appropriate values for variables */

for (l=0;(l<max_list)&&(f_list[l][0]!='\0');l++)
if ((fp=fopen(f_list[l],"r"))!=NULL)
{

/* Read in sequence of temperature,anneal time,v, g */
fgets(comments, 80, fp);
fscanf(fp,"%lf,%lf,%lf,%lf",&T,&annl_time,&v,&g);

/* Read in the data, and put it into N(Q)_2 and NQ_1*/

for (j=0;j<Q_bin;j++)
{
fscanf(fp,"%lf%lf",&Q[j],&NQ_2[j]);
NQ_1[j]=NQ_2[j];
}

fclose (fp);
```

```
tot_time=0.0;
i=0;

*/ The main part of program.  Finds time evolution of N(Q)'s */

while (tot_time<annl_time)
{
if ((i%2)!=0)
{
integral_1=N_integrate(NQ_2);
integral_2=N_eQ_integrate(NQ_2);
t_interval=find_t(NQ_2,integral_1,integral_2);

for (j=0;j<Q_bin;j++)
if (NQ_1[j]>0.0)
{
newN=NQ_2[j]-t_interval*(v/2.0)
*NQ_2[j]*(integral_1*exp(-Q[j]/(k*T))+integral_2);
if (newN<min_population)
NQ_1[j]=0.0;
else
NQ_1[j]=newN;
}
}
else
{
integral_1=N_integrate(NQ_1);
integral_2=N_eQ_integrate(NQ_1);
t_interval=find_t(NQ_1,integral_1,integral_2);

for (j=0;j<Q_bin;j++)
if (NQ_2[j]>0.0)
{
newN=NQ_1[j]-t_interval*(v/2.0)
*NQ_1[j]*(integral_1*exp(-Q[j]/(k*T))+integral_2);
if (newN<min_population)
```

```
NQ_2[j]=0.0;
else
NQ_2[j]=newN;
}
}
tot_time += t_interval;
i++;
}


/* change the file name to *.anl */

change_name(f_list[l]);

/* Write the values to file */

fp=fopen(f_list[l],"w");
fprintf(fp,"/* %s\n",comments);
fprintf(fp,"/* anneal time:\t%15.2f\n",annl_time);
fprintf(fp,"/* anneal temperature:\t%15.2f\n",T);
fprintf(fp,"/* anneal time:\t%15.2f\n",tot_time);

if ((i%2)!=0)
{
integral_1=N_integrate(NQ_2);

for (j=0;j<Q_bin;j++)
  fprintf(fp,"%15.8e\t%15.8e\n",Q[j],NQ_2[j]);

fprintf(fp,"Integral of N(Q) is:\n");
fprintf(fp,"%15.8e\n",integral_1);
}
else
{
integral_1=N_integrate(NQ_1);

for (j=0;j<Q_bin;j++)
```

```
  fprintf(fp,"%15.8e\t%15.8e\n",Q[j],NQ_1[j]);

fprintf(fp,"Integral of N(Q) is:\n");
fprintf(fp,"%15.8e\n",integral_1);

}
fclose(fp);
}
return 0;
}

/* function to integrate N(Q) */

double N_integrate(double NQ[])
{
int i;
double integral;
extern double Q[Q_bin];

integral=0.0;

for (i=1;i<Q_bin;i++)
integral+=((NQ[i]+NQ[i-1])/2.0)*(Q[i]-Q[i-1]);

return integral;
}

/* function to integrate exp(-Q)*NQ(Q) */

double N_eQ_integrate(double NQ[])
{
int i;
extern double T;
extern double Q[Q_bin];
double integral;

integral=0.0;
```

```
for (i=1;i<Q_bin;i++)
integral+=((NQ[i]+NQ[i-1])/2.0)*(Q[i]-Q[i-1])*exp(-Q[i]/(k*T));

return integral;
}

/* function to change the name to the output file name.*/
void change_name(char f_list[])
{
int i;

i=0;
while (f_list[i]!='\0')
i++;
f_list[i]='.';
f_list[i+1]='a';
f_list[i+2]='n';
f_list[i+3]='3';
f_list[i+4]='\0';
}

/* function to find time interval.  Returns the time */
/* needed for the lowest non-zero bin to decay by 10 percent */

double find_t(double NQ[],double integral_1,double integral_2)
{
extern double Q[Q_bin],v,T;
int i;
double time_found;

for (i=0;(NQ[i]==0.0)&&(i<Q_bin);i++)
;

time_found=0.1/((v/2.0)*(integral_1*exp(-Q[i]/(k*T))
+integral_2));
```

```
if (time_found>5.0)
return 5.0;

else
return time_found;

}
```

# Appendix C

# Code for Simulation of Irradiation

The following is the computer code for simulating defect dynamics during an irradiation, using the generalized activation energy theory of Chapter 3. The code is written in C. The code assumes presence of a file named "list.dpa", which contains the names of data files. The data file is assumed to contain a header line, then the values of irradiation temperature, irradiation dose, the dose rate, the minimum value of the activation energy to be considered, the maximum value of the activation energy to be considered, the reaction constant, and the generation rate, all in one line. The density of defect states, G(Q), from Chapter 2 is approximated by 4 segments of exponential functions.

The time evolution of the defects is simulated by letting

$$N(Q,t+\delta t) \;=\; N(Q,t)+\delta t \times \frac{dN(Q,t)}{dt},$$

where $\delta t$ is the time step. The value of time step is fixed to be 0.0002 sec. Integration is performed by simply trapezoidal approximation. Since the functions to be integrated are smoothly varying, the error in integration is estimated to be small. The simulation stops when the desired dose is reached. The results are then appended to data files, and written to the disk under the same name.

```
/*  Program for calculating time evolution of N(Q) */
/* during irradation It reads in data from files */
/* listed in 'list.dpa'. */

#include <stdio.h>
#include <math.h>

/* Time step used in simulation */
#define t_interval 0.00005

/* Bin size of activation energies */
#define Q_bin 200

/* Boltzmann constant */
#define k .0000862

#define max_list 20
#define name_length 15
```

```
double N_integrate(double NQ[]);
double N_eQ_integrate(double NQ[]);
void init_GQ(double GQ[]);
void init_NQ(double NQ[]);

/* Variables.  v = reaction constant g = generation term */
/* T = temperature low_Q = minimum activation energy used */
/* high_Q = maximum activation energy used */

double v,g;
double low_Q,high_Q,dose_rate,dose,T,Q_step;

main()
{
extern double v,g;
extern double low_Q,high_Q,dose_rate,dose,T,Q_step;
double newN,integral_1,integral_2;
double NQ_1[Q_bin], NQ_2[Q_bin], GQ[Q_bin];
char fname[name_length], comments[80],
f_list[max_list][name_length];
char name[name_length];
register unsigned long int i;
int j,l,str_length;
FILE *fp;

/* initialize f_list so that they are all EOF's */

for (l=0;l<max_list;l++)
f_list[l][0]='\0';


/* Read in the list of files*/

fp=fopen("list.dpa","r");
fgets(comments, 80, fp);
l=0;
do
```

```
{
fgets(name,name_length,fp);
str_length = strlen(name)-1;
name[str_length]='\0';
strcpy(f_list[l],name);
l++;
}
while ((l<max_list)&&(f_list[l-1][0]!='\0')&&
(f_list[l-1][0]!='\n'));

fclose(fp);

/* Read in temperature,dose,dose rate,low_Q,high_Q,v,g */

for (l=0;(l<max_list)&&(f_list[l][0]!='\0');l++)
if ((fp=fopen(f_list[l],"r"))!=NULL)
{
fgets(comments,80,fp);
fscanf(fp,"%lf,%lf,%lf,%lf,%lf,%lf,%lf",&T,&dose,&dose_rate,
&low_Q,&high_Q,&v,&g);
fclose (fp);

/* Initialze N(Q)'s to all zero, and initialize G(Q) */
init_NQ(NQ_1);
init_NQ(NQ_2);
init_GQ(GQ);

Q_step=(high_Q-low_Q)/Q_bin;

/* Main part of the program.  Finds time evolution of N(Q) */
for (i=1;(i*dose_rate*t_interval)<dose;i++)
{
if ((i%2)!=0)
{
integral_1=N_integrate(NQ_2);
integral_2=N_eQ_integrate(NQ_2);
for (j=0;j<Q_bin;j++)
```

```
{
newN=NQ_2[j]+t_interval*
(g*dose_rate*(1.0-NQ_2[j]/GQ[j])-(v/2.0)*NQ_2[j]*
(integral_1*exp(-(low_Q+j*Q_step)/(k*T))+integral_2));
if (newN<0)
NQ_1[j]=0.0;
else
NQ_1[j]=newN;
}
}
else
{
integral_1=N_integrate(NQ_1);
integral_2=N_eQ_integrate(NQ_1);
for (j=0;j<Q_bin;j++)
{
newN=NQ_1[j]+t_interval*
(g*dose_rate*(1.0-NQ_1[j]/GQ[j])-(v/2.0)*NQ_1[j]*
(integral_1*exp(-(low_Q+j*Q_step)/(k*T))+integral_2));
if (newN<0)
NQ_2[j]=0.0;
else
NQ_2[j]=newN;
}
}
}

/* Write the values to file by appending the input file */

fp=fopen(f_list[l],"a");

if ((i%2)!=0)
{
integral_1=N_integrate(NQ_2);

for (j=0;j<Q_bin;j++)
  fprintf(fp,"%15.8e\t%15.8e\n",j*Q_step+low_Q,NQ_2[j]);
```

```
fprintf(fp,"Integral of N(Q) is:\n");
fprintf(fp,"%15.8e\n",integral_1);
}
else
{
integral_1=N_integrate(NQ_1);

for (j=0;j<Q_bin;j++)
  fprintf(fp,"%15.8e\t%15.8e\n",j*Q_step+low_Q,NQ_1[j]);

fprintf(fp,"Integral of N(Q) is:\n");
fprintf(fp,"%15.8e\n",integral_1);

}
fclose(fp);
}
return 0;
}

/* function to initialize the NQ's */

void init_NQ(double NQ[])
{
int i;

for (i=0;i<Q_bin;i++)
NQ[i]=0.00;
}

/* function to initialize GQ, approximated by exponentials  */

void init_GQ(double GQ[])
{
int i;
double Q_step;
extern double low_Q,high_Q;
```

```
Q_step = (high_Q-low_Q)/Q_bin;

i=0;

while ((i*Q_step+low_Q)<1.29)
{
GQ[i]=7.808e18*exp(-0.459*(low_Q+i*Q_step));
i++;
}

while ((i*Q_step+low_Q)<2.26)
{
GQ[i]=2.53e19*exp(-1.38*(low_Q+i*Q_step));
i++;
}

while ((i*Q_step+low_Q)<2.55)
{
GQ[i]=2.3e20*exp(-2.3*(low_Q+i*Q_step));
i++;
}

while (i<Q_bin)
{
GQ[i]=1.604e18*exp(-0.409*(low_Q+i*Q_step));
i++;
}
}

/* function to integrate N(Q) */

double N_integrate(double NQ[])
{
int i;
extern double low_Q, high_Q;
double Q_step, integral;
```

```
integral=0.0;
Q_step = (high_Q-low_Q)/Q_bin;

for (i=1;i<Q_bin;i++)
integral+=((NQ[i]+NQ[i-1])/2.0)*Q_step;

return integral;
}

/* function to integrate exp(-Q)*NQ(Q) */

double N_eQ_integrate(double NQ[])
{
int i;
extern double low_Q, high_Q,T;
double Q_step, integral;

integral=0.0;
Q_step = (high_Q-low_Q)/Q_bin;

for (i=1;i<Q_bin;i++)
integral+=((NQ[i]+NQ[i-1])/2.0)*Q_step*
exp(-(low_Q+i*Q_step)/(k*T));

return integral;
}
```